Muscle LIM Protein and Nesprin-1 in Mechanotransduction

Inaugural-Dissertation
to obtain the academic degree
Doctor rerum naturalium (Dr. rer. nat.)

integrated in the International Graduate School for Myology MyoGrad
in the Department of Biology | Chemistry | Pharmacy
at the Freie Universität Berlin

in Cotutelle Agreement with the
Ecole Doctorale 515 "Complexité du Vivant"
at the Université Pierre et Marie Curie Paris

by

Christine Schwartz
(née Technau)

from Berlin

Berlin, 2016

This work was prepared from 08/12 to 05/16 under the supervision of Simone Spuler and Gisèle Bonne. I conducted the main part of my thesis in the laboratory of Christian Geier in Berlin. During my PhD, I worked in the laboratory of Gisèle Bonne under the supervision of Catherine Coirault for 11 months in Paris.

Dissertation Defense / Disputation / Soutenance de thèse: 29.09.2016

Reviewers

Simone Spuler, MD, Prof.	Reviewer, FU Berlin
Sigmar Stricker, PhD, Prof.	Reviewer, FU Berlin
Catherine Badens, PharmD, PhD, Prof.	1st external reviewer
Dieter Fürst, PhD, Prof.	2nd external reviewer

Contents

Summary

Striated muscle cells are constantly confronted with differing physical stimuli like changes in the stiffness of their surroundings, and stretch because of the movement of the muscles. Physical stimuli are translated into a biochemical signal by mechanotransduction. If mechanotransduction is disturbed in muscle cells and their precursors, cardiac or skeletal muscle diseases may develop. In this thesis, I studied three proteins that are participating in two different pathways of mechanotransduction.

Muscle LIM Protein (MLP) is a small striated muscle specific cytoplasmic protein. When cardiomyocytes in 2D cell culture are stretched, MLP shuttles to the nucleus. Without shuttling MLP, isolated cardiomyocytes fail to respond to the stretch stimulus. Although several interaction partners of MLP are known, its overall function is not completely understood. Human patients with mutations in the gene coding for MLP develop cardiomyopathies and have a high risk of sudden cardiac death. Mice with a functional knock-out of MLP develop a phenotype similar to dilated cardiomyopathy in humans.
I wanted to elucidate the role of MLP in these cardiomyopathies by expressing mutated MLP in isolated neonatal cardiomyocytes of mice without endogenous MLP ($MLP^{-/-}$ mice). I established cell culture of freshly isolated neonatal cardiomyocytes in 2D and 3D culture conditions and prepared viruses to transduce the isolated cardiomyocytes with mutated MLP. Surprisingly, I found that in 3D cultures of cardiomyocytes, MLP did not shuttle to the nucleus after stretching of the cells. Although I could not solve this issue during the time given, I prepared the setup for subsequent experiments in 2D.

Nesprin proteins, together with SUN proteins, form a nuclear envelope-spanning protein complex, the LINC complex. Inside the nucleus, the LINC complex interacts with Emerin and Lamin proteins. Outside the nucleus, it binds different parts of the cytoskeleton. Thus, information can be carried from the cytoskeleton directly into the nucleus. A patient with congenital muscular dystrophy harboring a nonsense mutation in the gene coding for Nesprin-1 should express a truncated protein Nesprin1-ΔKASH lacking the SUN binding domain, probably disturbing the LINC complex.
Nesprin1-ΔKASH was not present in isolated myoblasts from this patient. These cells displayed deformed nuclei and had defects in mechanosensitive responses similar to myoblasts from a second patient with congenital muscular dystrophy who lacks aminoacid K32 in A-type lamins (LMNA-ΔK32). When the cells were cultured on soft tissue culture dishes that resemble the stiffness of muscle fibers, both patient cell lines displayed an elevated level of stress fibers and focal adhesions, and the cells spread further than WT myoblasts in these conditions. I present data that this was not due to MLC kinase but because of activity of ROCK and SRC. A knockdown of the formin FHOD, a downstream target of ROCK and SRC, reduced the phenotype of ectopic stress fiber formation in the mutant cell lines.
While it is hypothesized that mutations in Nesprin and Lamin proteins lead to a mechanical instability of the nuclear envelope, these results indicate that signalling pathways through the nuclear envelope are disturbed as well.

Zusammenfassung

Quergestreifte Muskelzellen sind sich ständig ändernden physikalischen Stimuli wie Dehnung oder sich ändernder Festigkeit des sie umgebenden Gewebes konfrontiert. Der Prozess, mit dem diese physikalischen Stimuli in biochemische Signale übersetzt wird, heißt Mechanotransduktion. In dieser Dissertation wurden drei Proteine untersucht, die Teil von zwei verschiedenen Mechanismen der Mechanotransduktion sind.

Muscle LIM Protein (MLP) ist ein kleines Protein, das spezifisch in quergestreifter Muskulatur vorkommt. MLP migriert vom Zytoplasma isolierter neonataler Kardiomyozyten in deren Zellkern, wenn die Zellen in 2D-Kulturen gedehnt werden. Wird dies verhindert, zeigen die Zellen keine Adaptation an den Stimulus. Obwohl einige Interaktionspartner von MLP bekannt sind, ist dessen Funktion insgesamt nicht vollständig verstanden. Patienten mit Mutationen in dem Gen, das für MLP kodiert, entwickeln Herzmuskelerkrankungen und sind der Gefahr des plötzlichen Herztodes ausgesetzt. Mäuse mit einem Knockout von MLP ($MLP^{-/-}$ Mäuse) entwickeln einen Phänotyp, der der Dilatativen Kardiomyopathie beim Menschen ähnelt.
Ich wollte zeigen, dass MLP wegen der Mutationen der Patienten nicht mehr in den Zellkern transloziert und dies das Expressionsmuster der isolierten Kardiomyozyten nach Dehnung verändert. Ich etablierte die Kultur neonataler Kardiomyozyten in 2D und 3D Kulturbedingungen und bereitete Viren vor, die für verschiedene Mutationen von MLP kodierten, mit denen $MLP^{-/-}$ Kardiomyozyten transduziert werden sollten. Überraschenderweise translozierte MLP nie in den Zellkern von Kardiomyozyten, die in 3D- statt in 2D-Kulturen gedehnt wurden. Auch wenn ich in der gegebenen Zeit dieses Problem nicht vollständig lösen konnte, habe ich die notwendigen Methoden und Materialien für zukünftige Experimente in 2D etabliert.

Zusammen mit SUN-Proteinen formen große Nesprin-Proteine den die Kernmembran überspannenden LINC-Komplex. Dieser interagiert mit Emerin und Lamin-Proteinen im Inneren des Zellkernes und ist im Zytoplasma mit den verschiedenen Bestandteilen des Zytoskelettes verbunden. Ein junger Patient, der aufgrund eines fälschlich kodierten Stopp-Codons ein verkürztes Nesprin-Protein (Nesprin1-ΔKASH) produziert, litt an angeborener Muskeldystrophie. Nesprin1-ΔKASH fehlt die Domäne, mit der das Protein mit SUN-Proteinen interagiert. Somit ist bei diesem Patienten vermutlich der LINC-Komplex nicht vollständig funktionsfähig.
Während Nesprin1-ΔKASH in den Myoblasten des Patienten nicht exprimiert war, war die Lokalisation anderer, LINC assoziierter Proteine normal. Die Zellen hatten verformte Zellkerne und zeigten Defekte in der Reaktion auf verschiedene physikalische Stimuli. Dies ähnelte Myoblasten von Patienten, die Mutationen in Lamin-A/C hatten (LMNA-

ΔK32 Myoblasten). Dies deutet darauf hin, dass Nesprin-1 und Lamin-A/C am gleichen Mechanismus der Mechanotransduktion beteiligt sind. Wenn die Myoblasten auf weichen Petrischalen, die die Festigkeit von Muskelgewebe imitierten, kultiviert wurden, entwickelten die Zellen beider Patienten verstärkt Stressfasern, die normalerweise nur auf harten Untergründen gebildet werden. Daten in dieser Dissertation zeigen, dass die Stressfasern wegen einer Überaktivität von ROCK und SRC gebildet wurden. Knock-down des Formin Proteins FHOD1, das von ROCK und SRC aktiviert wird, reduzierte den beobachteten Phänotyp bei beiden Zelllinien.
Es wird bereits länger vermutet, dass Mutationen in Nesprin und Lamin Proteinen zu einer mechanischen Destabilisierung der Kernmembran führt. Die hier gezeigten Ergebnisse deuten darauf hin, dass nicht nur eine solche Destabilisierung vorliegt, sondern auch Signalwege, die durch die Kernmembran hindurch gehen, gestört sind.

Résumé

Les cellules musculaires striées sont constamment confrontées à différents stimuli physiques, comme les changements dans la rigidité de leur environnement, mais sont aussi extensibles en raison de leur rôle dans la contraction des muscles. Les stimuli physiques sont convertis en un signal biochimique par méchano-transduction. Si la méchano-transduction des cellules musculaires et de leurs précurseurs est perturbée, des maladies liées à la défaillance des muscles squelettiques et cardiaques peuvent se développer. Lors de ma thèse, j'ai étudié trois protéines qui participent à deux vois différentes de méchano-transduction.

La protéine musculaire « LIM » (MLP) est une protéine cytoplasmique spécifique du muscle strié. Dans une culture cellulaire in 2D, lorsque les cardiomyocytes sont étirés, MLP est transloqué vers le noyau. Sans translocation de MLP, les cardiomyocytes isolés ne parviennent pas à répondre à la stimulation de l'étirement. Bien que plusieurs partenaires interagissant avec MLP soient connus, sa fonction générale n'est pas totalement élucidée. Les patients porteurs de mutations dans le gène codant pour MLP développent une cardiomyopathie et présentent un risque élevé de mort subite. Les souris MLP knock-out (souris $MLP^{-/-}$) développent un phénotype similaire à la cardiomyopathie dilaté humaine.
Mon objectiv a été d'élucider le rôle de MLP dans ces cardiomyopathies en surexprimant une mutation de MLP dans les cardiomyocytes isolés à partir de souris $MLP^{-/-}$ néonataux. Pour cela, j'ai établi une culture cellulaire de cardiomyocytes néonataux fraîchement isolés en condition de culture 2D et 3D. J'ai également préparé les virus à transduire dans les cardiomyocytes $MLP^{-/-}$. Étonnamment, dans les cultures 3D de cardiomyocytes, MLP n'est pas transloqué vers le noyau après l'étirement des cellules. Bien que le temps imparti ne m'ai pas permis de résoudre ce problème, j'ai mis au point les expérience 2D nécessaires à la poursuite de ce project.

Les protéines nesprines et SUN forment ensembles un complexe protéique transmembranaire de l'enveloppe nucléaire, le LINC complexe. Dans le noyau, le complexe LINC interagit avec les protéines émerine et lamines. En dehors du noyau, il lie les différentes parties du cytosquelette. Ainsi, l'information peut passer directement du cytosquelette vers le noyau. Un patient souffrant de dystrophie musculaire congénitale porteur d'une mutation non-sens dans le gène codant pour Nesprin-1, devrait exprimer une protéine tronquée Nesprin1-ΔKASH ; une proteine dont le domaine de liason à SUN est manquant, induisant probablement une perturbation du LINC complexe.
La Nesprin1-ΔKASH n'était pas présente dans les myoblastses isolés de ce patient. Ces cellules présentaient des noyaux déformés, mais également des anomalies de réponses méchanosensibles, semblables à ceux observés sur les myoblastes d'un deuxième patient

souffrant de dystrophie musculaire congénitale (mutation LMNA-ΔK32). Lorsque les cellules ont été cultivées sur supports mous, mimant la rigidité des fibres musculaires, les deux lignées cellulaires de patients affichaient un niveau élevé de fibres musculaires stressées et d'adhésions focales. De plus, les cellules s'étalaient mieux que les myoblastes WT dans ces conditions. Les données ci-dessous démontrent que l'ensemble de ces événements n'est pas dû à la kinase MLC mais à l'activité de ROCK et SRC. Le knock-down de la formine FHOD, une cible en aval de ROCK et SRC, a réduit la formation de fibres ectopiques stressées dans des lignées cellulaires mutantes.
Bien que l'on ai émis l'hypothèse que les mutations dans les protéines nesprines et lamines conduisent à une instabilité mécanique de l'enveloppe nucléaire, ces résultats indiquent que les voies de signalisation, par le biais de l'enveloppe nucléaire sont perturbées aussi.

Acknowledgements

Many people accompanied me during my years as a PhD student. I am lost for words to show my gratitude towards you.

Christian Geier integrated me in his lab and gave me the MLP project to work on. Besides the things I learned at the bench, I got insights in the ways of politics at the institute and the problems to keep a lab running that I could not have gotten in a bigger group. I was sad when I learned that the contract of the lab at the ECRC was finally not extended, but I am glad that most members of our group found a new position. And I hope that Christian will have the opportunity to carry on his research projects in the future.
In our group and in the neighbouring groups with whom we shared office and lab space, I met wonderful people. We were a good team and I miss working with you!

Catherine Coirault and Gisèle Bonne were welcoming me in Paris. Catherine gave me the opportunity to work on the Nesprin project and she helped me staying focused. Martina Fischer and Feriel Azibani introduced me to the French way of lab life, which sometimes was surprisingly different from what I knew from German laboratories.

The concept of MyoGrad, the International Graduate School for Myology with a cooperation between German and French laboratories, is a wonderful opportunity for young scientists and I am glad that I could be part of it. Learning a new language, working abroad and meeting people with different sets of beliefs and values changes the way of thinking dramatically, which adds up to the things a PhD student should learn.
This thesis was funded with a PhD stipend by the Deutsche Forschungsgemeinschaft DFG and with a mobility aid from the Deutsch-Französische Hochschule (Université franco-allemande, DFH-UFA), which was both organized by MyoGrad.

Simone Spuler and Gisèle Bonne always gave their advice on project decisions. I have been happy to work with and get advice from such experienced group leaders.
The people forming my thesis committee were having a big impact on the thesis. We met twice over the years and after both meetings I was more optimistic and motivated than before.

Several people answered questions I had about different methods I used or wanted to use, both in Berlin at the Campus Buch and in Paris at the Pitié-Salpétrière. Because of the tight networks on these campuses, there was always an expert at hand when problems appeared or when I wanted to try something new.

Acknowledgements

The confocal pictures taken within the MLP project were possible because I could use the microscopes of the Advanced Light Microscopy group from Anje Sporbert at the Max Delbrück Center for Molecular Medicine (MDC) in Berlin.

During my time at Campus Buch, I joined the regular lab meetings of the group of Michael Bader at the MDC, which included discussions about papers and projects. It was good for me to get to know many more people, it was interesting to learn about the difficulties to organize a big team and I am grateful that I could participate.

Andrea Stöhr from the group of Thomas Eschenhagen at the Universitätsklinikum Hamburg-Eppendorf welcomed me in Hamburg to teach me the generation of 3D cultures of isolated neonatal cardiomyocytes. She also introduced me to Ingke Braren who is group leader of the HEXT Vector Facility, which enabled me to realize the production of adeno-associated viruses.

Finally, there is my husband. Without his love and support, most of this would not have become reality.

Thank you all.

Declaration

I, Christine Schwartz, hereby declare that I have prepared this dissertation by myself and without any inappropriate support. All sources of information are properly referenced. The contents of this dissertation have not been presented to any other university.

Christine Schwartz

Berlin, May 4th 2016

1 Introduction

1.1 Potential Implications of Mechanotransduction Defects in Muscle Diseases

The human body is constantly confronted with various phyiscal stimuli. Some stimuli like heat, touch or sound are recognized by us consciously. The reaction of the whole body to the stimulus is what we generally understand as reaction on physical stimuli.
However, it is not only our body as a whole that reacts on physical stimuli. Every cell in the body analyzes its surroundings, translates the physical stimuli into biochemical signals and reacts accordingly. This process is called mechanotransduction. For example, muscle contractions lead to stretching of some cells and result in compression of others. Or, during cellular migration, the stiffness of the surrounding tissue is an indication if the cell has reached its final destination. For embryonic development and maintenance of a healthy tissue, for muscle contraction and homeostasis, it is important that every cell interprets those stimuli and reacts properly.

If the pathways of mechanotransduction are disturbed, diseases of different severeness may occur. In the next two chapters, I will introduce some cardiac and skeletal muscle diseases that are connected to defects in mechanotransduction. Development, regeneration, contraction and homeostasis of these tissues depend on the correct recognition of the physical surrounding of muscle cells. Thus muscles react sensitively to mechanotransductional defects.

1.1.1 Mechanotransductional Defects in Cardiomypathies

The European Society of Cardiology defines a cardiomyopathy as a myocardial disorder in which the heart muscle is structurally and functionally abnormal (Elliott *et al,* 2007). Importantly, a cardiac disease is only classified as a cardiomyopathy if the myocardial abnormality is not caused by coronary artery disease, hypertension, valvular disease or congenital heart diseases (Elliott *et al,* 2007). Many cardiomyopathies have monogenetic causes, but until today, not all patients know the mutations that cause their disease.
Many patients harboring a cardiomyopathy have no restrictions regarding their day-to-day life, while others are more affected. However, sudden cardiac death is a common problem that occurs without warning, not only in elderly but also young patients (Basso *et al,* 2000). Especially when the heart is demanded to work hard, for example during sports and military service, an undetected cardiac disorder may lead to sudden cardiac death (Holdsworth *et al,* 2015; Sharma *et al,* 2015b). Cardiac screening of athletes is

recommended, but it may be challenging to distinguish a trained heart from a mildly diseased one (Sharma *et al,* 2015a).

Cardiomyopathies are grouped in several subsets. With a prevalence of 1:500, Hypertrophic Cardiomyopathy (HCM) is the most common myocardial disorder that is genetically transmitted (Maron *et al,* 1995). Up to 25% of the patients develop a serious phenotype with heart failure, atrial fibrillation and sudden cardiac death (Enriquez and Goldman, 2014). One of the major characteristics of HCM is the left ventricular hypertrophy, which is a thickening of the ventricular walls (fig. 1). This is accompanied by a smaller heart chamber volume. At an ultrastructural level, common findings in the myocardium of affected patients include myocardial disarray and interstitial fibrosis. Several years after the initial diagnosis, some of the patients develop a cardiac dilation (Biagini *et al,* 2005). Then the heart is remodeled, the chamber volume increases, the ventricular walls become thinner and softer and cannot contract properly (fig. 1). This characterizes the transition to overt heart failure.
For many years, HCM has been considered to be a disease of the sarcomere, as HCM causing mutations were only found in sarcomeric proteins (Thierfelder *et al,* 1994). In most of the cases, cardiac myosin binding protein C and β-myosin heavy chain are mutated (Barry and Maron, 2013). Today, about 1 400 different HCM associated mutations have been identified in 73 genes (listed by Roma-Rodrigues and Fernandes, 2014). Some phenotypes are not mono-genetic but a result of double-heterozygous mutations, leading to different phenotypes within one family (Van Rijsingen *et al,* 2009). Moreover, only 50% of HCM patients receive a genetic diagnosis, indicating many unknown factors (Maron *et al,* 2012). As some of the mutations known today are localized in genes coding for non-sarcomeric proteins, the hypothesis that HCM is a disease of the sarcomere is chal-

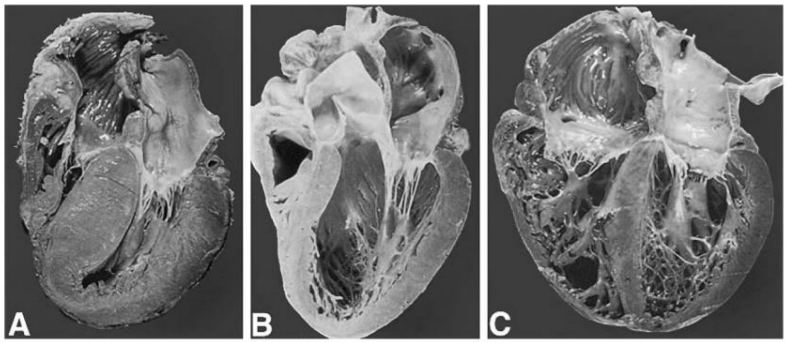

Figure 1: Cardiac Remodelling. Chamber volume and ventricular wall thickness change due to remodelling of the heart. In a hypertrophied heart (A), the ventricular walls are thicker and the chamber volume is reduced compared to a normal heart (B). During cardiac dilation, the ventricular walls become thinner while the chamber volume increases dramatically (C). If the cardiac remodelling results from a genetic mutation and is not acquired secondarily, physicians speak of hypertrophic or dilated cardiomyopathy, respectively. From Seidman and Seidman, 2001.

lenged. Many of the proteins mutated in patients with HCM are involved in pathways of mechanotransduction in cardiomyocytes, indicating the possibility that the disease is associated with defects in mechanotransduction (Lyon *et al,* 2015).
In the year 2003, Geier *et al* identified HCM causing mutations in the gene *CSRP3* (*cystein and glycine rich protein 3*). *CSRP3* is coding for Muscle LIM Protein (MLP), a striated muscle specific protein that is not exclusively found at the sarcomere but also in the cytoplasm and in the nucleus. Up to 1% of diagnosed patients with HCM have a mutation in *CSRP3* (Roma-Rodrigues and Fernandes, 2014). Interestingly, mutations of MLP are also associated with Dilated Cardiomyopathy (DCM).

The main characteristic of DCM is a left ventricular dilation, associated with systolic dysfunction (Elliott *et al,* 2007). Heart failure is one of the major complications of DCM. The prevalence of DCM increases with age and is rare in young children (McNally *et al,* 2013). In many cases, DCM is induced by viral infections, inflammation, drugs or toxins. DCM is also a complication that may develop during and after pregnancy (Tibazarwa *et al,* 2013). It is estimated that 25% to 50% of DCM patients have a familial DCM (Petretta *et al,* 2011). When the cause of the disease cannot be found, the patients are diagnosed with idiopathic DCM. Since genetic screening became more efficient and less cost intensive, many of the idiopathic DCM patients were found to be carrying mutations in various genes.
More than 40 different genes are associated with DCM (Spaendonck-Zwarts *et al,* 2013; Tesson *et al,* 2013). In a big cohort of index patients with idiopathic DCM, 25% were found to have a mutation in the sarcomeric protein titin (Herman *et al,* 2012). Other mutations that cause DCM are located in genes coding for proteins that localize at different parts of the sarcomere, costamere, and the nuclear envelope (McNally *et al,* 2013). Several of the genes found to trigger DCM were also mutated in patients with other cardiomyopathies. This raises the question how one mutation causes one or another form of cardiomyopathy. Many patients additionally suffer from muscular disorders, especially those harbouring mutations in the nuclear envelope proteins Nesprin, Emerin and A-type Lamins, that are part of or associated to the LINC complex (see chapter 1.2.3.5 on page 24*ff.*). Similar to HCM, many of the mutated genes in DCM are involved in mechanotransduction, indicating the importance of this mechanism in cardiac tissue diseases (Cook *et al,* 2014).

MLP contains two LIM domains and a nuclear localization sequence (fig. 2, Boateng *et al,* 2009; Schallus *et al,* 2009). The LIM domains are named after lin11, isl-1 and mec-3, homeodomain transcription factors of *Caenorhabditis elegans* and the rat, where the domains have firstly been described (Way and Chalfie, 1988; Freyd *et al,* 1990; Karlsson *et al,*

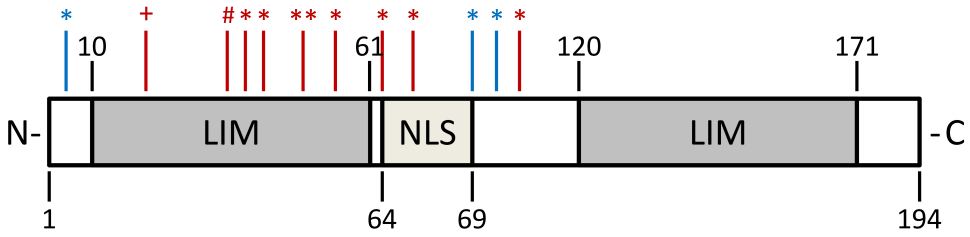

Figure 2: Protein Structure of MLP and its Mutations, Associated to Cardiomyopathies. Two LIM domains enclose the nuclear localization sequence (NLS) of MLP. Mutations that are associated with Hypertrophic Cardiomyopathy are indicated in red: (+) Y18QfsX194, (#) K42fsX165, (*) point mutations L44P, S46R, S54R/E55G, C58G, R64C, Y66C and Q91L. Mutations associated with Dilated Cardiomyopathy are indicated in blue: (*) point mutations W4R, K69R and G72R.

1990). A LIM domain forms two zinc fingers, binding one zinc ion each (fig. 3, Michelsen *et al,* 1993). They share the consensus sequence $[CX_2CX_{16\text{-}23}HX_2C]X_2[CX_2CX_{16\text{-}21}CX_2(C/H/D)]$ with X representing any aminoacid (Sadler *et al,* 1992).

At first, it has been suggested that the LIM domain was involved in protein-DNA interaction, because of its resemblance to GATA zinc fingers found in transcription factors (Sánchez-García and Rabbits, 1994). However, no LIM domain containing protein has been found that binds DNA by this domain. The LIM domain rather is involved in protein-protein interaction (Schmeichel and Beckerle, 1994). Proteins that contain one or several LIM domains have a multitude of interaction partners. This is also true for MLP (see chapter 1.2.3.3.1 on page 20). Because of their ability to function as scaffolding proteins, LIM domain containing proteins are involved in a variety of biological functions like carcinogenesis, cell lineage specification, axon guidance, muscle formation, and regulation of actin dynamics (Bach, 2000).

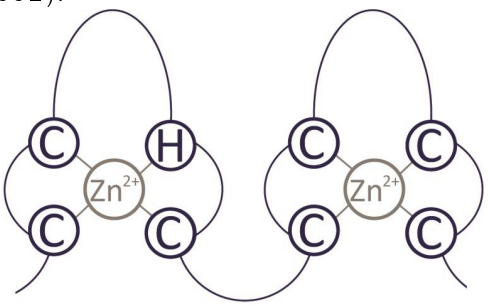

Figure 3: Schematic Representation of a LIM Domain. Cysteins (C) and histidins (H) of a LIM domain form two zinc fingers, binding two zinc ions (Zn^{2+}). Note that the last C can also be a histidine (H) or aspartic acid (D).

Until today, 12 mutations of MLP are known to cause either DCM or HCM (fig 2). Geier *et al* were first to describe mutations of MLP linked to HCM. They found three mutations (L44P, S54R/E55G and C58G) of MLP, all of them localized in the second zinc finger of the N-terminal LIM domain (Geier *et al,* 2003). Further studies revealed that MLP with the mutation C58G has a reduced interaction with α-actinin and N-RAP (Geier *et al,* 2003; Gehmlich *et al,* 2004). Additionally, this mutation prevents the formation of this second zinc finger (Gehmlich *et al,* 2004). Other mutations of MLP causing HCM are S46R, R64C, Y66C, Q91L and a frameshift mutation K42fsX165 (Bos *et al,* 2006;

Geier *et al,* 2008). An insertion of some bases into the gene after the codon for the 18th aminoacid completely changes the sequence of the following aminoacids (Y18QfsX194, Van Rijsingen *et al,* 2009). A double mutation of this insertion with a point mutation in the gene coding for myosin heavy chain results in a phenotype much worse than the single mutations (Van Rijsingen *et al,* 2009).

Three mutations were published to be the cause of DCM: W4R, K69R and G72R (Knöll *et al,* 2002; Mohapatra *et al,* 2003; Hershberger *et al,* 2008). The W4R mutation reduces the interaction of MLP with telethonin, another sarcomeric protein (Knöll *et al,* 2002). Mice lacking wildtype MLP but expressing W4R-MLP develop a phenotype similar to HCM in human (Knöll *et al,* 2010). And yet, it is not clear if this mutation is the sole cause for the cardiac disease, as the W4R mutation was found not only in patients with DCM, but also in HCM cohorts, in a patient with myocardial noncompaction, in control groups as well as not segregating with the disease (Mohapatra *et al,* 2003; Newman *et al,* 2005; Bos *et al,* 2006; Geier *et al,* 2008; Schweizer *et al,* 2014). Similar doubts are present for the K69R mutation (Mohapatra *et al,* 2003): MLP with this mutation has a reduced interaction with α-actinin-2, but the history of the studied family is not clear: two affected children share the mutation with an unaffected mother but not with the unaffected father. Both examples show that it is not always easy to find the right cause for a disease, as multiple influences may exist.

Different cardiomyopathy causing mutations of MLP are focus of study in the first part of this thesis (chapter 2).

1.1.2 Muscular Dystrophies Related to Mutations of Lamin and Nesprin Proteins

Muscular dystrophies are a heterogenous group of diseases that are characterized by progressive muscle weakness. They affect different parts of skeletal muscle to a various degree (fig. 4). Joint contractures, scoliosis and respiratory impairment are additional phenotypes. Heart and brain may also be affected. The age of onset of the disease (congenital, early childhood, adulthood), affected muscles, additional phenotypes, severety and progression of the disease as well as the type of inheritance are valuable information for clinical diagnosis, which is supported by genetic diagnosis.

The first muscular dystrophy has been described 180 years ago (Conte and Gioja, 1836). Today, classification of muscular dystrophies separates more than ten different diseases (listed by Mercuri and Muntoni, 2013). This classification is complicated by the fact that mutations in different genes may lead to the same phenotype as they are involved in the same pathway, while allelic mutations lead to different phenotypes although the same gene is affected.

An example for allelic mutations are mutations in the *LMNA* gene, coding for proteins Lamin A and Lamin C (A-type lamins or Lamin A/C). Mutations of *LMNA* not only lead to both autosomal dominant and recessive Emery-Dreifuss muscular dystrophy, limb girdle muscular dystrophy or congenital muscular dystrophy (which is a heterogenous group of muscular dystrophies that share an onset at birth) (Bonne *et al,* 1999; Barletta *et al,* 2000; Muchir *et al,* 2000; Quijano-Roy *et al,* 2008). Mutations in the *LMNA* gene can lead to a variety of diseases, commonly named laminopathies (Burke and Stewart, 2002; Worman and Bonne, 2007; Bertrand *et al,* 2011). Besides muscular dystrophies, mutations in *LMNA* are connected to cardiomyopathies, neuropathies, lipodystrophy and progeria (premature ageing syndrome) (Bertrand *et al,* 2011).
Lamin proteins are underlying the inner nuclear membrane, forming the nuclear lamina (see chapter 1.2.3.5.2 on page 28). They have multiple functions, for example they are working in the same way of mechanotransduction as Emerin and Sun proteins at the inner nuclear membrane and Nesprin proteins at the outer nuclear membrane (see chapter 1.2.3.5 on page 24). Thus, mutations in these proteins can lead to similar phenotypes.
Emerin was the first protein associated to X-linked Emery-Dreifuss muscular dystrophy (Bione *et al,* 1994). Mutations in the genes coding for Nesprin-1 and Nesprin-2 are causing this muscular dystrophy as well, in an autosomal-dominant way of inheritance (Zhang *et al,* 2007a). Additionally, a homozygous nonsense mutation in the gene coding for Nesprin-1 leads to congenital muscular dystrophy associated with adducted thumbs and mental retardation (Voit *et al,* 2002; Voit *et al,* 2007). A heterozygous mutation in the gene coding for Sun-1 is not disease-causing by itself, but worsens the phenotype of EDMD caused by a mutation of Emerin (Li *et al,* 2014).
Defects in mechanotransduction of myoblasts isolated from patients with congenital muscular dystrophy harboring mutations expressing a truncated Nesprin-1 (Nesprin1-ΔKASH) or A-type lamins missing one amino acid (LMNA-ΔK32) are subject of study in the second part of this thesis (chapter 3).

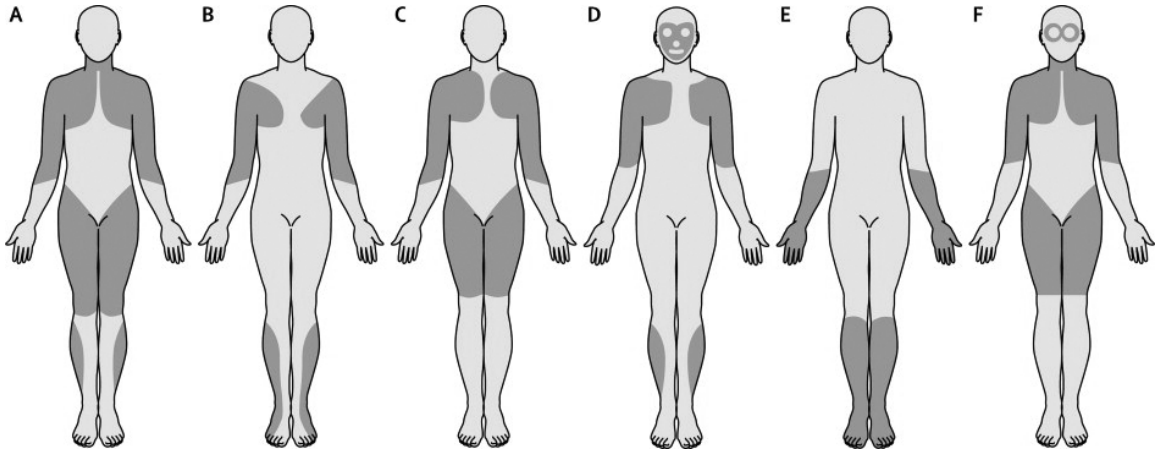

Figure 4: Pattern of Affected Muscles in Muscular Dystrophy. Dark parts represent muscle weekness. The pattern of affected muscle is a first indication about the type of muscular dystrophy. A: Duchenne and Becker muscular dystrophy. B: Emery-Dreifuss muscular dystrophy. C: Limb girdle muscular dystrophy. D: Facioscapulohumeral muscular dystrophy. E: Distal muscular dystrophy. F: Oulopharyngeal muscular dystrophy. From Mercuri and Muntoni, 2013.

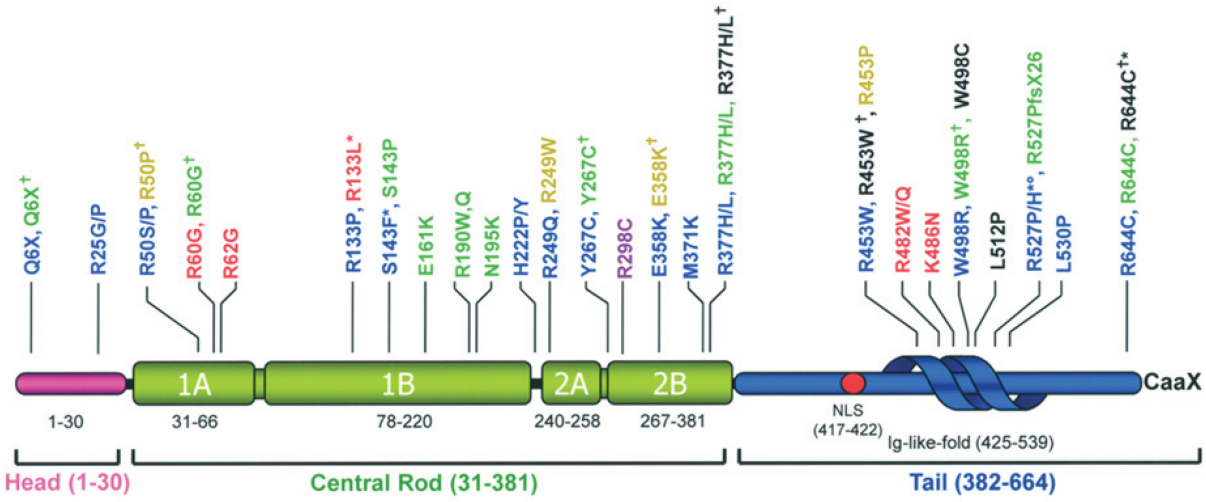

Figure 5: Domain Structure of Lamin-A, Mutations and Associated Laminopathies. A-type lamins consist of a head domain, a central rod domain and a tail domain. Different mutations lead to varying diseases: Emery-Dreifuss muscular dystrophy (blue), DCM (green), Limb girdle muscular dystrophy (black), , congenital muscular dystrophy (gold), familial partial lipodystrophy (red) and Charcot-Marie-Tooth disease (plum). '†' indicates that this aminoacid exchange causes other laminopathies as well. From Scharner *et al*, 2010.

1.2 Mechanisms of Mechanotransduction

In the previous chapters, we have seen that defects in mechanotransduction can have a severe effect on the human body. In this chapter, I will introduce the mechanisms of mechanotransduction, explain some of the physical and intracellular stimuli and the cellular reaction and I will talk about molecules that are important for mechanotransduction in striated muscle cells and muscle precursor cells (myoblasts).

As described before, mechanotransduction is the translation of a physical stimulus into a biochemical signal. The physical stimulus is transferred from outside the cell towards the mechanosensor. The mechanosensor is a protein, a protein complex or a cell organell within the cell or cell membrane that translates the stimulus into a biochemical signal and thus initiates mechanoresponsive signalling pathways (Fedorchak *et al,* 2014). Ion channels as well as proteins that are part of the actin cytoskeleton, the sarcomere or focal adhesion complexes are mechanosensors (Martinac, 2014; Luo *et al,* 2013; Puchner *et al,* 2008; Kuo, 2014). Additionally, the nucleus itself is thought to be a giant mechanosensor, as proteins localized at the nuclear membrane are mechanosensitive as well (Guilluy *et al,* 2014).
The biochemical signal can be a protein shuttling from cytoplasm to the nucleus, an intracellular calcium level increase or the starting of a phosphorylation cascade (Sharili and Connelly, 2014; Ruwhof *et al,* 2001). Ultimately, the biochemical signal results in an adaptation of the cell that depends on the physical stimulus.

1.2.1 Mechanical Forces Are Physical Stimuli

Cells are confronted with various physical stimuli, depending on their localization. Physical stimuli are mechanical forces like shear, compression and tension or stretch (fig. 6). If these forces act on an object, it is deformed. Stretch leads to elongation, shear may deform a square to a rhomb, and compression, the opposite of stretch, compresses the object. The deformation depends on the properties of the object, on how much it resists the force. Tensile strenght works against stretch, while compressive strength and shear strength oppose compression and shear forces. However, if the applied forces are too strong, the object might deform irreversibly or break.
Inside the body, these forces act on all cells. Mechanotransduction is the mechanism for a cell to understand these forces and to react accordingly, to adapt to a changing environment and to prevent irreversible damage. For example, muscle cells are repeatedly stretched and compressed, endothelial cells are exposed to shear stress because of blood flow. Contractile tension occurs if a cell is attached to a surface and tries to contract. The stiffer the surface, the higher are the forces the cell has to fight against to perform

the movement. Internal forces like tensions in the cytoskeleton are stimuli as well.

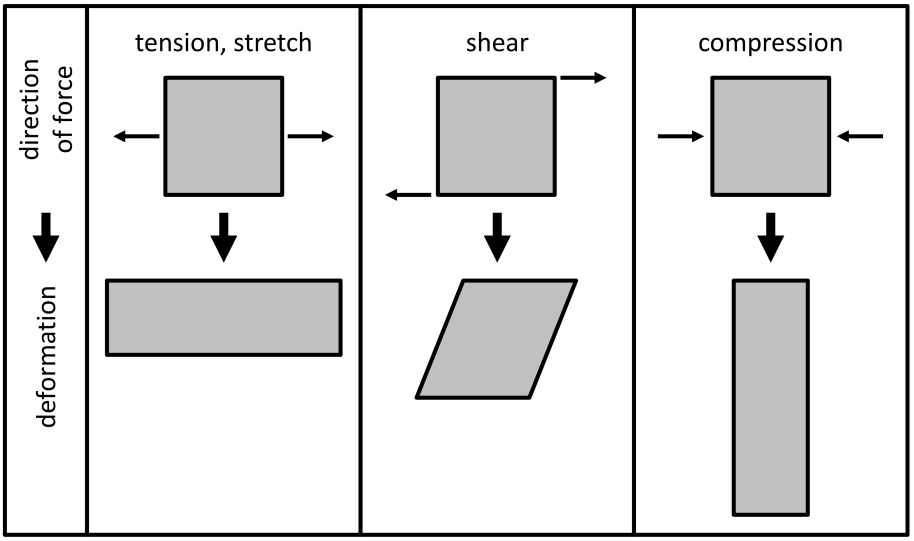

Figure 6: Mechanical Forces and Their Effects. The direction of force influences the deformation of an object. Tension, also named stretch, pulls on the object, thereby elongating it. Shear force also applies tension, but on different parts of the object, leading to sliding of its parts. Compression is the opposite of stretch. Cells developed technics to reduce the deformation.

1.2.2 Tension: Stretch and Surface Stiffness

Stretch has en effect both on cellular and on organ level. In the heart, intensified stretch of the cardiac muscle due to increased influx of blood into one of the ventricles leads to stronger contractions (Frank-Starling mechanism: Starling, 1918). This may lead to cardiac hypertrophy (fig. 1 A). Over-stretching of isolated papillary muscles induces a reduction in sarcomeric length and an increase of apoptosis (Cheng *et al,* 1995).
At single-cell level, cyclic stretch triggers nuclear rotation in fibroblasts and enhances proliferation, while reducing differentiation of C2C12 cells (Kook *et al,* 2008; Brosig *et al,* 2010). Isolated neonatal rat cardiomyocytes orient themselves to the direction of cyclic stretch, but different angles have been reported (Salameh *et al,* 2010; Dhein *et al,* 2014). Furthermore, stretch leads to hypertrophy of isolated cardiomyoctyes: increased cell size, enhanced sarcomerogenesis and the expression of a „hypertrophic gene program“ (upregulation of natriuretic peptides *ANP* and *BNP*, of β-*myosin heavy chain* and *skeletal* α-*actinin*) (Chien *et al,* 1991; Dorn *et al,* 2003; Frank *et al,* 2008).

Cells have to deal with contractile tension when they are in contact with stiff extracellular matrix. Fibroblasts actively probe the substrate rigidity with filopodia extensions before occupying an area (Wong *et al,* 2014). During cell migration, they prefer stiffer substrates over softer ones (Lo *et al,* 2000). On stiff surfaces, fibroblasts display reduced cell migration, which corresponds with a longer contact time between focal adhesions and the stiff surface (Fusco *et al,* 2015).

The stiffness of the matrix surrounding mesenchymal stem cells influences the differentiation of these cells (Engler *et al,* 2006): When cultured on matrix with a stiffness similar to brain tissue (very soft, 1 kPa), the differentiating cells express neurogenic markers and develop a branched morphology, similar to primary neurons. If the matrix has a stiffness similar to striated muscle (soft, 8 kPa to 17 kPa), the cells express myogenic markers. On hard surfaces (25 kPa to 40 kPa), differentiating mesenchymal stem cells express osteogenic markers and have a morphology similar to osteoblasts. This finding highlights the importance of cells to perform proper mechanotransduction during differentiation and development.

Differentiation of myoblasts also depends on matrix stiffness. Both too soft and too hard environments prevent the development of a striated pattern of fused myotubes (Engler *et al,* 2004). Similar phenotypes were found for neonatal cardiomyocytes (Engler *et al,* 2008; Jacot *et al,* 2008). In those cells, striation and autocontractions developed best when the cells were cultured on plates with a stiffness similar to that of cardiac tissue, in contrast to harder plates resembling fibrotic scars, or softer culture conditions.

In some experimental setups, the spreading area of cells also varies with the stiffness of the surface, with smaller spreading areas on softer matrices (Engler *et al,* 2004; Bertrand *et al,* 2014; Fusco *et al,* 2015). However, surface stiffness does not seem to generally influence the spreading area (Jacot *et al,* 2008; Fusco *et al,* 2015).

The different adaptations of different cell types to substrate stiffness are summarized in table 1.

Table 1: Adaptation to Differences in Stiffness of the Matrix. The elastic modulus of the surface is given in kPa. Abbreviations: CMC: cardiomyocyte, FA: focal adhesion, MSC: mesenchymal stem cell.

Stiffness	**Cell Type**	**Phenotype**	**Literature**
very soft matrix (1 kPa)	C2C12	elongation takes more time for <8 kPa, myosin striation: no	Engler *et al,* 2004
	chicken embryonal CMCs	approx. 60% striation	Engler *et al,* 2008
	rat neonatal CMC	hardly striated, no changes in spreading area	Jacot *et al,* 2008
	differentiating MSC	expression of neurogenic markers, branching	Engler *et al,* 2006
soft matrix (8-17 kPa)	C2C12	myosin striation at 8 and 11 kPa, but not at 17 kPa	Engler *et al,* 2004
	C2C12	optimal substrate stiffness: 12 kPa	Engler *et al,* 2004
	human myoblast	less cell spreading than on glass	Bertrand *et al,* 2014
	chicken embryonal CMCs	almost 100% striation	Engler *et al,* 2008
	rat neonatal CMC	well striated and aligned, no changes in spreading area, maximal force development	Jacot *et al,* 2008
	differentiating MSC	expression of myogenic markers	Engler *et al,* 2006
stiff matrix (25-50 kDa)	chicken embryonal CMCs	approx. 25% striation, slower contraction frequency, less cells contracting than on soft or very soft matrices	Engler *et al,* 2008
	rat neonatal CMC	stress fibers, unaligned striations, contraction only after stimulus with voltage	Jacot *et al,* 2008
	differentiating MSC	expression of osteogenic markers	Engler *et al,* 2006
glass	C2C12	cell area bigger the harder the matrix	Engler *et al,* 2004
	C2C12	myosin striation: no, but stress fibers + FA (vinculin)	Engler *et al,* 2004
	human myoblast	bigger cell area than on soft matrix	Bertrand *et al,* 2014

1.2.3 Important Players in Mechanotransduction

To translate a physical stimulus into a biochemical signal, several steps are needed, as discussed in the previous chapter. In the following part, proteins and protein complexes that are involved in mechanotransduction in striated muscle cells and myoblasts are presented. Fig. 7 summarizes two mechanisms used in mechanotransduction: direct force transmission from cell membrane to the nuclear envelope and translocation of proteins from cytoplasm to into the nucleus.

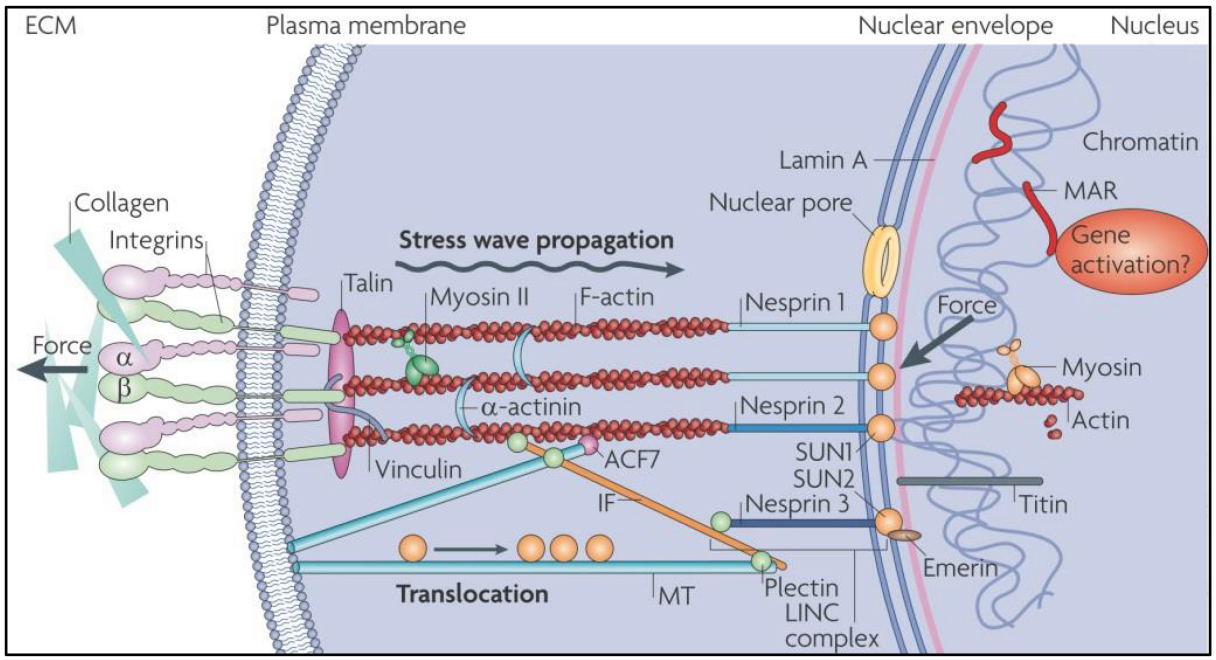

Figure 7: Mechanotransduction from the Extracellular Matrix to the Nucleus. Integrins are transmembrane proteins that connect the extracellular matrix (ECM) with the interior of the cell. Together with Talin, Vinculin and many more proteins, they form the multiprotein complex named focal adhesions. Focal adhesions are connected to the actin cytoskeleton. Mechanical forces can be transmitted directly towards the LINC complex that is situated at the nuclear envelope. The LINC complex contains Nesprin and Sun proteins, spans the nuclear envelope and connects the cytoskeleton with the nucleoskeleton. LINC complex associated proteins Lamin and Emerin are found directly below the nuclear envelope. The nuclear envelope with the LINC complex, Lamin and Emerin forms a huge mechanosensor. Alternatively, mechanotransductive signalling can occur via translocation of proteins from the cytoplasm to the nucleus. From Wang *et al,* 2009.

1.2.3.1 The Cytoskeleton: Actin Fibers

Actin fibers, also known as F-actin, are products of polymerization of monomeric G-actin. G-actin are small proteins with a molecular weight of 42 kDa. Cells maintain a pool of G-actin monomers (Pollard *et al,* 2000). G-actin either binds ATP (adenosine triphosphate) or ADP (adenosine diphosphate) (Straub and Feuer, 1950). For the generation of a new

actin fiber, ATP-G-actin self-associates to dimers and trimers during the nucleation phase. These complexes are kinetically unstable and dissociate easily, but they are stabilized by actin nucleation factors. Additional ATP-G-actin associates with the emerging fiber, thus elongating it, mainly at the barbed (plus) end. Within the fiber, the ATP gets hydrolyzed to ADP (Straub and Feuer, 1950). At the pointed (minus) end of the fiber, disassembly of the actin fiber occurs, refreshing the stock of monomeric ADP-G-actin. Although association and disassociation can occur at both ends of the actin fiber, this is not favoured by the various proteins orchestrating the actin dynamics.

Profilin and β-thymosins are the main G-actin binding proteins in vertebrates, with which they form 1:1 complexes (Carlsson *et al,* 1977; Safer *et al,* 1991; Schutt *et al,* 1993; Xue and Robinson, 2013). They are competing for overlapping binding sites of the actin monomer (Safer *et al,* 1997). It has also been reported that profilin, thymosin-β4 and G-actin form a ternary complex, but its function is not known (Yarmola *et al,* 2001; Xue *et al,* 2014). Thymosin-β4 sequesters G-actin molecules and thereby prevents not only their nucleation but also their integration into actin fibers (Yu *et al,* 1993). Profilin also prevents self-association of G-actin, and the binding of G-actin to the pointed end of an existing actin fiber (Pollard and Cooper, 1984). However, it accelerates the ADP to ATP exchange of G-actin and promotes the integration of the monomer into the barbed end of an actin fiber, which is mediated by formins (Pring *et al,* 1992; Selden *et al,* 1999; Kovar and Pollard, 2004). After the integration of the monomer, profilin is released from the filament and free to bind another G-actin (Tilney *et al,* 1983).

The nucleation inhibiting function of profilin can be overruled by formin proteins (Li and Higgs, 2003). After nucleation, the formin protein remains at the barbed end of the developing actin fiber (Pruyne *et al,* 2002). Profilin-G-actin complexes are recruited to the barbed end of the actin filament by formin binding to profilin (Imamura *et al,* 1997; Sagot *et al,* 2002; Kovar *et al,* 2003; Pring *et al,* 2003). Additionally, formin proteins promote the elongation of actin fibers by blocking the barbed end from capping proteins that inhibit the elongation, a process known as *processive capping* (Pruyne *et al,* 2002; Zigmond *et al,* 2003; Bombardier *et al,* 2015; Shekhar *et al,* 2015).
In mammals, 15 genes are coding for formin proteins that are recognized by their FH1 and FH2 domains that bind profilin and mediate actin assembly, respectively (Higgs and Peterson, 2005; Goode and Eck, 2007). The elongation of an actin fiber is orchestrated in a linear way by formins (Kovar and Pollard, 2004).
Some formin proteins have additional functions like bundling, severing or depolymerization of actin (Harris *et al,* 2004; Moseley and Goode, 2005; Chhabra and Higgs, 2006; Harris *et al,* 2006). For example, the Formin Homology Domain Protein 1 (FHOD1) is

not involved in actin fiber elongation but has a capping function and bundles existing actin fibers, thereby stabilizing them (Schönichen *et al,* 2013). Furthermore, FHOD1 is involved in formation of stress fibers, which are contractile actin fiber bundles characterized by the presence of Non-muscle Myosin IIa (NMMIIa, see chapter 1.2.3.2.3) (Gasteier *et al,* 2003; Takeya *et al,* 2008).

Another protein complex mediating the nucleation of actin is the arp2/3 complex. Arp2/3 was the first actin nucleating factor identified (Goley and Welch, 2006). In contrast to formins that can create actin filaments *de novo*, the arp2/3 complex adds a new branch of actin to an existing actin filament at an angle of 70° (Mullins *et al,* 1998; Amann and Pollard, 2001). By mimicking the barbed end of actin fibers, arp2/3 provides a starting point for further actin fiber elongation (Robinson *et al,* 2001; Nolen *et al,* 2004). The arp2/3 complex needs nucleation promoting factors for activation (Goley and Welch, 2006).

Vinculin is part of focal adhesions. It has the ability to nucleate actin and to initiate the generation of new actin fibers (Wen *et al,* 2009). Furthermore, vinculin bundles existing actin fibers (Wen *et al,* 2009). It also recruits the arp2/3 complex to the focal adhesion sites (DeMali *et al,* 2002; Moese *et al,* 2007). Thus, vinculin connects the emerging actin cytoskeleton with focal adhesions. Vinculin and focal adhesions are discussed in more detail in chapter 1.2.3.4 on page 23.

Capping proteins bind the barbed end of actin fibers and prevent their elongation, thereby antagonizing formin proteins (Bombardier *et al,* 2015). A variety of proteins with capping activity have been identified, with a protein suitably named capping protein (also known as β-actin and CapZ) beeing the most abundant one (Maruyama *et al,* 1977; Isenberg *et al,* 1980; Edwards *et al,* 2014). By preventing the elongation of actin filaments, they are an important factor for actin regulation. For example, together with arp2/3, they produce nets of actin filaments with short branches, which is important in cell movement (Miyoshi *et al,* 2006; Akin and Mullins, 2008; Edwards *et al,* 2014).

1.2.3.2 Force Generating Players

Some of the players in mechanotransduction not only receive and process the information about a physical stimulus. Both the sarcomere of striated muscle cells and actin stress fibers of other cell types not only have important functions in mechanotransduction, but can actively generate tension themselves.

1.2.3.2.1 The Sarcomere

In striated muscle, which means skeletal and cardiac muscle, the sarcomere is the elementary force-generating unit. According to the sliding filament theory, thick and thin filaments of the sarcomere slide over each other and thus generate muscle force (Huxley and Niedergerke, 1954; Huxley and Hanson, 1954). In electron microscopic pictures from the sarcomere, the different structures of the sarcomere are clearly distinguishable (fig. 8). The thick filament is mainly composed of myosin, while actin is the main component of the thin filament. α-actinin is the main crosslinker of actin fibers in the Z-line, but a variety of other proteins are found there as well (Blanchard *et al,* 1989; Knöll *et al,* 2011; Burgoyne *et al,* 2015).

Titin forms a third subset of filaments of the sarcomere (Wang *et al,* 1979). With a molecular weight of up to 4 MDa, it is the biggest protein known (Bang *et al,* 2001). The N-terminal region is bound to the sarcomeric Z-line, while the C-terminus is fixed in the M-line. Thus, one titin protein spans half a sarcomere.

When the sarcomere is stretched, a passive force is generated to oppose this stretch. Titin

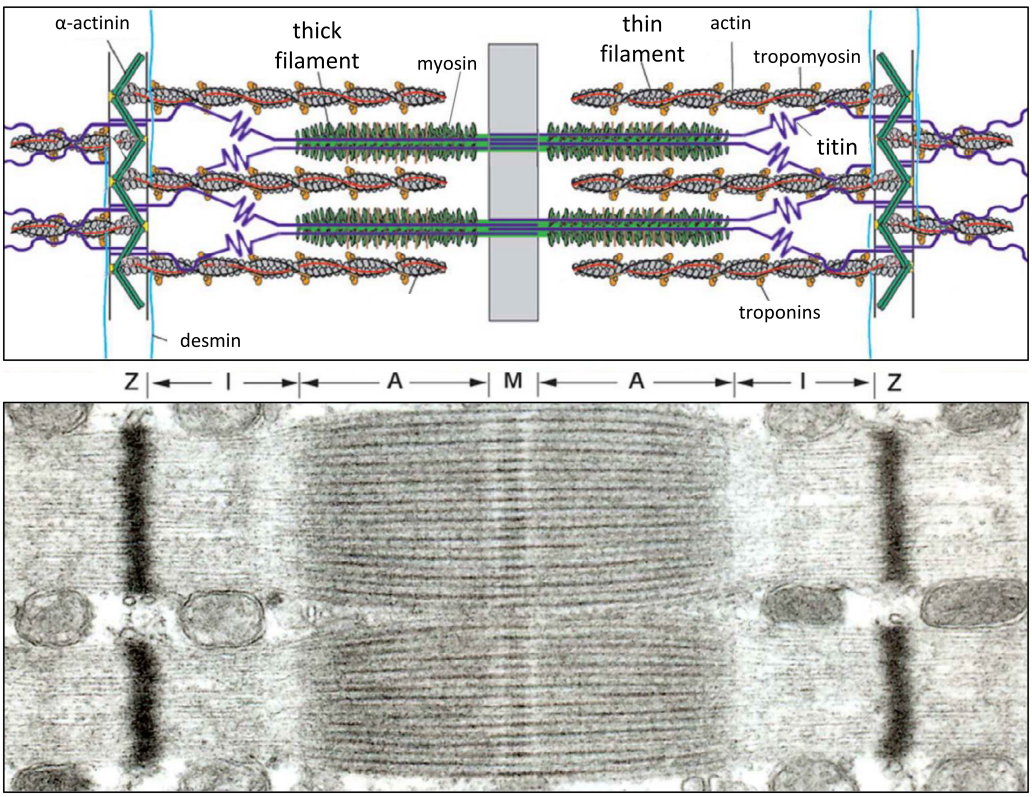

Figure 8: The Sarcomere. A simplified model of the sarcomere is depicted on top. In the Z-line, α-actinin crosslinks the thin filaments that are mainly composed of actin. Thick filaments mainly contain myosin. Titin filaments spans from the Z-disk to the M-line. In the bottom, the different bands are clearly distinguishable in the electron microscopic picture. From Ottenheijm *et al,* 2008.

is known to be an elastic protein and one of the main causes for passive force development (Maruyama *et al,* 1976; Granzier and Irving, 1995). The elastic part of titin is located in the I- and A-band of the sarcomere (Trombitás *et al,* 1995). Upon stretch of the sarcomere, its elastic parts unfold, and re-fold once the stretch is released (Minajeva *et al,* 2001). Titin also functions as a mechanosensor: When stretched, a serine/threonine protein kinase domain of titin, localized in the M-band, gets activated (Puchner *et al,* 2008). This subsequently changes gene expression and protein turnover (Lange *et al,* 2005).

Muscle LIM protein (MLP) is a small stiated muscle specific protein that localizes to the Z-disk of the sarcomere. However, it is not tightly fixed in this position but also found interacting with proteins at the costameres, the actin cytoskeleton and the intercalated disk of cardiomyocytes (Louis *et al,* 1997; Flick and Konieczny, 2000; Gehmlich *et al,* 2004; Geier *et al,* 2008). Furthermore, MLP localizes to the nucleus during development, chronic cardiac pressure overload and after stretching of isolated cardiomyocytes (Arber *et al,* 1994; Ecarnot-Laubriet *et al,* 2000; Boateng *et al,* 2009). MLP was thought to be a stretch-sensor (Knöll *et al,* 2002), but because of its structure and as it is not tightly fixed at the sarcomere, it is more likely that the protein is part of the mechanotransduction pathway in cardiomyocytes (Gehmlich *et al,* 2010).

Telethonin, also known as T-cap, connects two titin molecules that the same half of the sarcomere in the Z-disk (Zou *et al,* 2006). However, it does not seem to be necessary for a proper fixation of titin at the Z-disk, as telethonin-KO mice display no phenotype under basal conditions at an age of four month (Knöll *et al,* 2011). Only after pressure overload, these mice have an elevated level of apoptosis and develop heart failure (Knöll *et al,* 2011).
As telethonin interacts with MLP, telethonin was also thought to be part of the stretch-sensing pathway in cardiomyocytes (Knöll *et al,* 2002; Knöll *et al,* 2010). However, others doubt this hypothesis: As the interaction between telethonin and titin is one of the strongest known, it is unlikely that the MLP-telethonin-titin complex is part of a stretch sensor (Bertz *et al,* 2009).

1.2.3.2.2 Actin Stress Fibers

More than 100 years ago, stress fiber-like cytoplasmic fibers were described in intestine epithelial cells (Heidenhain, 1899). At first, they were disposed as fixation artifacts, as they were not seen in other tissue samples (Burridge and Wittchen, 2013). But when cells are cultivated on stiff plastic or glass, they also develop stress fibers (Lewis and Lewis,

1924). Now we know that actin stress fibers are long, contractile protein complexes mainly composed of actin and an ATPase named non-muscle myosin (Perdue, 1973; Weber and Groeschel-Stewart, 1974; Isenberg *et al,* 1976; Kreis and Birchmeier, 1980). They are bundles of 10 to 30 actin fibers with alternating orientation of barbed and pointed ends (Cramer *et al,* 1997). The actin filaments in stress fibers are cross-linked by α-actinin (Lazarides and Burridge, 1975). Because of the non-muscle myosin content and the alternated orientation of actin fibers, stress fibers are contractile and thus have the ability to generate tension within the cell (Kreis and Birchmeier, 1980; Harris *et al,* 1981; Katoh *et al,* 1998).

Four different types of stress fibers have been found in metazoan cells (fig. 9): transverse arcs, dorsal and ventral stress fibers and the perinuclear actin cap (Soranno and Bell, 1982; Small *et al,* 1998; Khatau *et al,* 2009). They are classified by the number of focal adhesions they are bound to: transverse arcs are not connected to focal adhesions, dorsal stress fibers interact with them on one end and both ventral stress fibers and the perinuclear actin cap interact on both ends with focal adhesions (Heath and Dunn, 1978; Heath, 1983; Burridge, 1986; Khatau *et al,* 2009). Furthermore, the perinuclear actin cap is connected to the nucleus by the LINC complex (Khatau *et al,* 2009). Fibers of the

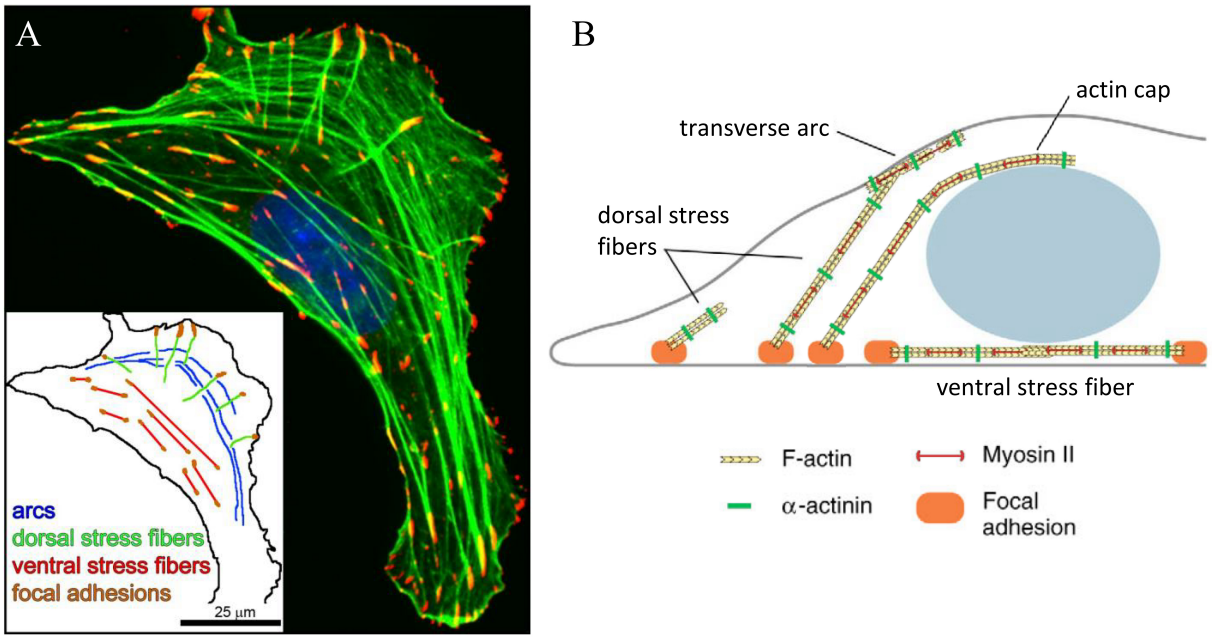

Figure 9: Four Types of Stress Fibers. Stress fibers are composed of actin and nonmuscle myosin and are crosslinked by α-actinin. In contrast to transverse arcs, ventral and dorsal stress fibers as well as stress fibers of the perinuclear actin cap are connected to focal adhesions. A: A fluorescent microscopic image visualizes actin fibers in green, focal adhesions in red and the nucleus in blue, seen from top. The inlay clarifies the localization of the three different stress fiber types found in this cell. From Burridge and Wittchen, 2013. B: In this graphic, the localization of the different stress fiber types is depicted, seen from the side. After Pellegrin and Mellor, 2007 and Khatau *et al,* 2009.

actin cap are not only involved in shaping the nucleus, they also control nuclear rotation and orientation and thus have an effect on cell migration (Khatau *et al,* 2009; Kim *et al,* 2014; Tamiello *et al,* 2015). Compared to the other stress fiber types, actin cap fibers have a higher turnover rate (Kim *et al,* 2012).
Stress fibers of all types interact directly with each other to form a network throughout the cell (Hotulainen and Lappalainen, 2006). Dorsal stress fibers and transverse arcs can transform to ventral stress fibers (Hotulainen and Lappalainen, 2006).

1.2.3.2.3 Inhibition of Stress Fiber Formation Signalling

Stress fiber formation and contractility depend on the activity of non-muscle Myosin IIa (NMMIIa): Both a knock-down by siRNA as well as inhibition of the myosin ATPase activity by blebbistatin reduce stress fibers in isolated cells (Cai *et al,* 2006; Goeckeler *et al,* 2008). Blebbistatin is a small compound specifically inhibiting many members of the myosin II family, including NMMIIa, by affecting the ATPase function of the protein (Straight *et al,* 2003; Limouze *et al,* 2004).

A reduced amount of stress fibers can also be found when cells are treated with Y27632 (Uehata *et al,* 1997). Y27632 is a synthetic compound that competes with ATP for binding to the ATP binding pocket of rho-associated coiled-coil forming protein serine/threonine kinases (ROCK), thereby inhibiting their kinase function (Uehata *et al,* 1997; Ishizaki *et al,* 2000; Jacobs *et al,* 2006). Fibroblasts that were treated with this inhibitor of ROCK proteins lost their stress fibers, although only the central ones, while peripheral stress fibers were still present (Katoh *et al,* 2001). Besides other functions in the cell, ROCK regulate stress fiber formation (Leung *et al,* 1996). They either directly phosphorylate the myosin regulatory light chain or inhibit myosin phosphatase (Amano *et al,* 1996; Kimura *et al,* 1996). Both phosphorylation reactions increase the phosphorylation level of myosin light chain, leading to an activation of myosin and subsequently increasing actin cross-linking by moysin (Narumiya *et al,* 2009).

ROCK are activated by RhoA via phosphorylation (Leung *et al,* 1995). Consequently, injection of constitutivly active Rho into fibroblasts leads to stress fiber development, while RhoA inhibition reduces stress fibers (Paterson *et al,* 1990; Goldyn *et al,* 2009). Furthermore, RhoA activity increases when static force is applied to the cells in an integrin-dependant way (Guilluy *et al,* 2011).

A variety of activators has been found upstream of RhoA. G-protein coupled receptors, stretch and SRC (from the word SaRComa) kinases are involved in RhoA activation (Zhao

et al, 2007; Schramp *et al,* 2008; Yu and Brown, 2015). The small compound SU6656 inhibits SRC kinases and was used to study the function of the SRC kinase family (Blake *et al,* 2000). SRC kinases have been reported to both activate and inhibit RhoA activity or to have no effect on the kinase (Arthur *et al,* 2000; Knock *et al,* 2008; Schramp *et al,* 2008; Cicha *et al,* 2014; Takito *et al,* 2015). The effect of ROCK inhibitor Y27632 and SRC kinase inhibitor SU6656 are identical and if both inhibitors are combined, the effect does not get stronger, showing that the inhibitors function in the same pathway (Knock *et al,* 2008).

Stress fibers in the cell periphery that have not been affected by ROCK inhibition are sensitive towards treatment with ML7, an inhibitor of myosin light chain kinase (MLC kinase) (Katoh *et al,* 2001). Both MLC kinase and ROCK phosphorylate NMMIIa at the same serine residue (Katoh *et al,* 2001).

Besides NMMIIa, ROCK has other targets for phosphorylation. FHOD1 (Formin Homology 2 Domain Containing Protein 1, see chapter 1.2.3.1 on page 13) is one of them. Usually present in an autoinhibited conformation, FHOD1 gets activated via phosphorylation by ROCK in a SRC-dependant manner (Gasteier *et al,* 2003; Koka *et al,* 2003; Hannemann *et al,* 2008; Takeya *et al,* 2008; Schönichen *et al,* 2013). Constitutively active FHOD1 leads to thicker actin fiber bundles and more stress fibers (Gasteier *et al,* 2003; Takeya *et al,* 2008).

Taken together, actin stress fibers are formed upon different cell signalling cascades. NMMIIa and FHOD1 are important targets downstream in these cascades (fig. 10).

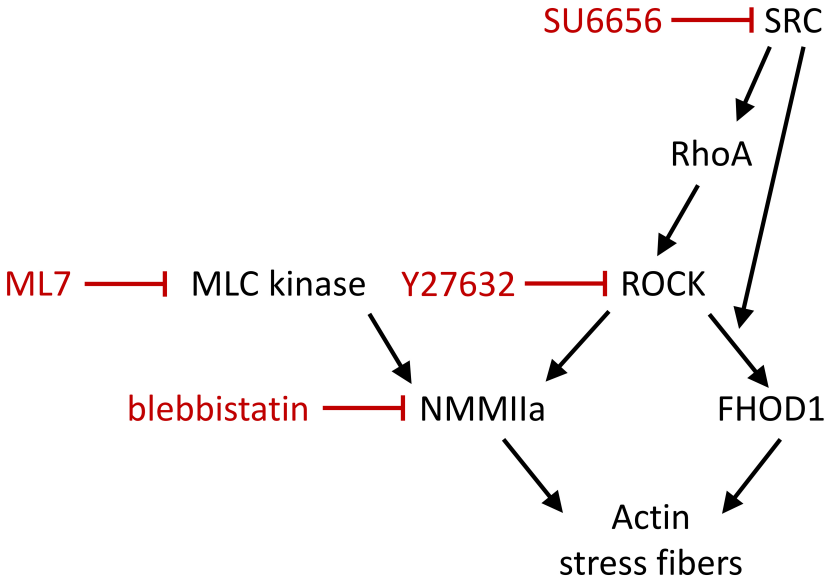

Figure 10: Pathways of Stress Fiber Formation. Formation of stress fibers depends on the activity of NMMIIa and FHOD1. NMMIIa can be activated both by MLC kinase and ROCK. RhoA and SRC are found upstream of ROCK. ROCK also activates the formin FHOD1. This activation is mediated by SRC. Compounds for inhibition of the proteins at different levels are indicated in red.

1.2.3.3 Muscle LIM Protein (MLP)

Muscle LIM Protein (MLP) is a small evolutionary conserved protein, mainly found in striated muscle cells (Arber *et al,* 1994; Levin *et al,* 2014). As presented in this chapter, the overall function of MLP is not completely understood. By shuttling into the nucleus, MLP participates in mechanotransduction (Boateng *et al,* 2009).

1.2.3.3.1 A Short History of MLP

Muscle Lim Protein (MLP, also cystein and glycin-rich protein 3 or CRP3), encoded by the gene *CSRP3*, is a small protein with 194 amino acids. It contains two independantly functioning LIM domains, each followed by a small glycine-rich region, and a nuclear localization sequence (NLS) between the two LIM domains (fig. 2, Boateng *et al,* 2009; Schallus *et al,* 2009). MLP belongs to the CRP (cystein and glycin-rich protein) family. Its members share a high degree of evolutionary conservation in vertebrates, insects, protozoa and plants (Weiskirchen and Günther, 2003). This conservation indicates an important role of the protein family.
Although many groups studied MLP both *in vivo* and *in vitro* with various methods, its overall function is still not fully understood. Initially, MLP was found because of its expression in denervated skeletal muscle (Arber *et al,* 1994). Until today, it is reported to be a promotor of myogenesis, to be involved in calcium-signalling via calcineurin, to be a part in the stretch-sensing pathway and to have a function in actin bundling and stabilization (Arber *et al,* 1994; Knöll *et al,* 2002; Costa *et al,* 2007; Boateng *et al,* 2009; Hoffmann *et al,* 2014).
Human patients with chronic heart failure due to a cardiomyopathy have a 50% lower protein level of cardiac MLP, while mRNA level were normal (Zolk *et al,* 2000). Contrary to this finding, Boateng *et al* report an upregulation of MLP in human failing heart samples (Boateng *et al,* 2007). However, they do not further describe the patients, thus a direct comparison of the two publications is not possible. On the other hand, myocardiac infarction in mice and rat as well as aortic banding in rat lead to upregulation of MLP in cardiac tissue (Heineke *et al,* 2005; Wilding *et al,* 2006; Boateng *et al,* 2007). Nevertheless, all these publications indicate that MLP is affected by cardiac disease.

The LIM domain is a domain suited to bind a variety of proteins (Schmeichel and Beckerle, 1994). Thus it is not surprising that MLP serves as a backbone for protein-protein interaction of many proteins in different parts of the cell. MLP interacts with xyxin at the intercalated disk that connects two cardiomyocytes, with telethonin and α-actinin at the Z-disk of the sarcomere, with transcription factors MyoD, myogenin and MRF4 in the nucleus, and it recrutes calcineurin to the Z-disk (Kong *et al,* 1997; Louis *et al,* 1997;

Knöll *et al,* 2002; Heineke *et al,* 2005). Mutations of MLP induce both hypertrophic and dilated cardiomyopathy in humans (Geier *et al,* 2003; Mohapatra *et al,* 2003; Bos *et al,* 2006; Geier *et al,* 2008; Hershberger *et al,* 2008).

MLP was originally described to be a striated muscle specific protein, promoting myogenesis (Arber *et al,* 1994). The *CSRP3* gene is strongly expressed in the heart and shows a weak expression in adult skeletal muscle (Arber *et al,* 1994). No MLP mRNA was found in other tissues (Arber *et al,* 1994). However, new findings indicate that the protein is also present in retinal neurons during embryonic development (Levin *et al,* 2014). MLP was found in the cytoplasm and in the dendrites of these neurons, but not in the nucleus. Its function in these cells however is still unknown. In skeletal muscle, MLP is weakly expressed in muscles containing predominantly slow fibers like soleus and hardly detectable in *Tibialis anterior* which is built of fast muscle fibers (Schneider *et al,* 1999). It is upregulated in fast muscle fibers during fast-to-slow fiber transition (Willmann *et al,* 2001). However, mice lacking MLP have no changes regarding the fiber-type distribution, indicating that MLP is not necessary for slow fiber development (Barash *et al,* 2005). In the heart, MLP is constantly expressed in atrial and ventricular cardiomyocytes during embryonal development and in the adult (Zolk *et al,* 2000).

The role of MLP in mechanotransduction has been subject of some research. Initially, MLP deficient isolated neonatal cardiomyocytes were found not to adapt properly to stretch stimuli (Knöll *et al,* 2002). Later, it was discovered that MLP shuttled to the nucleus as a reaction to tension (Boateng *et al,* 2007): Both the increase of tension within the cardiac muscle of a mouse by aortic constriction as well as the stretching of isolated neonatal cardiomyocytes triggered the shuttling of MLP. When the translocation of MLP to the nucleus is inhibited, the cells fail to adapt to the cyclic stretch stimulus similar to MLP deficient cardiomyocytes (Boateng *et al,* 2009). Nevertheless, MyoD, myogenin and MRF4 are the only found nuclear interaction partners of MLP until today, and neither is expressed in the heart (Miner *et al,* 1992; Louis *et al,* 1997). Thus, the nuclear function of MLP in mechanotransduction remains elusive.

1.2.3.3.2 MLP in the Mouse Model

Mice with a functional knockout of *MLP* ($MLP^{-/-}$) were first described by Arber *et al,* 1997. The authors distinguished between an early and a late phenotype. 35% – 65% of all neonates displayed a severe hypertrophy of all four cardiac chambers within the first week after birth and died (Arber *et al,* 1997). Interestingly, the homozygous offspring of heterozygous crossings had a higher mortility rate than pups of homozygous mice.

The authors concluded that the genetic background modulated the difference in neonatal survival rates.
The hearts of neonates of our MLP$^{-/-}$ mice with a C57BL/6N background were hypertrophied and softer compared to those of wildtype mice, but we did not observe such a high morbidity rate, although we had offspring from the Arber-mice (see chapter 2.1.2.1 on page 39). The mice of other groups also lack the early phenotype (Heineke *et al,* 2010; Unsöld *et al,* 2012), encouraging the hypothesis about the influence of the genetic background.

The animals described by Arber *et al* without a severe early phenotype develop a late phenotype around the age of four weeks with cardiac hypertrophy and heart failure, resembling dilated cardiomyopathy in humans (Arber *et al,* 1997). Although force development and contractility of the heart are normal at this age, the level of B-type natriuretic peptide (BNP) is elevated (Unsöld *et al,* 2012). BNP is induced by stretch of the tissue and its expression correlates with the end-diastolic wall stress of the left ventricle (Tokola *et al,* 2001; Iwanaga *et al,* 2006). This shows that the hearts of the young MLP$^{-/-}$ mice are already altered.

Mice that are expressing a constitutivly active form of calcineurin develop cardiac hypertrophy and heart failure (Molkentin *et al,* 1998). If those mice are crossed with MLP$^{-/-}$ mice, they develop an even stronger cardiac hypertrophy, although they displayed an improved left ventricular function (Heineke *et al,* 2010). Interestingly, a mild inducible overexpression of calcineurin resulted in an improved cardiac function without the development of cardiac hypertrophy (Heineke *et al,* 2010).

Heterozygous mice (MLP$^{+/-}$) display no phenotype at baseline level (Heineke *et al,* 2005). However, there are some indications that these mice develop a phenotype when confronted with stress: After induction of myocardial infarction, heterozygous mice have a higher mortality rate and developed worse left ventricular ejection fraction and left ventricular dilation compared to wildtype mice, while the usual hypertrophic reaction of the cardiomyocytes was reduced (Heineke *et al,* 2005).

As MLP is upregulated after aortic banding and myocardial infarction, and to further understand the role of MLP in cardiac function, a mouse line overexpressing MLP was generated (Kuhn *et al,* 2012). Surprisingly, these mice were indistinguishable from WT litter mates, both at base line and after aortic constriction leading to cardiac pressure overload. As an overexpression of MLP rescues the phenotype of MLP$^{-/-}$ mice, the construct was functionally active. The authors conclude that MLP neither causes nor

modulates cardiac hypertrophy *in vivo* (Kuhn *et al,* 2012).

Taken together, MLP is a small striated muscle specific protein with various interaction partners. Mutations of MLP may cause different forms of cardiomyopathy, but the overall function of MLP remains unknown.

1.2.3.4 Focal Adhesions

Focal adhesions are multiprotein complexes that connect the cell with the adjacent extracellular matrix (fig. 11). More than 50 proteins are associated to focal adhesions and function as coactivators, inhibitors of activation or as scaffolding proteins (Geiger *et al,* 2001; Kuo, 2014). I will explain the function of some of them in this chapter.

As transmembrane proteins, integrins connect the cell with its surroundings. They were named integrins because of their integral membrane structure and their role in keeping the integrity of the link between the extracellular matrix and the cytoskeleton (Tamkun *et al,* 1986). Integrins are receptor proteins with a large extracellular and a small cytoplasmic part. Different α- and β-integrin subunits noncovalently form αβ-heterodimers in all metazoans. In mammals, 24 different heterodimers are created from a subset of 18 α and 8 β subunits which selectively bind to various ligands (Hynes, 2002). Ligands include

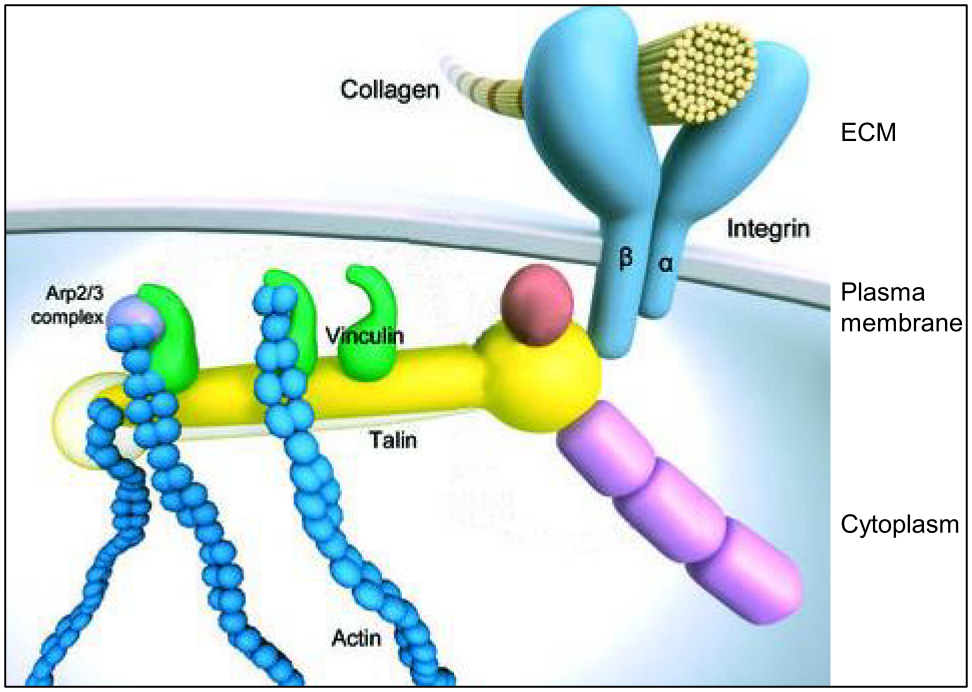

Figure 11: Simplyfied Model of a Focal Adhesion. Focal Adhesions are multiprotein complexes. In this figure, only some components are depicted, due to simplicity. The transmembrane proteins integrins connect the cell with the extracellular matrix. The interaction of talin with integrins activates the receptors. Vinculin recruits the arp2/3 complex to the focal adhesion and connects the protein complex with actin fibers. After Brakebusch and Fässler, 2003.

components of the extracellular matrix like fibronectin, laminin, fibrinogen and collagen as well as counter-receptors like cadherins (Flier and Sonnenberg, 2001; Humphries *et al,* 2006).
Integrins can signal bidirectionally: outside-in and inside-out. From inside the cell, integrins get activated. Several different pathways activate integrins, but they all have in common a final step, when talin binds to the intracellular part of the integrin β-subunit (Tadokoro *et al,* 2003; Bouaouina *et al,* 2012). The outer part of integrin subsequently undergoes a conformational change which enables the protein to bind its ligands (Iwamoto and Calderwood, 2015). Outside-in, several different pathways may be activated, leading to cell spreading, proliferation, mobility, cell survival or differentiation, depending on the cell type and the ligand (Shen *et al,* 2012; Hu and Luo, 2013).

Vinculin regulates the formation of focal adhesions, the activation of integrins and is a mechanical force transmitter by connecting talin to actin fibers (Humphries *et al,* 2007). Upon stretch of cells, vinculin is recruited to the adhesion complexes (Guilluy *et al,* 2011). As already presented in chapter 1.2.1, the size of focal adhesions corresponds to the stiffness of the surface of the cell culture plate with bigger focal adhesions on harder surfaces (Fusco *et al,* 2015).

1.2.3.5 The LINC Complex and Associated Proteins

The LINC complex is a multiprotein complex spanning the nuclear envelope. It directly connects the cytoskeleton with nuclear proteins. In this chapter, I will discuss the components of the LINC complex, its associated proteins localized at the inner nuclear envelope as well as their importance in muscle cells.

1.2.3.5.1 The LINC Complex

The LINC complex is the **Li**nker of **N**ucleus and **C**ytoplasm (Crisp *et al,* 2006). It is composed of members of two transmembrane protein families. SUN domain proteins at the inner nuclear membrane and KASH (Klarsicht/ANC-1/ homology) domain proteins spanning the outer nuclear membrane interact within the perinuclear space (fig. 12). This protein complex is evolutionary conserved, although the number of SUN and KASH domain proteins varies between different species (Kim *et al,* 2015). Three members of each protein family interact with each other in a promiscuit way, meaning that every KASH domain can interact with every SUN domain (Stewart-Hutchinson *et al,* 2008; Sosa *et al,* 2012).
One function of the LINC complex is to connect the nucleoskeleton with the cytoskeleton. It is involved in mechanotransduction, nuclear migration, positioning and anchoring,

telomere positioning and centrosome migration (Ding *et al,* 2007; Dawe *et al,* 2009; Lei *et al,* 2009; Méjat, 2010; Zhang *et al,* 2010; Guilluy *et al,* 2014).
Inside the nucleus, SUN domain proteins directly interact with proteins of the nuclear lamina, which are part of the nucleoskeleton, and emerin (Haque *et al,* 2006; Haque *et al,* 2010). Interestingly, while the localization at the nuclear envelope of SUN domain proteins depends on lamin proteins in some species (e.g. humans), their localization is independent from the nuclear lamina in other species (e.g. *Caenorhabditis elegans*) (Lee *et al,* 2002; Hasan *et al,* 2006). The localization of KASH domain proteins at the outer nuclear envelope depends on the KASH domain and on the presence of SUN domain proteins (Crisp *et al,* 2006; Lei *et al,* 2009; Roux *et al,* 2009). Without SUN domain proteins, the KASH domain protein is floating into the adjacent endoplasmic reticulum (Crisp *et al,* 2006; Lei *et al,* 2009).
Outside the nucleus, KASH domain proteins are connected to actin filaments, microtubules and intermediate filaments (Zhang *et al,* 2002; Wilhelmsen *et al,* 2005; Roux *et al,* 2009; Yu *et al,* 2011; Luxton *et al,* 2011). Thus the LINC complex is building the bridge from the nuclear proteins to the cytoskeleton (fig. 12).

In mammals, the KASH domain protein family includes the **N**uclear **E**nvelope **Sp**ectrin **R**epeat Prote**in**s Nesprin-1 to Nesprin-4 as well as KASH-5, encoded by the genes *SYNE-1* to *SYNE-4* and *CCDC155*, respectively (Meinke and Schirmer, 2015). However, KASH-5 is only expressed in the germ line and the expression of Nesprin-4 is mainly restricted to secretory tissue (Roux *et al,* 2009; Morimoto *et al,* 2012; Horn *et al,* 2013).
Nesprin-1, also known as Enaptin, SYNE-1 or MYNE-1, and Nesprin-2, also named Nuance and SYNE-2, are giant proteins with a molecular weight of 1 MDa and 800 kDa, respectively. The proteins share a high homology: Both contain an N-terminal actin binding domain, a long rod formed of spectrin repeats and a C-terminal KASH domain (fig. 13). While Nesprin-1 giant protein contains 46 spectrin repeats, Nesprin-2 giant only contains 18 (Warren *et al,* 2005). Several smaller isoforms exist from both proteins. These isoforms are due to alternative promotors or are splicing variants and lack parts of the N- or C-termini of the giant isoforms (Zhang *et al,* 2001; Rajgor *et al,* 2012).
As part of the LINC complex, the giant Nesprin-1 is located at the nuclear envelope (fig. 12). Smaller isoforms with a KASH domain, like Nesprin-1-α (fig. 13), are found at the inner nuclear membrane, directly interacting with Lamin proteins and Emerin (Mislow *et al,* 2002; Wheeler *et al,* 2007). In figure 13, Nesprin-1 isoforms are depicted that are found in the heart, isolated cardiomyocytes, skeletal muscle, myoblasts or myotubes (Rajgor *et al,* 2012; Duong *et al,* 2014). During development, the composition of Nesprin-1 isoforms changes. While in human myoblasts and myotubes only the giant isoform is present, Nesprin-1-α and Nesprin-1-β are strongly expressed in adult skeletal muscle,

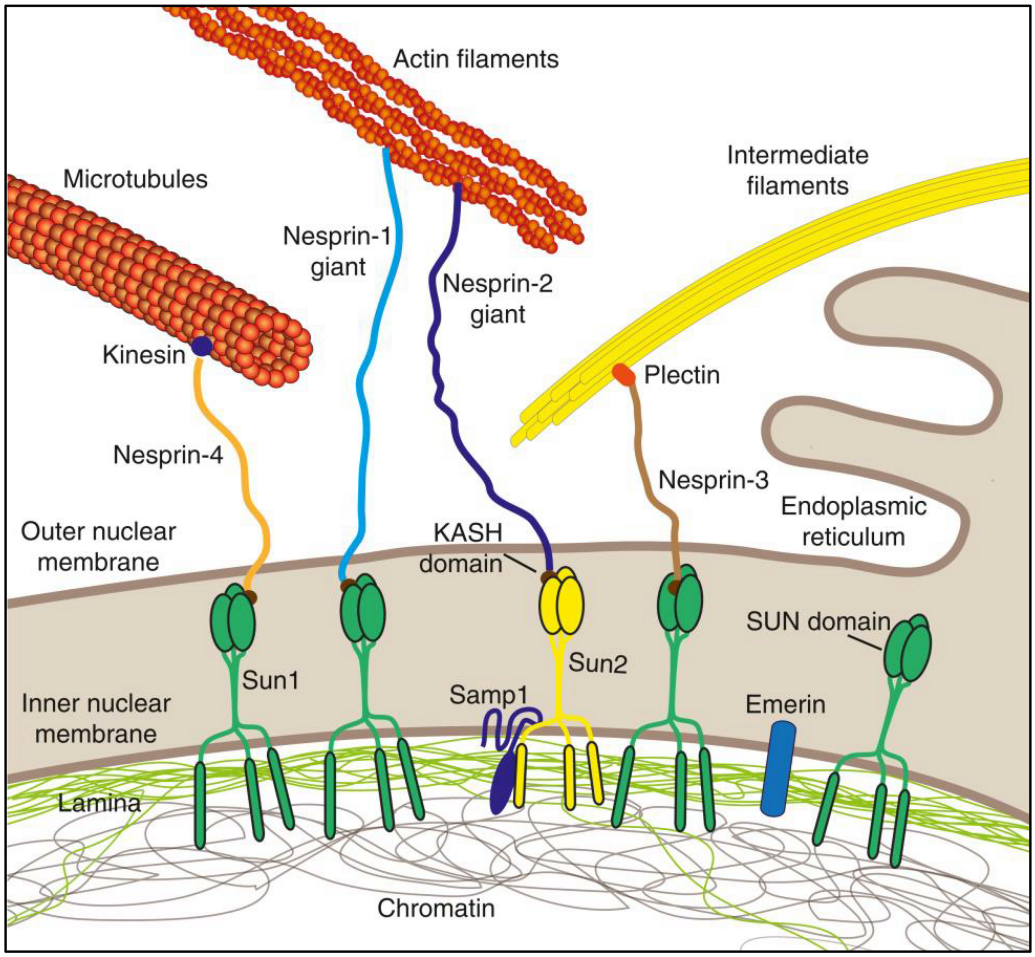

Figure 12: The LINC Complex at the Nuclear Envelope. Nesprin proteins that are connected to the different parts of the cytoskeleton interact via their KASH domain with SUN domain proteins in the perinuclear space. SUN domain proteins span the inner nuclear membrane and interact with different proteins inside the nucleus, including lamin proteins. Thus the LINC complex that is composed of KASH and SUN domain proteins links the cytoskeleton with nuclear proteins. From Isermann and Lammerding, 2013.

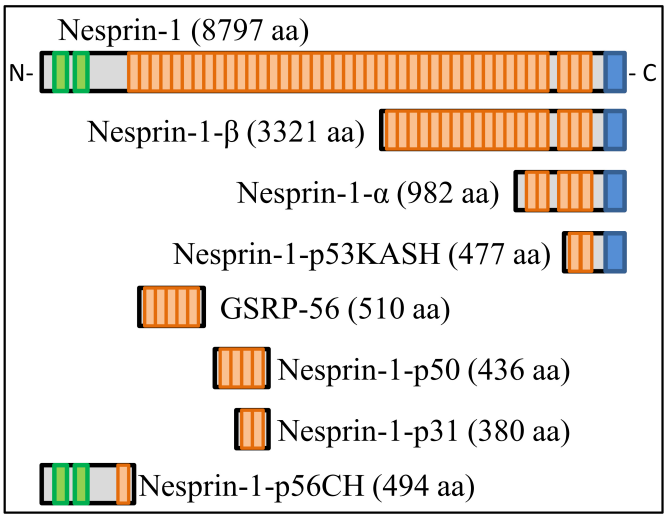

Figure 13: Nesprin-1 Protein Structure and Striated Muscle Specific Splice Variants. The giant Nesprin-1 protein contains an actin binding domain (green), 48 spectrin repeats (orange) and a KASH domain (blue). Alternative splicing events generate a variety of smaller isoforms that lack parts of the N- or C-termini. After Rajgor *et al*, 2012.

while the giant isoform is downregulated compared to myoblasts (Randles *et al,* 2010). It is important to note that only antibodies recognizing the C-terminus of Nesprin-1 have been used in this study, isoforms lacking this part could not be analyzed. Nesprin-1-α also is strongly expressed in cardiomyocytes (Mislow *et al,* 2002). Nesprin-1 isoform GSRP-56 has been found in isolated cardiomyocytes and heart protein extracts, in C2C12 cells as well as adult skeletal muscle (Kobayashi *et al,* 2006). While the KASH domain directs Nesprin-1 isoforms towards the nuclear envelope, Nesprin-1 isoforms lacking the KASH domain are not restricted to that localization and can be found in other compartments of the cell like golgi (Kobayashi *et al,* 2006). The other isoforms shown in fig. 13, Nesprin-1-p53KASH, Nesprin-1-p50, Nesprin-1-p31 and Nesprin-1-p56CH have been detected in heart tissue by PCR (Rajgor *et al,* 2012). Skeletal muscle has not been tested in this study. When expressed ectopically in different cell lines, the KASH-less isoforms localized to the nucleolus, stress fibers, focal adhesions or microtubules, depending on the isoform and the transfected cell line (Rajgor *et al,* 2012).

Mouse models with mutations in *Syne-1*, *Sun1* and *Sun2* have been generated to further understand the function of LINC complex and to find models for human diseases. The first mouse model for studying the function of nesprin-1 overexpressed the KASH domain of nesprin-1 (Grady *et al,* 2005). The excessive KASH domain displaced the KASH domain isoforms of nesprin-1 from the nuclear envelope. This lead to disturbed positioning of synaptic nuclei, which are important for muscle innervation. Due to a lack of antibodies, it is not known if nesprin-2 also was replaced from the nuclear envelope. The mice were not described further.

Three mouse models exist that lack the KASH domain of nesprin-1 or KASH-domain containing isoforms (Zhang *et al,* 2007b; Puckelwartz *et al,* 2009; Zhang *et al,* 2010). Mice of all three lines had changes in positioning of synaptic and non-synaptic nuclei. Zhang *et al* (2007b) replaced the exon coding for the KASH domain by a neomycin cassette. Brain-specific isoforms that lack this exon are not affected. No phenotype was reported for these mice.

Puckelwartz *et al* deleted the KASH domain of nesprin-1 as well. Due to the deletion, abnormal splicing added 61 aminoacids with no homology to any known protein domain at the C-terminus of the truncated protein. Half of the homozygous mice died perinatally because of respiratory failure. Surviving mice developed a phenotype similar to Emery-Dreifuss muscular dystrophy with centralized nuclei, hindlimb weakness, progressive muscle wasting and cardiac conduction defects, but a normal organization of the sarcomere. Although the mutant nesprin-1 still localized to the nuclear envelope, it did no longer interact with sun-2. This contradicts previous publications that reported that the interaction with sun proteins is important for a localization of nesprin proteins at

the nuclear envelope (Crisp *et al,* 2006; Lei *et al,* 2009; Roux *et al,* 2009). However, it is possible that the additional amino acid chain mediates the localization of the mutant nesprin-1 (Puckelwartz *et al,* 2009).
In the third mouse line, the 16th exon counted backwards from the last exon was removed, leading to a premature stop codon (Zhang *et al,* 2010). This resulted in a knock-out of nesprin-1-α and other isoforms that contained the C-term, including the brain-specific isoforms without the KASH domain. 60% of homozygous pups died during the first days after birth, probably because of an inability to suckle, which lead to feeding problems. Surviving mice had normal cardiac functions and no histopathological changes in skeletal muscle, except centrally placed nuclei. They developed growth retardation and had a decreased tolerance for excercise. Nuclei were not deformed, but the anchorage of nuclei at muscle fibers was disrupted. Furthermore, when strain was applied on isolated muscle fibers, nuclei from mutant mice elongated less than those from WT mice. This indicates that the nesprin-1 KASH domain is important in strain transmission.
Mice with a knock-out of *Sun-1* but not *Sun-2* display disturbed myonuclear positioning, indicating that the function of both proteins is not completely redundant (Lei *et al,* 2009). Furthermore, a knock-out of *Sun-1* leads to infertility (Ding *et al,* 2007). A double knock-out of both *Sun-1* and *Sun-2* is lethal, but additional neuron-specific expression of *Sun-1* increased the survival rate (Lei *et al,* 2009). Furthermore, *Sun-1* knock-out mice develop a phenotype similar to cerebellar ataxia in humans (Wang *et al,* 2015). Before the generation of *Sun-1* knock-out mice, this disease had been associated with mutations in *SYNE-1* in humans (Dupré *et al,* 2007; Gros-Louis *et al,* 2007). Taken together, the different mouse models confirm that nesprins and SUN domain proteins function in the same pathway.

1.2.3.5.2 LINC Associated Proteins: Lamins and Emerin

For transmission of a stretch signal into the nucleus and for a proper signal response, not only Nesprins, Sun-1 and Sun-2 are necessary, but also the nuclear lamina and Emerin (Lee *et al,* 2007; Guilluy *et al,* 2014). Furthermore, cells with a functional knock-out of *LMNA* display defects in mechanotransduction (Lammerding *et al,* 2004). Thus, Lamin A/C and Emerin are treated as LINC complex associated proteins.

The nuclear lamina is a meshwork underlining the inner nuclear envelope. It is mainly composed of A- and B-type Lamin protein filaments that are encoded by the genes *LMNA*, *LMNB1* and *LMNB2*. Lamin proteins are specific for Metazoa, meaning that they are only expressed in animals (Dittmer and Misteli, 2011). Splice variations of *LMNA* lead to several isoforms of A-type lamins with Lamin-A and Lamin-C (Lamin-A/C) being the

main isoforms (Azibani *et al,* 2014).

Shortly after fertilization, an embryo is very soft (0.4 kPa) (Majkut *et al,* 2013). During development, some tissues like striated muscle (10 kPa to 11 kPa) stiffen, while others like brain (0.3 kPa) remain soft (Majkut *et al,* 2013; Swift *et al,* 2013; Young *et al,* 2014). The composition of the nuclear lamina correlates with the stiffness of the tissue, with A-type lamins being more prominent in stiffer tissue and B-type lamins dominating in softer tissue (Swift *et al,* 2013). The stiffness of a tissue also correlates with a higher phosphorylation level of A-type lamins in soft cell culture conditions (Swift *et al,* 2013). Phosphorylation of A-type lamins leads to a higher solubility of the proteins, while non-phosphorylated A-type lamins polymerize (Omary *et al,* 2006; Dittmer and Misteli, 2011). Polymerization of A-type lamin proteins leads to a stiffening of the nucleus, protecting its contents against physical damage (Swift and Discher, 2014).

A-type lamins consist of a head domain, a central rod domain and a tail domain (fig. 5) (Herrmann and Aebi, 2004). They have several functions: Polymerized into a stiff network underneath the nuclear envelope, the nuclear lamina can be dilated, but not easily compressed (Dahl *et al,* 2004). Thus it stabilizes the nucleus from the inside. Mutations in *LMNA* lead to nuclear deformations both in the cell culture and in patients (Capell and Collins, 2006; Kandert *et al,* 2007; Bertrand *et al,* 2014). Furthermore, A-type lamins are associated to the LINC complex and interact with Emerin, SUN domain proteins and a short isoform of Nesprin-1 that is localized at the inner nuclear membran (Sakaki *et al,* 2001; Mislow *et al,* 2002; Haque *et al,* 2006). Thus they are involved in the functions of the LINC complex. For example, both a knock-out of *LMNA* and components of the LINC complex lead to defects in mechanotransduction (Lammerding *et al,* 2004; Zhang *et al,* 2010). Finally, A-type lamins also interact with transcription factors and chromatin (Meier *et al,* 1991; Lloyd *et al,* 2002; Guelen *et al,* 2008). Thus, mutations of *LMNA* might directly interfere with gene regulation.

Diseases that are associated with the nuclear lamina are commonly named laminopathies (Burke and Stewart, 2002; Worman and Bonne, 2007; Bertrand *et al,* 2011). Interestingly, various diseases are caused by mutations in the *LMNA* gene which often but not always specifically affect only some organs: muscular dystrophies and cardiomyopathies, neuropathies, lipodystrophies and premature ageing (see chapter 1.1.2 on page 5). Sometimes, one mutation of *LMNA* causes different phenotypes and varying onset of the disease in patients from one family (Bertrand *et al,* 2011). A second mutation in another gene might be modifying the phenotype of the patients, but this is not always identified (Brodsky *et al,* 2000; Ben Yaou *et al,* 2007).

A clear genotype-phenotype relationship is not obvious for laminopathies (Scharner *et al,* 2010). Only few mutations can clearly be connected to a certain phenotype (Scharner *et al,* 2010). However, mutations leading to phenotypes involving the skeletal muscle seem

to destabilize the protein, suggesting that an instability of A-type lamins leads to skeletal muscle disorder (Krimm *et al,* 2002; Scharner *et al,* 2014).

Emerin is encoded by the gene *EMD/STA* and was first identified because of its involvement in Emery-Dreifuss Muscular Dystrophy (EDMD) (Bione *et al,* 1994). The protein localizes at the nuclear envelope in a Lamin dependent manner (Manilal *et al,* 1996; Östlund *et al,* 2006). By directly interacting with Sun-1 and Sun-2, it is connected to the LINC complex in the nucleoplasm (Haque *et al,* 2010). Although Emerin is ubiquitously expressed in differenciated cells, only skeletal muscle, heart and tendons are affected by knock-out of *EMD/STA* (Manilal *et al,* 1996; Tunnah *et al,* 2005; Koch and Holaska, 2012). Emerin was shown to interact with various transcription factors and a deletion of Emerin subsequently leads to misexpression of several members of canonical myogenic signalling pathways, for example: Notch-signalling, which preserves the undifferentiated state of satellite cells, is upregulated, while Wnt-signalling, which is important for differentiation of myogenic progenitors and fusion of myoblasts into myotubes, is reduced (Brack *et al,* 2008; Pansters *et al,* 2011; Koch and Holaska, 2012; Koch and Holaska, 2014). Emerin knock-out mice display a mild phenotype with minimal motor and cardiac dysfunctions and defects in muscle regeneration (Melcon *et al,* 2006; Ozawa *et al,* 2006). Emerin plays an important role in mechanotransduction. Defective mechanotransduction leads to apoptosis of isolated Emerin deficient fibroblasts after cell straining (Lammerding *et al,* 2005). Furthermore, mechanosensitive genes like *egr*-1 are not upregulated by stretch in these cells, while they are rapidly upregulated in WT cells (Morawietz *et al,* 1999; Lammerding *et al,* 2005). Guilluy *et al* show that phosphorylation of Emerin is necessary for a proper response of the cell on stretching stimuli transmitted via Integrins and the LINC complex (Guilluy *et al,* 2014). Furthermore, fibroblasts plated on stiff culture plates contain an elevated level of phosphorylated Emerin compared to cells grown on softer plates (Guilluy *et al,* 2014).

Taken together, the LINC complex with the associated proteins Emerin and A-type lamins is not only important for proper mechanotransduction through the nuclear membrane, but has additional functions. Mutations in the different genes coding for LINC complex and associated proteins may lead to the same disease. For example, the neuromuscular disorder Emery-Dreifuss muscular dystrophy is caused by mutations in Lamin-A/C, Emerin, Nesprin-1 or Nesprin-2 (Bione *et al,* 1994; Bonne *et al,* 1999; Zhang *et al,* 2007a).

1.3 Aims of this Thesis

Mechanotransduction is the translation of a physical stimulus into a biochemical signal and the reaction of a cell on the stimulus. If mechanotransduction is disturbed, diseases of different kinds, like cardiomyopathies or muscular dystrophies may develop, depending on the affected tissue.
Hypertrophic cardiomyopathy (HCM) is a frequent genetic heart disease. It is the most frequent cause of sudden cardiac death in the young and in athletes. Whereas most of the currently known disease genes encode sarcomeric proteins, recent findings indicate that mutations in non-sarcomeric proteins may also cause HCM. Missense mutations in Muscle LIM Protein (MLP) were identified as a novel cause of HCM in several German families some years ago. Striated muscle specific MLP is not exclusively a sarcomeric protein, but also found in the cytosol and the nucleus. In the heart, MLP seems to be essential for a correct signal transduction in response to mechanical stretch. One aim of this thesis was to elucidate the signalling pathways of MLP and the role of HCM-associated MLP mutations in the pathogenesis of HCM. My hypothesis was that mutated MLP was no longer able to shuttle to the nucleus, which resulted in a misreaction of isolated cardiomyocytes towards stretch stimuli. To test the hypothesis, the following steps were necessary:

1. Establishment of the isolation of neonatal cardiomyocytes from wild type (WT) mice and from mice with a functional knock-out of MLP ($MLP^{-/-}$ mice).

2. Optimization of the culture of isolated neonatal cardiomyocytes. This included

   a) the optimization of 2D cell culture (plating and culture conditions), as well as stretching of these cultures,

   b) the establishment of 3D cell culture techniques and stretching of cells within these cultures and

   c) the reduction of the amount and/or proliferation of fibroblasts.

3. Cloning for the generation of wild type and mutant MLP constructs. The mutations were either associated to cardiomyopathies, mimicked the phosphorylation of aminoacids that are known to be phosphorylated or changed the charge of aminoacids within the nuclear localization sequence of MLP.

4. Insertion of MLP constructs into isolated neonatal cardiomyocytes from $MLP^{-/-}$ mice by transfection or transduction with the aim to analyze

   a) whether mutated MLP shuttles to the nucleus after stretching of the cells (immunofluorescence),

b) if the response of cardiomyocytes to stretch is impaired if mutated MLP is present (quantitative real-time PCR) and

c) to compare gene expression of stretched cardiomyocytes expressing WT or mutated MLP constructs (Illumina Gene Expression Chip)

I started the PhD project in Berlin in the laboratories of Christian Geier. At point 3, I stopped the project on MLP to work in a cooperating laboratory of Gisèle Bonne in Paris to fulfill the cotutelle requirements of working in both countries. In Paris, I worked with Catherine Coirault on mechanotransduction in muscle precursor cells (myoblasts).
In myoblasts and skeletal muscle cells, the LINC complex and its associated proteins Emerin and A-type lamins have a function in mechanotransduction. The LINC complex spans the nuclear envelope and thus connects the nuclear interior with the cytoskeleton. I wanted to adress the question if the KASH domain of Nesprin-1, which is part of the LINC complex, is required for mechanotransduction in human muscle precursor cells. I worked with human myoblasts from two patients with congenital muscular dystrophy and from a control person. One patient carried a nonsense mutation in the gene coding for Nesprin-1 (Nesprin1-ΔKASH), the other patient a mutation in the gene coding for A-type lamins, lacking one amino acid (LMNA-ΔK32). I analyzed them with the following experiments:

5. Characterization of Nesprin1-ΔKASH myoblasts:

   a) Subcellular localization of Nesprin1-ΔKASH and LMNA-ΔK32 (immunofluorescence).

   b) Analysis of the localization of other proteins of the nuclear envelope (Sun proteins, Emerin, and Nesprin-2) (immunofluorescence).

   c) Analysis whether Nesprin-2 compensates for Nesprin1-ΔKASH (quantitative real-time PCR).

   d) Quantification of nuclear deformations and changes in nuclear size (immunofluorescence)

6. Assessment of the role of Nesprin-1 and A-type lamins in myoblast mechanosensibility:

   a) Orientation of Nesprin1-ΔKASH and WT myoblasts in 3D culture (immunofluorescence)

   b) Test whether Nesprin1-ΔKASH and LMNA-ΔK32 myoblasts recognize stiffness of substrate (indicators: spreading area, actin stress fibers, focal adhesion sites)(immunofluorescence)

7. Analysis of actin cytoskeleton dynamics in Nesprin1-ΔKASH and LMNA-ΔK32 myoblasts.
    a) Detection of actin stress fibers (immunofluorescence) after usage of the following inhibitors:
        i. MLC kinase inhibitor ML7.
        ii. ROCK inhibitor Y27632.
        iii. SRC inhibitor SU6656.
    b) Analysis of FHOD1 function in Nesprin1-ΔKASH and LMNA-ΔK32 myoblasts:
        i. FHOD1 expression (immunofluorescence, quantitative real-time PCR)
        ii. knock-down of FHOD1 by small interfering RNA (immunofluorescence)
8. Determination whether the transduction with a mini-Nesprin-1 construct (containing actin binding site, some spectrin repeats and KASH domain) ameliorates mechanotransduction of Nesprin1-ΔKASH myoblasts:
    a) Generation of a vector containing mini-Nesprin-1 for generation of lentivirus.
    b) Production of lentivirus for transducing mini-Nesprin-1.
    c) Infection of Nesprin1-ΔKASH and WT myoblasts with the lentivirus, establishment of stably transfected cell lines.
    d) Repetition of experiments on mechanosensibility from point 6 with stable cell lines expressing mini-Nesprin-1.

Lentivirus production (point 8b) and subsequent experiments were taken over by other members of the team when I returned to Berlin.

2 Muscle LIM Protein in Mechanotransduction

2.1 Material and Methods

2.1.1 Material

2.1.1.1 Buffer and Solutions

If not further specified, buffers and solutions were prepared as aqueous solutions and stored at room temperature. If indicated, the solutions were sterile filtered or autoclaved for 30 min at 121 °C.

Name of Buffer	**Contents**
ADS	116.36 mM NaCl, 1 mM NaH_2PO_4, 5.55 mM glucose, 5.37 mM KCl, 0.83 mM $MgSO_4$, 20 mM Hepes, pH 7.4, filter sterilized
CBFHH	136 mM NaCl, 5.4 mM KCl, 0.81 mM $MgSO_4$, 0.44 mM KH_2PO_4, 0.34 mM Na_2HPO_4, 5.6 mM glucose, 20 mM HEPES, pH 7.4-7.5, sterile filtered. Add 4% pen/strep directly before use.
DNA loading dye, 6 x	0.4 g/mL sucrose, 25 mg/mL bromophenol blue
Ear buffer	100 mM Tris, pH 8.5, 5 mM EDTA, 200 mM NaCl, 0.2% SDS, 1 mg/mL proteinase K
Gold buffer	20 mM Tris/HCl, pH 7.5, 155 mM NaCl, 2 mM EGTA, 2 mM $MgCl_2$, autoclaved
PBS	0.14 M NaCl, 2.7 mM KCl, 10.1 mM Na_2HPO_4, 7.3 mM KH_2PO_4, autoclaved
TBE, 10 x	1 M tris base, 1 M boric acid, 20 mM EDTA
TE/RNase	10 mM Tris/HCl, pH 8.0, 1 mM EDTA, 20 µg/mL RNase A

2.1.1.2 Culture Media and Supplements for *E. coli* and Neonatal Cardiomyocytes

Culture medium	Contents or Manufacturer, Reference
3D medium	10% horse serum, 2% CEE (2.1.2.6), 0.1% insulin, 0.1% aprotinin, in light medium, sterile filtered
Ampicillin	50 mg/mL
Aprotinin	Sigma, A1153. Stock: 33 mg/mL
AraC	Sigma, C1768
2,3-Butanedione monoxime (BDM)	Sigma, B0753
Collagen R solution	Serva, 47254.01
DARK medium	10% horse serum, 5% FCS, in light medium, sterile filtered
DMEM	Gibco, 31885-049
DMEM, 2x	20% 10x DMEM, 20% horse serum, 2% pen/strep, 4% CEE (2.1.2.6), steril filtered
DMEM, 10x	133 mg DMEM (powder), ad 10 mL with H_2O, steril filtered
DMEM (no glucose)	Gibco, 11966-025
DMEM (powder)	Gibco, 52100-021
Fibrinogen	Sigma, F8630. Stock: 200 mg/mL in 0.9% NaCl
Fibronectin	Sigma, F1141
Gelatine	Sigma, G1890
Glucose free medium	10% horse serum, 2% CEE (2.1.2.6), 0.1% insulin, 0.1% aprotinin, 0.1% lactate, 1% pen/strep, in DMEM (no glucose), sterile filtered
Glutamine	Gibco, 25030-024

Insulin	Sigma, I9278
Lactate	Sigma, 71718
Light medium	75% DMEM, 25% medium 199, 1% 1 M HEPES, 1% pen/strep, sterile filtered
Matrigel	BD Bioscience, 356234
Medium 199	Gibco, 31153-026
PBS	Gibco, 10010-015
Pen/strep	Invitrogen, 15140122
Thrombin	Sigma, T7513. Stock: 100 U/mL

2.1.1.3 Cell Culture Plates, by Flexcell International Corporation

Culture Plate	**Reference**
TissueTrain, for 3D	TT-4001U
UniFlex, laminin pre-coated	UF-4001L
UniFlex, collagen pre-coated	UF-4001C

2.1.1.4 Antibodies

Antigen	**source**	**Dilutions IF**	**Manufacturer, Reference**
α-actinin	mouse	1:500	Sigma, A7811
goat-488	donkey	1:250	Invitrogen, A11055
MLP (79D2)	mouse	1:100	Geier *et al,* 2008
MLP (everest)	goat	1:100	Everest Biotech, EB09104
MLP (GeneTex)	rabbit	1:100	GeneTex, GTX103219
MLP (Santa Cruz)	rabbit	1:100	Santa Cruz, sc98827
mouse-488	donkey	1:500	Invitrogen, A21202
mouse-488	goat	1:250 (MLP, YAP), 1:500 (α-actinin)	Invitrogen, A11001
mouse-555	goat	1:250 (MLP, YAP), 1:500 (α-actinin)	Invitrogen, A21424
rabbit-488	goat	1:250	Invitrogen, A11034
rabbit-594	goat	1:250	Invitrogen, A11012
YAP	mouse	1:100	Santa Cruz, sc101199

2.1.1.5 Kits

Method	Product, Manufacturer, Reference
DreamMix PCR	DreamTaq Green PCR Master Mix (2X), ThermoFisher Scientific, K1081
GelGreen	GelGreen Nucleic Acid Gel Stain, Biotium, 41004
Mini Prep	Invisorb Spin Plasmid Mini Two, stratec biomedical, 1010140300

2.1.1.6 Oligonucleotides for Cloning

In the sequence, bases inserting the mutation are in small letters, bases being complementary to the template in capital letters. Bases belonging to the mutated codons are underlined.

Name	Sequence
pGG2-MLP-fw	5'-CTC ACT ATA GGC TAG CAT GCC-3'
pGG2-MLP-rev	5'-TAA AGG GAA GCG GCC GCT CAC TCC-3'
MLP-L44P-rev	5'-T GCT GTC agG AGC TTT CCT GC-3'
MLP-L44P-fw	5'-G AAA GCT Cct GAC AGC ACC AC-3'
MLP-S46D-rev	5'-TGT GGT atc GTC CAG AGC-3'
MLP-S46D-fw	5'-CTG GAC gat ACC ACA GTG G-3'
MLP-S46R-rev	5'-TGT GGT cCT GTC CAG AGC-3'
MLP-S46R-fw	5'-CTG GAC AGg ACC ACA GTG G-3'
MLP-C58G-rev	5'-GCA CAC CTT ACc GTA GAT CTC-3'
MLP-C58G-fw	5'-GAG ATC TAC gGT AAG GTG TGC-3'
MLP-R64D-rev	5'-CC ATA CCT Gtc CCC ATA GC-3'
MLP-R64D-fw	5'-C TAT GGG gaC AGG TAT GGC-3'
MLP-R65D-rev	5'-GCC ATA atc GCG CCC ATA GC-3'
MLP-R65D-fw	5'-GG CGC gat TAT GGC CCC-3'
MLP-R65DK69A-rev	5'-GAT CCC ggc aGG GCC ATA ATC G-3'
MLP-Tripel-rev	5'-CC ATA ATC Gtc CCC ATA GC-3'
MLP-Tripel-fw	5'-C TAT GGG gaC GAT TAT GGC-3'
MLP-K69A-rev	5'-GAT CCC ggc aGG GCC ATA CC-3'
MLP-K69A-fw	5'-TAT GGC CCt gcc GGG ATC GGG-3'
MLP-S95D-rev	5'-G CTT TGG atc TTG TTG GAA CTG C-3'
MLP-S95D-fw	5'-C CAA CAA gat CCA AAG CCA GC-3'

2.1.1.7 DNA Molecular Weight Markers

Name	Product, Manufacturer, Reference
100 bp low ladder	PCR 100 bp Low Ladder, Sigma, P1473
GeneRuler 100 bp Plus	GeneRuler 100 bp Plus DNA Ladder, ThermoFisher Scientific, SM0321

2.1.2 Methods

2.1.2.1 Animals

The mice used for the experiments in this thesis were kept and bred at the animal facility from Max Delbrück Center for Molecular Medicine according to animal welfare practices. Neonatal mice were sacrificed by decapitation with scissors, adult mice were sacrificed by cervical dislocation.

Mouse Line	**Genetic Information**	**Received From**
WT	C57Bl6/N, inbred line	Charles River, Sandhofer Weg 7, 97633 Sulzfeld
$MLP^{-/-}$	Knock out: MLP gene, neoR replacing MLP exon2 including the ATG (Arber *et al,* 1997)	AG Karl-Ludwig Laugwitz, German Heart Centre Munich

Cardiac slices from rat were a kind gift from AG Michael Bader at Max Delbrück Center for Molecular Medicine.
Heart tissue samples from domestic pig (*Sus scrofa domestica*) were a kind donation from a butcher in Berlin, Germany.

2.1.2.2 Preparation of Cardiac Tissue Slices for Immunofluorescence

An adult mouse (14 to 30 weeks old) was quickly sacrificed and the sternum opened with scissors to remove the heart. Isopentane was frozen in liquid nitrogen and thawed at room temperature until it started melting. The heart was washed with PBS, dried on a paper towel and frozen in the melting isopentane. The heart was subsequently embedded in Tissue-Tek and snap-frozen in liquid nitrogen. Until further use, it was stored at −80 °C. Tissue samples from domestic pig were directly snap-frozen embedded in Tissue-Tek.
The heart samples were cut into 6 µm thick slices using a cryostat-microtome. After mounting on microscopic slides and drying at room temperature, the slides were stored at −80 °C until fixation (protocol 2.1.2.8) and immunofluorescence (protocol 2.1.2.9.3).

2.1.2.3 Isolation of Neonatal Cardiomyocytes

Neonatal mice were sacrificed at their day of birth or one day later and their sternum was opened without damaging the gut. The contracting hearts were removed from the bodies by pressing gently on the sternum and washed with ice cold ADS buffer. The atria were removed and the hearts were collected in a reaction tube with ADS on ice.
When all hearts were collected, they were cut into small pieces with scissors inside the reaction tube. To remove blood, the heart fragments were washed once with cold ADS

buffer. ADS buffer was removed and substituted by 1.8 mL prewarmed collagenase solution. The heart fragments were gently moved on a shaker at 37 °C for 6 min. This first collagenase solution was discarded afterwards.
A fresh aliquot of prewarmed collagenase solution was added to the tissue fragments. The fragments were gently moved on a shaker at 37 °C for 10 min. The collagenase solution containing isolated cells was mixed with 250 µL horse serum. The cells were pelleted at 200 x g for 10 min and collected in custodiol on ice. These three steps (collagenase solution at 37 °C, horse serum and pelleting at room temperature, collecting in custodiol on ice) were repeated until the heart fragments were completely dissolved.
Then the custodiol with the pooled cardiac cells was sifted with a 100 µm cell strainer to remove big chunks of non-dissolved cells. The cell strainer was washed with DARK medium. The sifted cells were pelleted as before, solved in DARK medium and left for one hour on a conventional petri culture dish at 37 °C and 5% carbondioxide in the cell culture incubator. During this time, non-cardiomyocytes started to adhere on the surface of the plate, while cardiomyocytes remained floating. Thus, the portion of non-cardiomyocytes was reduced.
After the one hour incubation, the supernatant was removed, pelleted and the cell pellet was resolved in 10 mL DARK medium. An aliquot of the solution was used for counting the cardiac cells in a Neubauer chamber. 700 000 cells were plated in each well of a flexcell plate. 1 500 000 to 3 000 000 cells were used to generate one 3D gel.

2.1.2.4 Coating of UniFlex Plates and 2D Culture

As the flexible bottom of the UniFlex® culture plates were made of silicone and thus needed additional coating, I tested several coating agents. I used plates that were pre-coated with collagen or laminin and tested different combinations of collagen (from Sigma, 86 µg/3 mL water or PBS per well; or from Serva, 1.6 mL + 200 µL 9% NaCl and 0.17% NaOH each), gelatine (1% w/v in ADS) and fibronectin (36 µg/3 mL PBS per well). The best coating for neonatal cardiomyocytes from mice were pre-coated laminin plates with either collagen from Sigma or fibronectin coating.
For the coating with collagen from Sigma, the plate was incubated with the collagen solution for several hours at 37 °C. Then the solution was removed and the plate dried over night. The cells only adhered if the bottom of the well was completely dry prior to plating.
For coating with fibronectin, collagen from Serva or gelatine, the coating solution was added to the plate several hours before plating of the cells (usually 3 h prior to the plating). Directly before the plating of the cells, the solution was removed and the well rinsed with PBS.

Neonatal cardiomyocytes were plated on the UniFlex plates and cultured in DARK medium at 37 °C and 5% CO_2. Medium was changed every two days. The cells were kept in culture for seven days befor treating with stretch and fixation.
For infection with AAV, virus particles were added to the cardiomyocytes three days after isolation in the concentration mentioned in the results text.

2.1.2.5 Casting of 3D Gels and Their Culture

For the the gel, 1 500 000 to 3 000 000 cells were mixed with 5.6% 2x DMEM, 2.6% fibrinogen, 10% matrigel and 3% thrombin in a final volume of 150 µL on ice. As soon as the thrombin was added, the polimerization of the fibrinogen to fibrin started.
The mastermix was pipetted between two anchors of a TissueTrain culture plate well (fig. 14). The plate was positioned on top of Through Loader posts in the FX-4000T system. A continuous vacuum of 20% was applied to generate the Through Bay. The polymerization within these Through Bays was for 1.5 h to 2 h at 37 °C. Afterwards, the TissueTrain plate was removed from the FX-4000T system, 3D medium or glucose free medium was added to each well and the cells were kept at 37 °C and 5% CO_2. Medium was changed every two days. For some experiments, cytosine arabinoside (AraC) was added once to the culture medium five days after casting at a final concentration of 25 µM.
During the culture, the gels adhered at the bottom of the well. This is not wanted as it changed the tensions within the gel. One week after the preparation of the gels, they were removed from the bottom of the wells with flat forceps without rupturing the gel. Afterwards, the gels were connected with the well only at the side of the anchors. The gels were stretched after three weeks of culture (protocol 2.1.2.7).

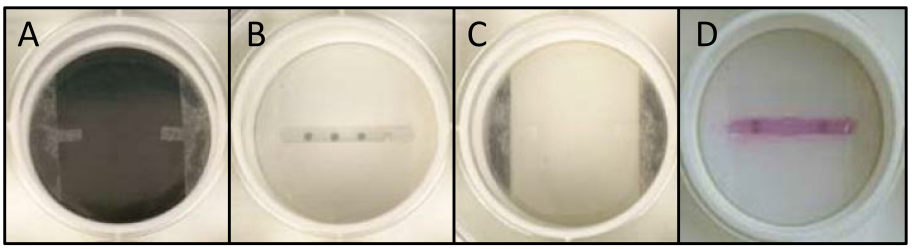

Figure 14: TissueTrain Culture Wells for 3D Cell Culture. A: empty well. The anchors to fix the gel are clearly visible, the flexible membrane is translucent. B: Through Loader beneath the flexible membrane for casting the gels. C: Arctangle loading post beneath the flexible membrane for application of uniaxial stretch along the length of the gel. D: Polymerized 3D gel between the two anchors.

2.1.2.6 Preparation of Chick Embryo Extract (CEE)

60 hatched eggs at 9th day of hatch were desinfected with 70% ethanol. They were a kind gift from the group of Sigmar Stricker at the Max Planck Institute for Molecular

Genetics in Berlin. The eggs were opened and the embryo removed from the egg with sterile tweezers. It is important not to hurt the yolk or blood vessels at this step and not to transfer any yolk with the embryo. The embryo was decapitated and both head and body collected in 300 mL CBFHH on ice in several 50 mL-reaction tubes. The embryos and especially the eyes were cut further with scissors and homogenized on ice (Polytron® homogenizer; 6 x 15 s; mode 11). After centrifugation for 15 min at 60 g and 4 °C, the supernatant was collected and the pellets pooled and resuspended in 150 mL CBFHH. The resuspended pellet was homogenized again and centifuged as above. All supernatants were pooled, aliquoted at 14 mL and stored at −20 °C.
After the first thawing, the chick embryo extract was centrifuged at 2000 rpm for 10 min. The middle phase was transferred to a new tube. The chick embryo extract could be re-frozen. After every thawing, it was centrifuged at 2000 rpm and only the supernatant was used for the cell culture medium.

2.1.2.7 Application of a Stretch Stimulus

To stretch the cells either in 2D or 3D culture, a FX-4000T system was used with FX-4000 V4.0 software. The UniFlex or TissueTrain culture plates were placed on top of Arctangle loading posts (fig. 14 C). If not indicated otherwise, a 10% stretch stimulus was applied to the cells for 24 h at a frequency of 1 Hz. During this time, the cells were kept in the incubator at 37 °C and 5% CO_2.

2.1.2.8 Fixation of Cardiomyocytes and Cardiac Tissue Slices

To preserve the state of the cells, they were fixed with 4% paraformaldehyde (PFA).
Cells in 2D cultures were washed two times with PBS and fixated for 10 min with 4% PFA. They were subsequently washed two times with PBS and either stored with fresh PBS at 4 °C or directly used for immunofluorescence (protocol 2.1.2.9.1).
3D culture gels were washed two times with PBS to remove the medium. To prevent contraction of cardiomyocytes during the fixation procedure, they were treated with 30 mM BDM (2,3-butanedione monoxime) in PBS for 20 min. After two more washing steps with PBS, they were fixed with 4% PFA for 30 min. Two more washing steps with PBS removed the PFA and the gels were either stored with fresh PBS at 4 °C or directly used in immunofluorescence (protocol 2.1.2.9.2).
Frozen tissue slices were fixed in 4% PFA for 15 min and washed three times with PBS to remove the PFA. This was directly followed by immunofluorescence staining procedures (protocol 2.1.2.9.3).

2.1.2.9 Immunofluorescence

2.1.2.9.1 Neonatal Cardiomyocytes on 2D UniFlex Plates

To visualize the subcellular localization of proteins within the cardiomyocytes plated on 2D UniFlex culture plates, the fixed cells were washed with 0,25% tween in PBS for 5 min. The cells were permeabilized with 1% triton X-100 in PBS for 15 min, followed by three washing steps with PBS to remove the triton. To reduce unspecific binding of the antibodies, 3% BSA/PBS was used as blocking for 1 h at room temperature. To reduce the amount of buffer needed, the flexible membrane was removed from the wells and further incubated in smaller 24-well plates.
The first primary antibody was diluted in 1% BSA/PBS. If the antibody 79D2 against MLP was used, gold buffer was used instead of PBS. The cells were incubated with the primary antibody for 24 h at 4 °C. Non-bound antibodies were removed by five washing steps with PBS. The secondary antibody coupled to a fluorophore was diluted in 1% BSA/PBS or gold buffer and incubated with the cells for 1 h at room temperature. Again, excessive antibodies were removed with 5 washes with PBS. For double-staining, the cells were incubated with a second pair of primary and secondary antibodies, as described for the first pair.
To mount the latex membranes, the membrane was glued to the surface of a microscope slide with DAKO, with the cells on top. Hardening vectashield containing DAPI was used to fix a glass cover slip on top of the membrane.

2.1.2.9.2 Neonatal Cardiomyocytes in 3D Gels

To detect the proteins in cardiomyocytes cultured in 3D gels, the protocol for immunofluorescence was slightly changed. All steps were performed on a rocking shaker.
Blocking with 3% BSA in PBS and permeabilization with 0.5% triton X-100 was performed in one step for 6 h at room temperature. Primary antibodies were mixed for one double staining procedure and diluted with 1% BSA/PBS and 0.5% triton X-100. After 24 h at 4 °C incubation of cells with the diluted antibodies, the gels were washed several times with fresh PBS: 5 min, 10 min and 30 min at room temperature, then for over night at 4 °C and again for 1 h at room temperature. The secondary antibodies and DAPI were diluted in 1% BSA/PBS and 0.5% triton X-100 and incubated with the gels at 4 °C for 24 h. The next day, the gels were washed three times for 1 h at room temperature with PBS and mounted with DAKO.

2.1.2.9.3 Cardiac Tissue Slices

The freshly fixed and washed slides were permeabilized with 0.2% triton X-100 for 30 min, followed by three washes with PBS. The slides were blocked with 5% BSA/PBS and 0.03% triton X-100 for 1 h. The primary antibody was diluted with 1% BSA/PBS and incubated with the slides over night at 4 °C in a wet chamber. Non-bound antibodies were removed with three washing steps with 0.05% tween/PBS. Then the slides were incubated with secondary antibody diluted with PBS for 1 h and washed three more times with PBS to remove all excessive antibodies. For double-staining, the incubation with primary and secondary antibodies was repeated for another set of antibodies. Finally, a glass cover slip was added together with a drop of hardening Vectashield containing DAPI.

2.1.2.10 Cloning for AAV Production

2.1.2.10.1 Isolation of mRNA from Cardiac Tissue

A mouse heart was isolated as described in chapter 2.1.2.2 and snap-frozen in liquid nitrogen. The tip was cut off the heart and added to 1 mL TRIzol in a Peqlab tube containing 2.8 mm ceramic beads. The tissue was homogenized using a FastPrep (speed 4.0, time 40 s, 1-3 times) and incubated at room temperature for 5 min. 200 µL chloroform was added to the mixture, vortexed for 15 s and again incubated for 5 min at room temperature. After centrifugation at 12 000 g for 10 min at 4 °C, the upper phase was transferred to a new reaction tube. 500 µL isopropanole was added to precipitate the RNA, inverted and incubated at room temperature for 10 min. After another centrifugation step, the supernatant was removed and the pellet washed with 70% ethanol. After a third centrifugation step, the supernatant was removed, the pellet air-dried and afterwards resolved in water. The concentration of the RNA was measured with a NanoDrop.

2.1.2.10.2 Reverse Transcription

To transcribe isolated mRNA into cDNA, Superscript III was used with 1 µg RNA and poly$(dT)_{20}$ primers, according to the manufaturer's instructions.

2.1.2.10.3 Polymerase Chain Reaction

To amplify a specific part of the cDNA, polymerase chain reaction (PCR) was used. In 25 to 35 cycles, the DNA template was thermically denatured. By reducing the temperature, primers annealed with the single stranded template. The polymerase elongated these primers complementary to the template (tab. 2). The annealing temperature depends on the length and the sequence of the primers, while the lengths of the different steps of

the PCR depend on the polymerase and the length of the amplified piece of DNA. The elongation time was estimated with 1000 bases per 1 min.

Table 2: Example for a PCR program

Initialization	94 °C	2 min	
Denaturation	94 °C	15 sec	35 cycles
Annealing	55 - 60 °C	30 sec	
Elongation	72 °C	1,5 - 3 min	
Final elongation	72 °C	10 min	

For a PCR with Taq polymerase, 1x PCR buffer, 2.5 mM $MgCl_2$, 200 µM of dATP, dTTP, dGTP and dCTP each, 0.14 µM forward and reverse primer, 0.3 µl cDNA and 5 U Taq polymerase were used in a final volume of 50 µL. Primer sequences are listed in chapter refMLP-primer.

2.1.2.10.4 Agarose Gelelectrophoresis

The molecular weight of a DNA fragment was analyzed by agarose gelelectrophoresis. 1-2% agarose were heated in 1 x TBE buffer until melted completely and mixed with GelGreen. The samples were mixed with 6 x DNA loading dye. GeneRuler 100 bp Plus DNA Ladder or PCR 100bp Low Ladder were applied to the gel next to the samples as reference for the molecular weight of DNA fragments (fig. 15). The DNA was separated according to its molecular weight by electrophoresis for 30 min at 80 V in TBE buffer. The DNA in the agarose gel was visualized with an UV-transilluminator.

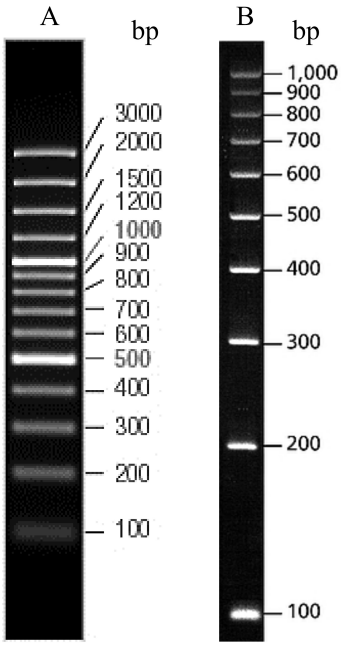

Figure 15: DNA Ladders. A: GeneRuler 100bp Plus, ThermoFisher Scientific, SM0321. B: PCR 100bp Low Ladder, Sigma, P1473.

2.1.2.10.5 Ligation with pGemT-easy

For singularization and further analyzation of the products of a PCR reaction (2.1.2.10.3), the polymerase was inhibited by three freeze-thaw-cycles with dry ice and the PCR product ligated with pGemT-easy according to the instructions of the manufacturer.

2.1.2.10.6 Transformation of *E. coli*

An aliquot of TOP10 chemically competent bacteria was thawed on ice. 2 µL ligation reaction were added to the bacteria and incubated on ice for 30 s. After a heat shock at 42 °C for 40 s, the cells were incubated again on ice for 2 min and subsequently plated on blue-white selection agar plates containing ampicillin.

2.1.2.10.7 Isolation of Plasmid DNA from Bacteria: Mini-Prep

To isolate plasmid DNA from *E. coli* in an analytical amount, selective LB medium was inoculated with a single white colony of a transformation (2.1.2.10.6) and incubated overnight at 37 °C. For isolation of the plasmid DNA, the kit Invisorb Spin Plasmid Mini Two was used according to the directions of the manufacturer.

2.1.2.10.8 Mutagenesis of MLP

To prepare the different mutations of MLP, several steps with PCR were necessary. The sequence of WT MLP was used as a template, with primers 1 and 2 amplifying the full length sequence (fig. 16). Primers 3 and 4 were designed that included the respective mutation. PCR, part A and PCR, part B using primer pairs 1 and 3 or 4 and 2, respectively, resulted in two PCR products with an overlapping part, containing the mutation (fig. 17). PCR C using primers 1 and 2 and both PCR products as a template resulted again in the full length sequence of MLP with the desired mutation. This PCR product was ligated with pGemT-easy and sequenced. Final constructs were send to the HEXT vector facility at the Universitätsklinikum Hamburg-Eppendorf for production of adeno-associated viruses. Fig. 18 shows the final vector for generation of adeno-associated viruses coding for wild type MLP in control of the cardiomyocyte specific TnT promotor that was generated by the HEXT vector facility. To facilitate the optimization procedure of infection of cardiomyocytes with these viruses, one virus was generated where the MLP sequence was replaced by GFP.
The double mutation of MLP (R65DK69A) was generated by further mutating the clone of R65D. For the tripel mutant (R64DR65DK69A), the double mutant was mutated again.

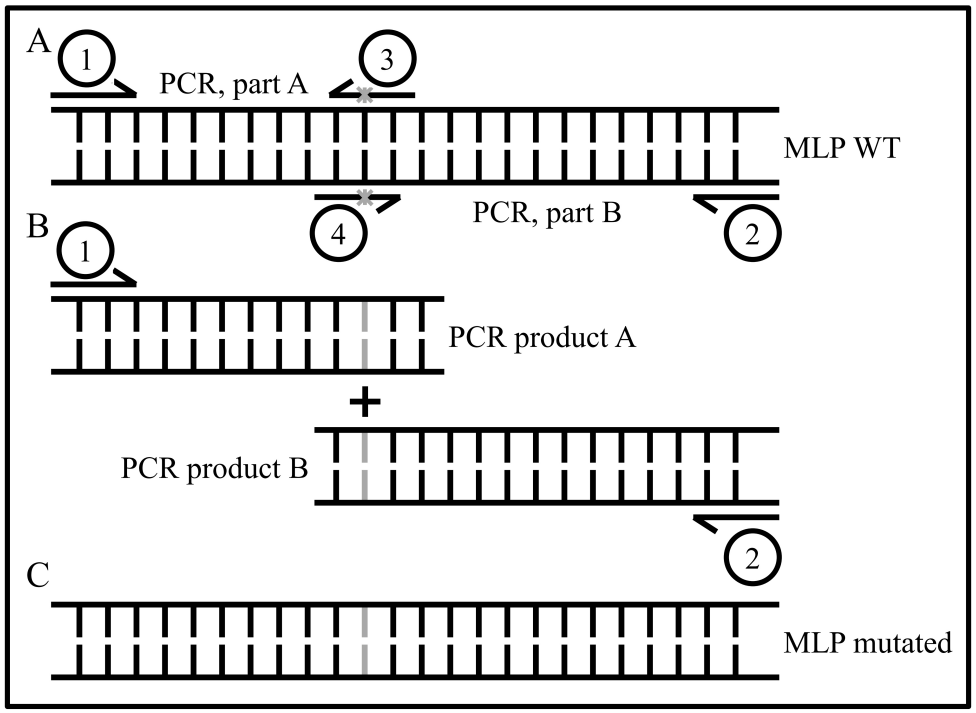

Figure 16: Plan for Mutagenesis of MLP by PCR. A: WT MLP was used as the template for the subsequent mutation of the sequence. The position of the primers is indicated. Primer pairs 1,3 and 4,2 are combined in PCR, part A and PCR, part B. B: These PCRs resulted in two overlapping PCR products A and B that contained the required mutation. A third PCR, using the two previous PCR products as templates and primers 1 and 2 was used to fuse the two PCR products. C: The fusion resulted in a full length MLP sequence with the intended mutation.

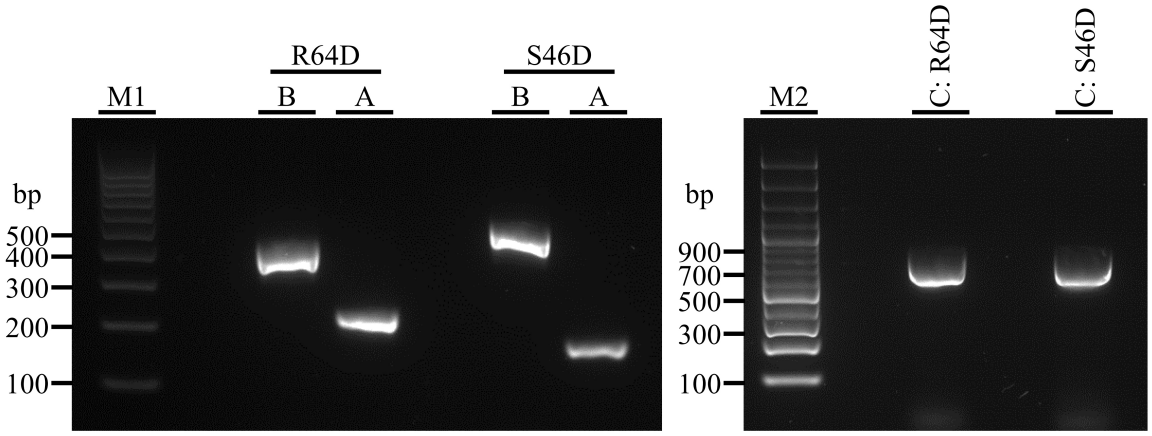

Figure 17: Examples of the Mutagenesis of MLP by PCR, agarose gel electrophoresis. Aliquots of PCR, part A and PCR, part B introducing the mutations R64D and S46D are shown in the left figure. On the right, the third PCR with the mutated full-length sequence of MLP is shown. M1: 100 bp low ladder. M2: GeneRuler 100 bp plus.

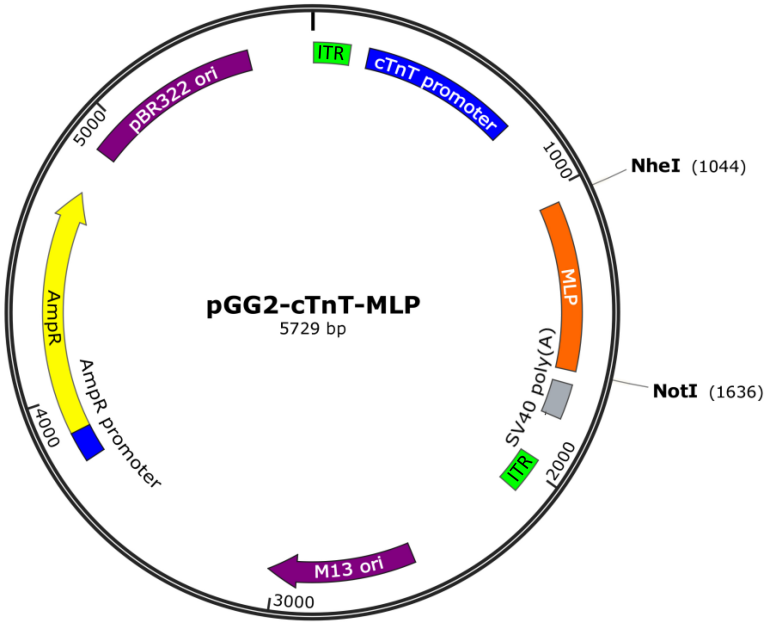

Figure 18: Final Vector for Production of Adeno-Associated Viruses Coding for MLP. MLP was subcloned from pGemT-easy with *Nhe*I and *Not*I. For optimization of viral protocols, MLP was replaced by GFP sequence. MLP (and GFP) expression is regulated by a cardiomyocyte specific TnT promotor (blue). The SV40 poly(A) sequence (grey) will protect the mRNA after transcription. The virus will contain the DNA between the two ITR sections (green). For amplification of the vector in bacteria, a gene coding for resistancy against ampicillin (yellow) as well as an origin of replication (purple) are present.

2.1.2.11 Genotyping

2.1.2.11.1 Isolation of Genomic DNA from Ear Biopsy

To differentiate between WT, $MLP^{-/-}$ and $MLP^{+/-}$ mice, the pieces of ears that were cut off the animals for labeling them were collected in the animal facility and frozen until further use. The biopsies were incubated with 100 µL ear buffer for 2 h or more at 55 °C, shaking and regularly vortexed, until completely dissolved. The proteinase was inactivated by heat (5 min at 95 °C). After cooling to room temperature, the mixture was diluted with 750 µL TE/RNase and stored at 4 °C.

2.1.2.11.2 PCR for Genotyping

2 µL of the genomic DNA from ear biopsy was used with water, DreamMix, 1 pm forward and reverse primers in a final volume of 25 µL. One pair of primers was used to detect WT sequence, one pair of primers to detect the knock-out sequence. Two PCR reactions with separate primer pairs were necessary.

2.2 Results

2.2.1 Setting Up Cell Culture of Neonatal Cardiomyocytes from Mice

2.2.1.1 Litter Size of MLP$^{-/-}$ Mice

Cultivation of isolated neonatal cardiomyocytes from mice is more complicated than from rat neonatal cardiomyocytes. However, our group had access to mice with a functional knock-out of MLP (MLP$^{-/-}$ mice) and corresponding WT control mice with the same genetic background (C75Bl/6N). Thus, we decided to establish the isolation and cell culture of neonatal mouse cardiomyocytes.

Isolation of neonatal cardiomyocytes from mice was established according to a protocol of the Christensen research group in Oslo with some modifications (Finsen *et al,* 2011). While our WT mice had a mean litter size of 8.5 pups, the litter of MLP$^{-/-}$ mice were much smaller with a mean of nearly five pups and a maximum of 7 pups per litter (fig. 19). In addition, the number of cages in the animal facility for breeding was restricted. Thus I had to downscale the protocol from 50 to 100 animals used in Oslo per isolation to five to twenty of our neonatal mice that were born preferably on the same day or on two consecutive days. Cardiomyocytes from older pups were less viable and the cultures contained more fibroblasts and other non-contracting mesenchymal cells.

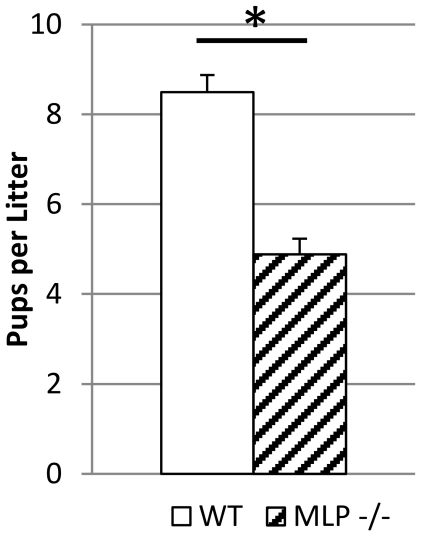

Figure 19: Litter Size of WT and MLP$^{-/-}$ Mice. Few pups were born from MLP$^{-/-}$ mice. This complicated the breeding organization for the preparation of neonatal cardiomyocytes. *: two-sided T-test with $p<0.001$. WT n=43, MLP$^{-/-}$ n=18.

2.2.1.2 Reduction of Non-Cardiomyocytes

Besides cardiomyocytes, other cell types including cardiac fibroblasts, endothelial cells and smooth muscle cells are present in the heart (Nag, 1979). Cardiomyocytes account for around 30% of all cardiac cells, but they represent more than 70% of the cellular volume within the heart (Jugdutt, 2003). These numbers vary depending on species and specimen age (Banerjee *et al,* 2007; Snider *et al,* 2009; Souders *et al,* 2009).

During the isolation of neonatal cardiomyocytes, those other cells, of course, are also isolated and result in a „contamination“ of the cardiomyocytes by non-cardiomyocytes.

While embryonic cardiomyocytes still possess the ability to proliferate, adult cardiomyocytes „grow“ by hypertrophy (Soonpaa *et al,* 1996). The switch from hyperplasia (organ growth by cell division) to hypertrophy (organ growth by increasing cell size) happens during the first days after birth (Li *et al,* 1996). However, the proliferation rate of neonatal cardiomyocytes is slow. Fibroblasts proliferate faster and soon outgrow the cardiomyocytes when kept in co-culture (Ieda *et al,* 2009). To remove a big portion of the fibroblasts, I made use of the observation that mesenchymal cells adhere faster to plastic petri dishes than neonatal cardiomyocytes (Blondel *et al,* 1971). Within 1 h, many of the mesenchymal cells but only few cardiomyocytes adhered to the surface of the dish. The supernatant containing an enriched amount of cardiomyocytes was used for cardiomyocyte culture.

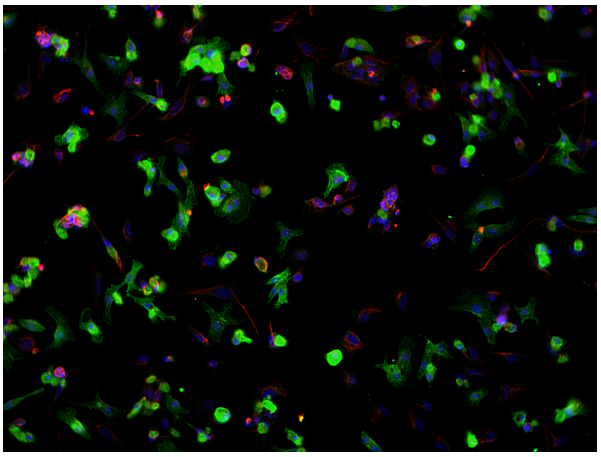

Figure 20: Discrimination of Cardiomyocytes and Mesenchymal Cells by Immunofluorescence. While cardiomyocytes are positive for $\alpha-actinin$ (green), mesenchymal cells like fibroblasts contain vimentin (red). Nuclei of all cells are stained with DAPI (blue).

Cardiomyocytes can be distinguished from non-cardiomyocytes by different methods. In a culture dish, most cardiomyocytes contract, thus I could estimate the quality of an isolation directly in the culture dish. For quantitative analysis, I used immunofluorescence. While cardiomyocytes were positive for α-actinin, fibroblasts and other mesenchymal cells could be stained by vimentin. An exemplary picture is shown in fig. 20. The proportion of non-cardiomyocytes was up to 50%. This varied between the isolations.

3D cultures were sustained for a much longer time than 2D cultures. Although I enriched the percentage of cardiomyocytes, fibroblasts still proliferated too much. As staining for vimentin did not work in 3D, I estimated the amount of fibroblasts by comparing the contractions between two gels. Some days after the generation of a 3D gel, cells within the gel started to contract. However, after some more days, the content of fibroblasts increased, which led to stiffening of the culture gels and resulted in fewer contractions. To diminuish the proliferation of fibroblasts, I tested several protocols.

AraC is a cytostatic drug that is cytotoxic during the S-phase of the cell cycle (Cozzarelli, 1977). When I incubated the 3D cultures for 3 days with the compound, contraction rates increased slightly, compared to the non-treated gels.

In another attempt, I replaced glucose in the medium for 3D cell cultures by lactate. While cardiomyocytes remain viable in these culture conditions, fibroblasts starve and

reduce their proliferation rate (Tohyama *et al,* 2013). This treatment markedly improved contraction rates within the gel, compared to both non-treated gels as well as AraC-treated 3D cultures. Thus, I cultured 3D gels in glucose-free medium.

2.2.1.3 Coating of UniFlex Culture Plates

As MLP is part of the stretch sensing pathway, I wanted to stretch our isolated neonatal cardiomyocytes. However, the flexible silicone membrane of the UniFlex® wells needs coating for the cells to adhere properly. While rat neonatal cardiomyocytes easily grow on plates that were pre-coated with collagen-I or simply coated with gelatine (Salameh *et al,* 2010; Dhein *et al,* 2014; Koivisto *et al,* 2014; Niu *et al,* 2015), this was not sufficient for mouse neonatal cardiomyocytes: With these conditions, only few of the attached cells were contracting cardiomyocytes which did not elongate but remained small and round. I tested UniFlex® plates pre-coated with laminin or collagen or coated the plates in our lab with collagen, gelatine, fibronectin and a combination of those coating agents. A combination of pre-coated laminin plates with additional coating with collagen or fibronectin was best for a lasting attachment of the cardiomyocytes.

2.2.2 Subcellular Localization of MLP

2.2.2.1 Specificity of Antibodies Detecting MLP

Several different anti-MLP antibodies are cited in the literature (Arber *et al,* 1994; Boateng *et al,* 2007; Geier *et al,* 2008; Gupta *et al,* 2008; Kuhn *et al,* 2012; Levin *et al,* 2014). While some are commercially available, most of them are not. We had one

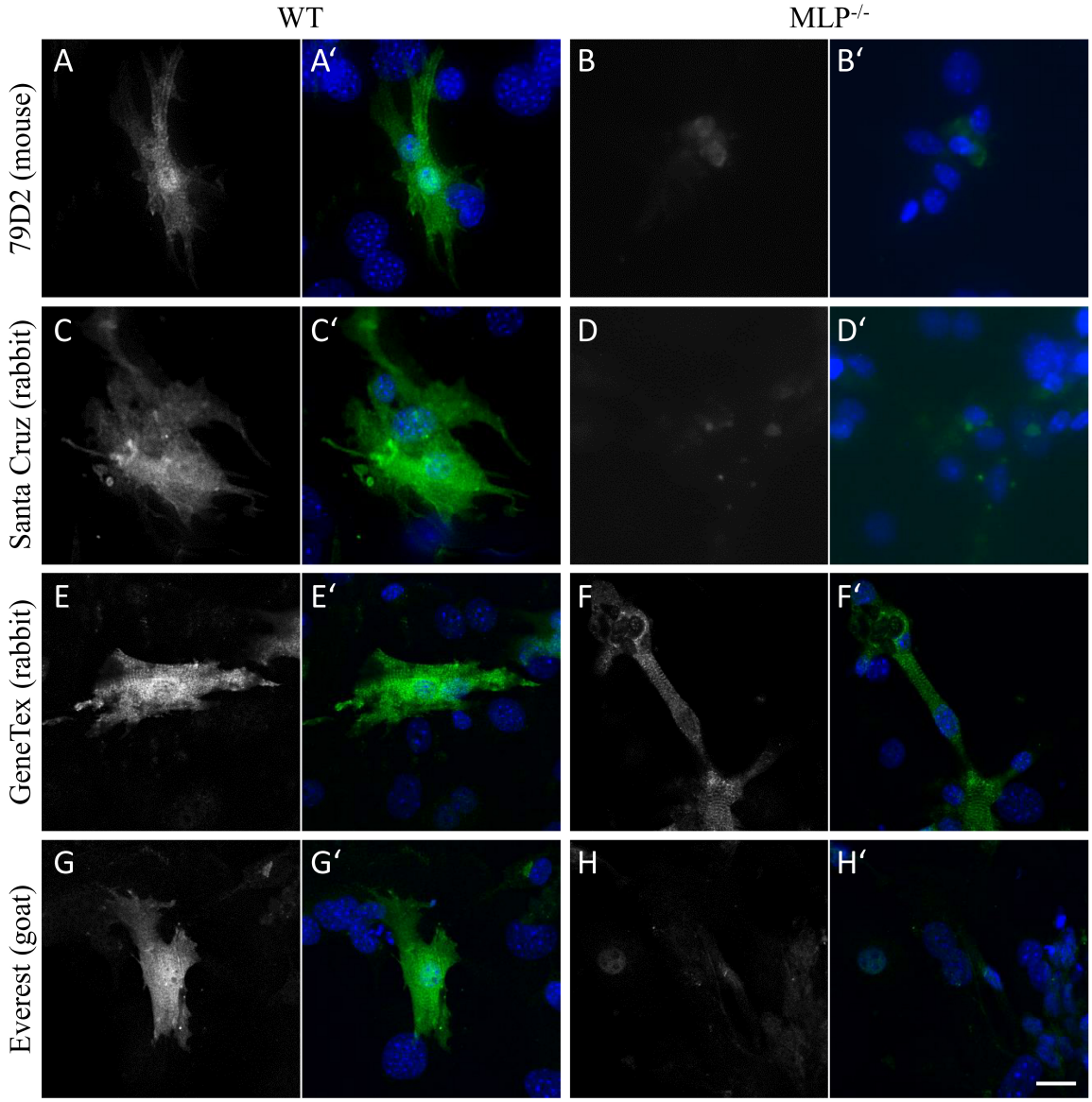

Figure 21: Specificity of Antibodies Against MLP. Our self-made mouse monoclonal antibody against MLP (clone 79D2) detected the protein specifically in WT cardiomyocytes (A), whereas MLP$^{-/-}$ cardiomyocytes remained free of antibody signal (B). The rabbit polyclonal antibody from Santa Cruz Biotechnology (sc-98827) was specific as well (C,D), but the exposure time was three times longer to get a similar result in WT cells. I doubted the specificity of the rabbit polyclonal antibody against MLP from GeneTex (GTX110536). The antibody did not only give a strong staining in WT cardiomyocytes (E), but also in cardiomyocytes from MLP$^{-/-}$ mice (F). The best commercially available antibody against MLP I found was the goat polyclonal antibody from Everest Biotech (EB09104). It specifically and strongly targeted cardiomyocytes from WT (G) but not MLP$^{-/-}$ mice (H). Exposure times from MLP$^{-/-}$ pictures were always the same as the times from the corresponding WT pictures. Scale bar: 20 µm.

monoclonal antibody in our stock (79D2) that targets the 21 C-terminal aminoacids of the protein (Geier *et al,* 2008). As this antibody was raised in mouse cells, I experienced the usual „mouse-on-mouse"-problem when detecting MLP in mouse tissue samples.

In order to avoid this problem and to have alternatives in the combination of antibodies for immunofluorescence, I searched for other commercially available antibody against MLP that were not raised in mouse. While one of them (Santa Cruz) only gave a very faint staining of MLP in WT cells, others (like the one from GeneTex) stained cells of $MLP^{-/-}$ mice as well, raising doubts about their specificity (fig. 21). Only the anti-MLP antibody from Everest gave a sufficient staining in WT but not in $MLP^{-/-}$ cardiomyocytes.

The anti-MLP antibody from Everest was working well in 2D cultures, but when I tested the antibody for detection of MLP in 3D cell cultures, it was not working as expected (fig. 22). Instead of staining the same cells as the myocyte marker α-actinin, the Everest antibody preferably stained cells that were not cardiomyocytes. On the other hand, the 79D2 antibody still specifically stained the cytoplasm of cardiomyocytes.

Taken together, not all commercially available antibodies that claim to detect MLP were specific, while others were specific but rather weak. Both our 79D2 and the antibody from Everest have been specific in 2D staining. However, in 3D, only the 79D2 antibody has been working properly.

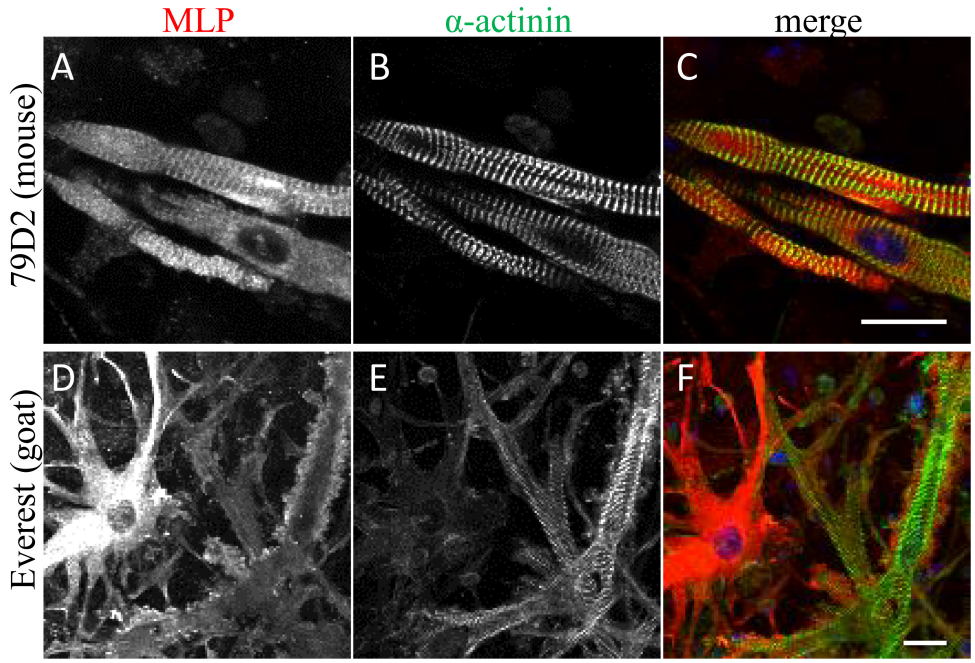

Figure 22: Specificity of Antibodies Against MLP in 3D. When I tested the antibodies in whole mount stainings of 3D culture gels, the 79D2 antibody strongly detected cardiomyocytes (A-C). Surprisingly, the Everest antibody against MLP did not stain cardiomyocytes (D) but cells that were not positive for the cardiomyocyte marker α-actinin (E, F). Scale bar: 20 µm.

2.2.2.2 Subcellular Localization of MLP in Cardiac Tissue Sections

I tested the subcellular localization of MLP in slices of the left ventricle of WT mouse, rat and domestic pig (*Sus scrofa domestica*). MLP never co-localized with nuclear DAPI staining, but was present in the cytoplasm of cardiomyocytes (fig. 23). Depending on the orientation of the section, a striation of the MLP staining was detectable that co-localized with α-actinin. α-actinin localizes to the sarcomeric Z-disk, indicating that MLP also localized there. A striation pattern was more easily found the bigger the donor animal was.

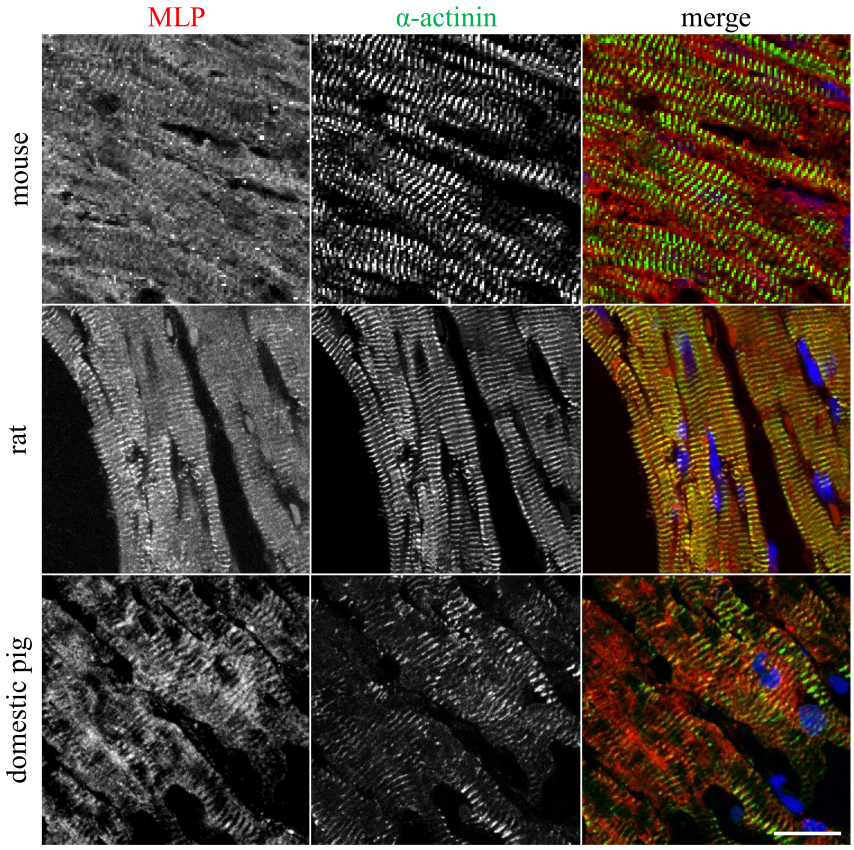

Figure 23: MLP in Cardiac Tissue Sections. In three different mammalian species (mouse, rat and domestic pig), MLP showed a predominant Z-disk pattern co-localizing with α-actinin with more (mouse, rat) or less (domestic pig) obvious general cytoplasmic staining. MLP was never found in the nucleus. Merge: green: α-actinin, red: MLP, blue: DAPI. Scale bar: 20 µm.

2.2.2.3 Subcellular Localization of MLP in Neonatal Cardiomyocytes

In 2D cultures of WT neonatal cardiomyocytes from mice, MLP usually localized to the cytoplasm of isolated cardiomyocytes without any pattern of striation (fig. 24). In these cells, α-actinin staining revealed a striated pattern of the sarcomere. MLP could not be detected in the nucleus of the cells. When the cardiomyocytes were treated for 24 h with a cyclic stretch of 10% and a frequency of 1 Hz prior to fixation, MLP could be detected in the nuclei of WT cardiomyocytes.

The culture of cardiomyocytes on 2D substrates is not at all recapitulating the situation of the cells within the heart. 3D cultures, although still not perfect, at least embedd the

cardiomyocytes within their fibrous networks.
In 3D cell cultures, MLP also localized to the cytoplasm of the WT cardiomyocytes, but not to the nucleus (fig. 25 A). Unexpectedly, stimulating the 3D cultures for 24 h at frequency of 1 Hz with 10, 15 or 18% stretch did not lead to a nuclear relocation of MLP (fig. 25 B-C).

For antibodies to pass through the cell membrane and the nuclear membrane, permeabilization is an important step during the staining procedure. To ensure that the non-nuclear localization of MLP in fig. 25 was not due to an insufficient permeabilization of the nuclear membrane, I used antibodies against proteins that localize to the nucleus of cardiomyocytes. I could show with the same protocol for immunofluorescence that in 3D gels, Yes-Associated Protein (YAP) localized in the nucleus of cardiomyocytes (fig. 26). This proves that MLP indeed did not localize to the nucleus of cardiomyocytes in our system of 3D cultures. More tests are necessary to determine if a misfunction of the stretch machine was the cause for this result, if MLP does not shuttle to the nucleus in 3D cultures or if the structure and/or the geometry of our 3D culture system prevents the shuttling process. Whatever the problem of the 3D culture system is, it was not suitable to test the hypothesis if mutant MLP no longer shuttles to the nucleus after a stretch stimulus. Thus, 2D cultures where used for the following experiments.

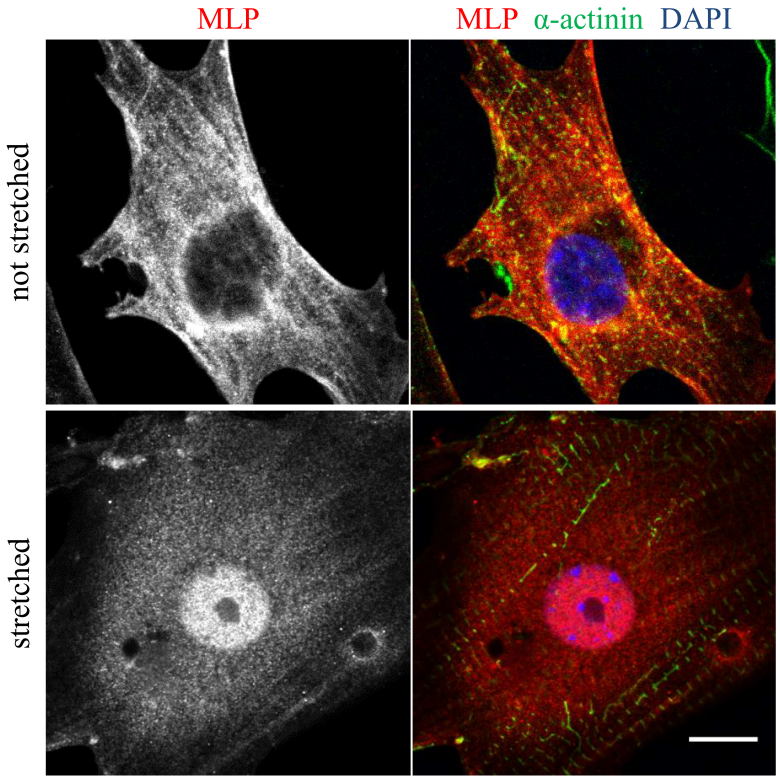

Figure 24: MLP in WT Cardiomyocytes, in 2D. In cardiomyocytes from neonatal WT mice, MLP was predominantly found in the cytoplasm of the cells. After stretching the cells, MLP was found in the nucleus. Scale bar: 10 µm.

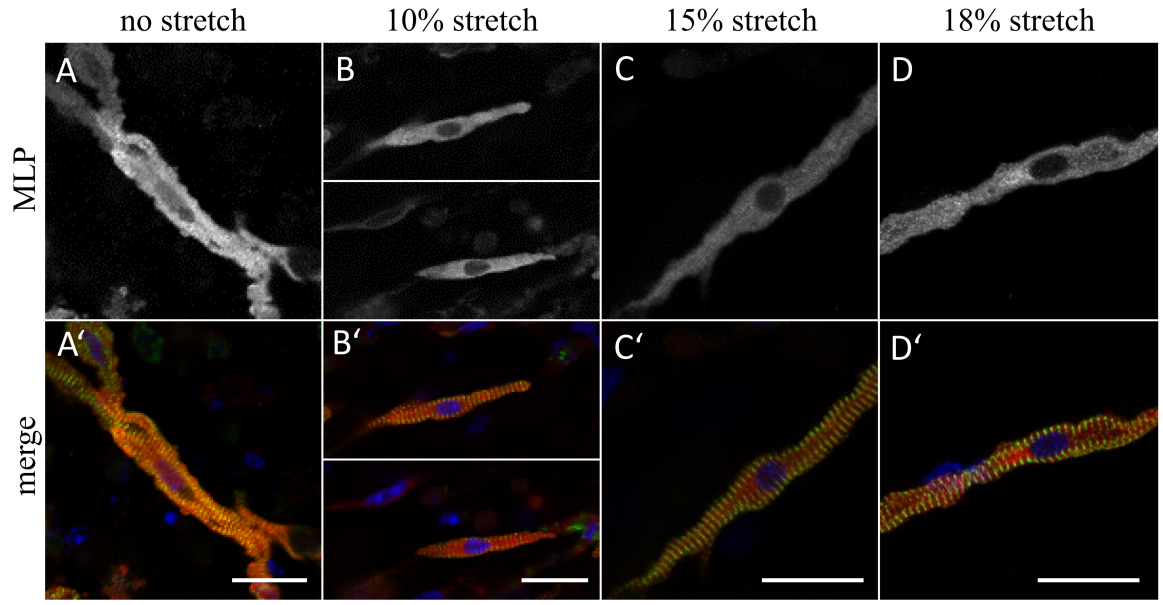

Figure 25: MLP Localization in 3D Gels. In 3D tissue cultures of WT neonatal cardiac cells, MLP was found in the cytoplasm of cardiomyocytes (A). It did not co-localize with DAPI. When the cells were stretched 10% for 24 h at a frequency of 1 Hz, MLP was still found in the cytoplasm, but never in the nucleus of the cells (B). The same was found when the stretching was increased to 15% (C) or 18% (D). Red: MLP, green: α-actinin, blue: DAPI. Scale bars: 25 µm.

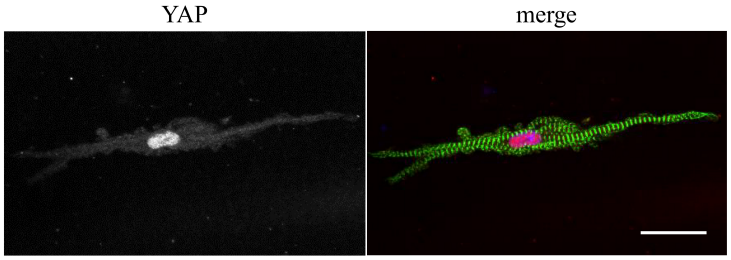

Figure 26: YAP Localization in the Nucleus of Cardiomyocytes in 3D Culture. To verify that nuclear proteins are properly stainded with my IF methods, I used antibodies against YAP, which is localized in the nucleus of cardiomyocytes in 3D cultures. Red: YAP, green: α-actinin, blue: DAPI. Scale bar: 25 µm.

2.2.3 Transduction of Isolated Cardiomyocytes with Mutated MLP

Several mutations of MLP cause hypertrophic or dilated cardiomyopathy in human patients. We hypothesize that the shuttling of MLP into the nucleus is required for a proper mechanosignalling within cardiomyocytes. I aimed to investigate whether the different mutations prevent the nuclear shuttling of MLP to answer the question if defective mechanosignalling is a trigger of diseases.

As I could not isolate cardiac cells from patients to stretch them, I planned to express mutant isoforms in isolated neonatal cardiomyocytes from $MLP^{-/-}$ mice. Thus I wanted to ensure that no endogenous WT MLP masked the subcellular localization of the mutated proteins.

In cooperation with the HEXT Vector Facility at the Universitätsklinikum Hamburg-Eppendorf, I prepared adeno-associated virus (AAV) vectors coding for WT MLP and mutated isoforms (tab. 4). Some of the mutations were chosen as they cause either HCM or DCM in human patients (L44P, S46R, C58G, K69R). The mutations S46D and S95D should mimique a constant phosphorylation of the serine residues. S46D was chosen as a patient with the MLP mutation S46R has been previously published (Geier *et al,* 2008). S95D was chosen as MLP gets phosphorylated at this serine residue (Højlund *et al,* 2009). Mutants R64D, R65D, K69A, R65DK69A and R64DR65DK69A were generated to destroy the integrity of the nuclear localization signal that is required for nuclear relocation of MLP (Weiskirchen and Günther, 2003; Boateng *et al,* 2009).

Table 4: Mutations of MLP, Generated for Further Studies.

Mutation	Comment	Reference
none	WT protein	
L44P	patient, HCM	Geier *et al,* 2003
S46R	patient, HCM	Geier *et al,* 2008
S46D	constant phosphorylation	Klede, 2011
C58G	patient, HCM	Geier *et al,* 2003
R64D	nuclear localization signal	Weiskirchen and Günther, 2003; Boateng *et al,* 2009
R64DR65DK69A	nuclear localization signal	
R65D	nuclear localization signal	
R65DK69A	nuclear localization signal	
K69A	nuclear localization signal	
S95D	constant phosphorylation	Højlund *et al,* 2009

2.2.3.1 Transduction Protocol for Adeno-Associated Viruses

To find the best number of virus particles per cell (MOI - multiplicity of infection), I incubated cardiomyocytes with AAV expressing GFP at an MOI of 3 000, 7 000 or 10 000

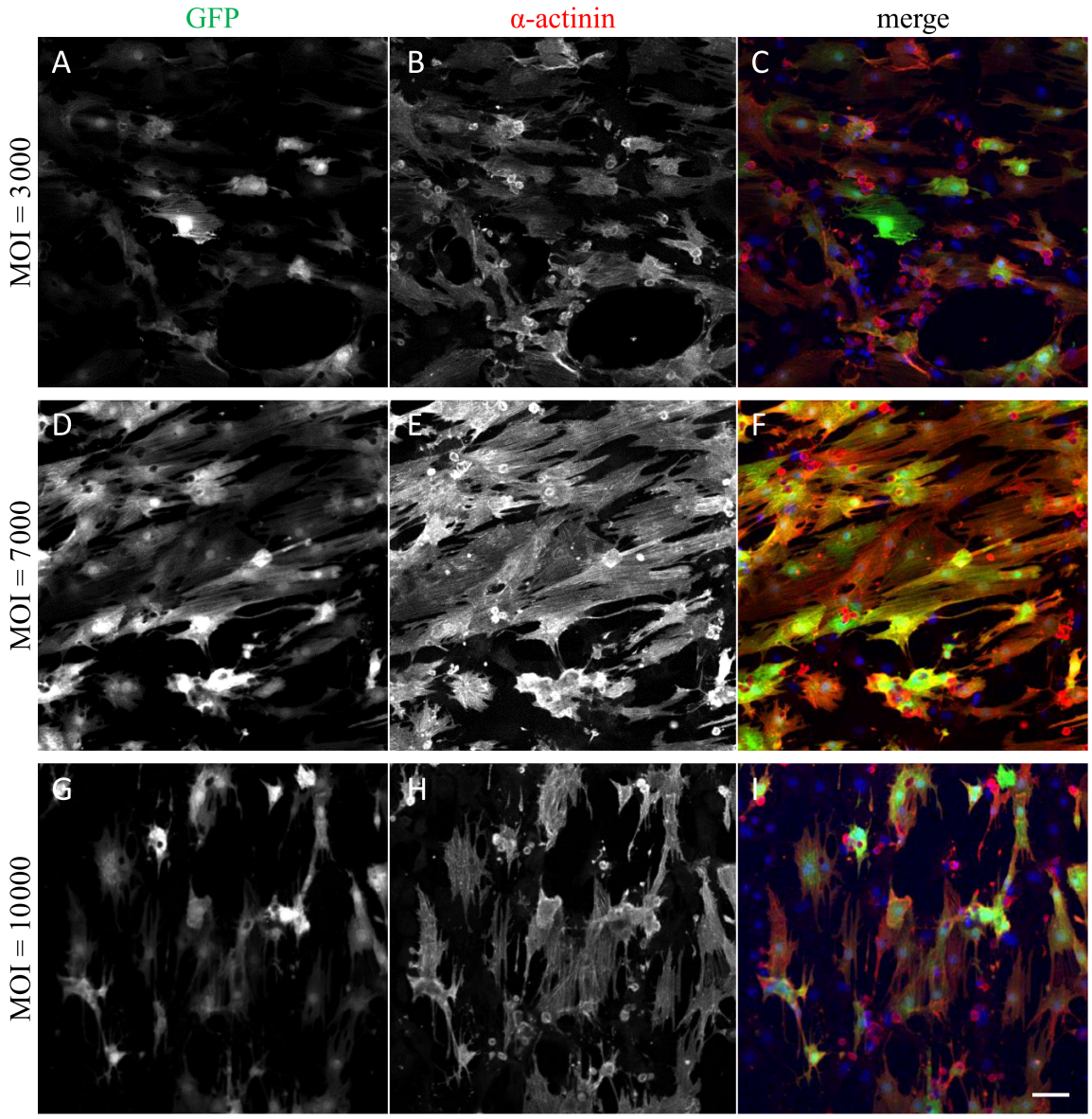

Figure 27: AAV: Optimization of Multiplicity of Infection. I tested several concentrations of virus particles per cell (MOI) that coded for GFP. At an MOI of 3 000, most cardiomyocytes expressed GFP, but many of those very weakly (A, C). At an MOI of 7 000, the GFP signal was more intense (D, F). Raising the MOI to 10 000 did not further improve the GFP intensity (G, I). Cardiomyocyte-specific α-actinin was used to confirm that only cardiomyocytes were GFP positive (B, E, H). Scale bar: 50 µm.

(fig. 27). To confirm that the infected cells were cardiomyocytes, I co-stained the cells for cardiomyocyte-specific α-actinin.

For all three concentrations of virus particles I hardly found a non-cardiomyocyte that was GFP-positive. This indicates that the combination of AAV serotype 6 and a cardiac troponin T promoter lead to a cardiomyocyte specific expression of the gene of interest. At an MOI of 3 000, most but not all cardiomyocytes were expressing GFP. The intensity of GFP was weak in many cells. Raising the MOI to 7 000 lead to a higher intensity of GFP expression within the cells. An MOI of 10 000 did not further ameliorate the GFP intensity. Thus, I decided to use AAV with an MOI of 7 000.

The expression of GFP within the cardiomyocytes revealed a myofibrillar and nuclear localization of GFP (fig. 28). In some places, a striated pattern was visible (arrowheads), colocalizing with α-actinin. This indicates that GFP is interacting with some sarcomeric and Z-disk proteins.

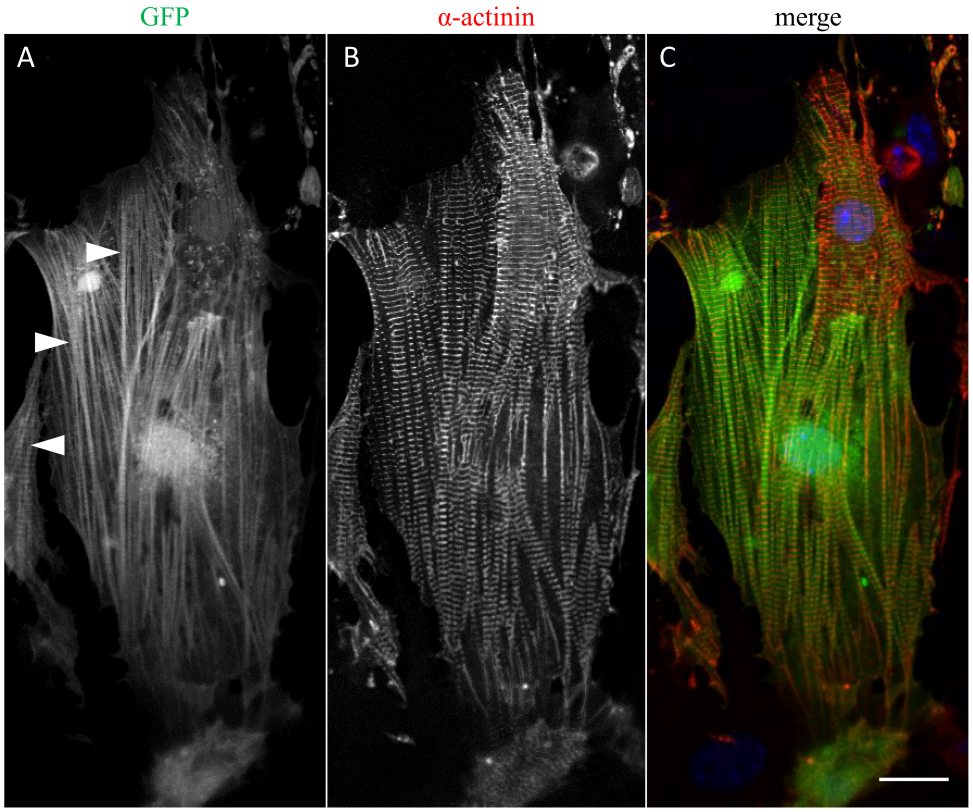

Figure 28: Subcellular Localization of GFP at the Sarcomere of Cardiomyocytes. Expressed in cardiomyocytes, GFP was not evenly distributed throughout the cell, but formed lines along the length of the cell (A). Those lines followed the α-actinin striation (B) and thus presumably visualized the sarcomeres within the cardiomyocyte. In some parts of the cells, a weakly striated pattern of GFP was found (arrowheads), which co-localized with α-actinin. Scale bar: 20 µm.

2.2.3.2 Infection of Cardiomyocytes With AAV Coding for MLP

When I transduced MLP$^{-/-}$ cardiomyocytes with AAV coding for WT MLP, the MLP localized in the cytoplasm of the cells (fig. 29). Occasionally, MLP co-localized with α-actinin. After treatment with 10% cyclic stretch for 24 h, WT MLP was also found in the nucleus of the cell, although a cytoplasmic staining was still present.
Due to shared time between Berlin and Paris, I did not have the possibility to evaluate the effect of the mutated forms of MLP.

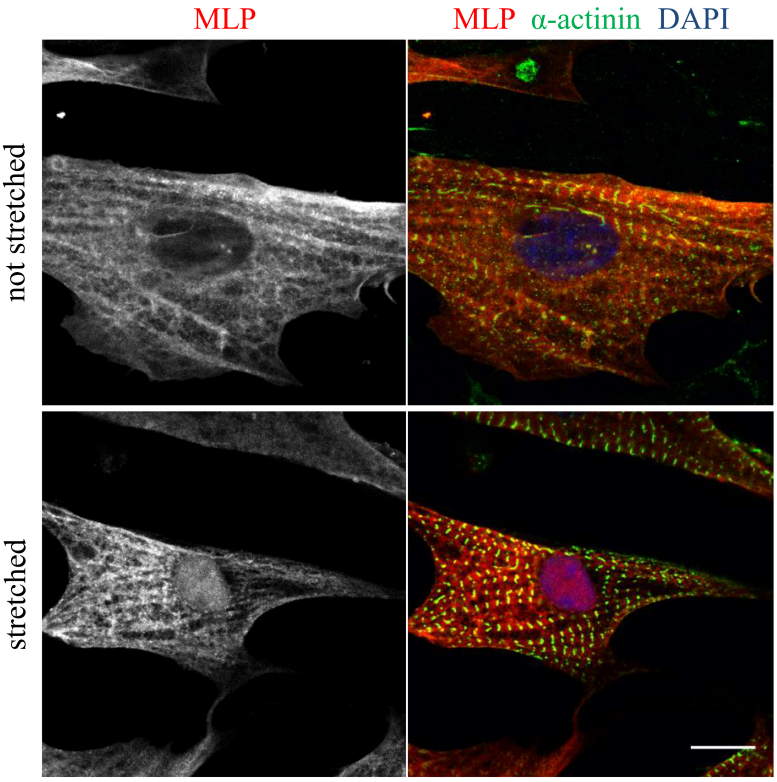

Figure 29: MLP$^{-/-}$ Cardiomyocytes Transduced with WT MLP. Cardiomyocytes from neonatal MLP$^{-/-}$ mice were transduced with WT MLP. When the cells were not stretched, MLP (red) was found in the cytoplasm of the cardiomyocytes, partially co-localizing with α-actinin (green). It did not localize to the nucleus. After stretching the cells for 24 h, MLP was additionally found in the nucleus of the cardiomyocytes. Nulei were visualized with DAPI. Scale bar: 10 µm.

2.3 Discussion

2.3.1 Cell Culture of Isolated Neonatal Cardiomyocytes

Cell culture of neonatal cardiomyocytes from mice is more complicated than from rat neonatal cardiomyocytes. Neonatal rat hearts are bigger and contain more cardiomyocytes, isolated cells adhere more easily to cell culture dishes and, as many antibodies are produced in mice but few in rat, the species-problem during immunostaining is hardly present.
On the other hand, mice are smaller and thus easier and cheaper to breed in the animal facility. Furthermore, with the first genetically modified rat generated in 2009, transgenic rat models are not yet common in the laboratories around the world (Geurts *et al,* 2009; Kawaharada *et al,* 2015). As we got MLP$^{-/-}$ mice (from Arber *et al,* 1997, via Laugwitz group at the German Heart Centre), we started the isolation of neonatal cardiomyocytes from mouse hearts despite the known difficulties in the cell culture.

It has not been reported before that the litter from MLP$^{-/-}$ mice was smaller in number than that of WT mouse lines. As the offspring of MLP$^{+/-}$ mice were born in the expected mendelian ratio (own observations and Arber *et al,* 1997), the fewer number of pups is not because homozygous knock-out pups die prenatally. It is more likely that the cardiac phenotype of the MLP$^{-/-}$ mothers lead to an insufficient supply with nutrients of the embryonic pups.

Besides cardiomyocytes, there are fibroblasts, endothelial cells, smooth muscle cells and other cell types present in the heart (Nag, 1979). 90-95% of non-cardiomyocytes are cardiac fibroblasts (Eghbali *et al,* 1988). During the first days after birth, the portion of cardiac fibroblasts rises dramatically, reducing the percentage of cardiomyocytes (Banerjee *et al,* 2007). At this time, the heart is remodeled to adapt to the changes in blood pressure due to the switch from embryonic to neonatal blood flow.
Cardiac fibroblasts largely contribute to the extracellular matrix within the heart (Fan *et al,* 2012). Cardiomyocytes are embedded in a tightly regulated frame of collagen fibers, which are the major contents of the extracellular matrix. These fibers protect the cells against tension and, at the same time, enable the intercellular communication. Both biosynthesis and degradation of the contents of the extracellular matrix are important to keep a healthy heart.
In addition to the production of components of the extracellular matrix, cardiac fibroblasts seem to regulate cardiomyocyte growth and proliferation: Embryonic cardiac fibroblasts induced proliferation of embryonal cardiomyocytes, while adult fibroblasts induced their hypertrophy (Ieda *et al,* 2009). Thus, somewhere between embryonic day E 12.5 and an

age of eight weeks that were tested by Ieda *et al*, cardiac fibroblasts change their influence on cardiomyocytes. We cannot exclude that neonatal cardiac fibroblasts still have an influence on the proliferation ability of neonatal cardiomyocytes, which in neonatal rat are still proliferating during the first days after birth (Li *et al,* 1996; Li *et al,* 2005; Paradis *et al,* 2015).

With all these positive influences of fibroblasts, it was not my intention to completely remove these cells from the isolated cardiac cells. However, as non-cardiomyocytes proliferate fast, they soon overgrow the slowly or not proliferating cardiomyocytes (Ieda *et al,* 2009). For 2D cell culture, which were kept for a week, pre-plating was sufficient to remove a big portion of non-cardiomyocytes and to ensure that cardiomyocytes were not overgrown by fibroblasts during the culture time. In 3D culture, which I kept for three weeks, fibroblasts still proliferated too much, even after pre-plating. Fewer contractions within the gel were an easily visible result. AraC is cytotoxic during the S-phase of the cell cycle (Cozzarelli, 1977). Thus treatment of the 3D cultures probably not only diminuished the proliferating fibroblasts, but also affected the portion of proliferating cardiomyocytes. This led to only a small improvement of the contractility within the 3D gels. The depletion of glucose from the culture medium proved more effective. While non-cardiomyocytes depend on glucose for nutrition, cardiomyocytes can use lactate as source for metabolism, energy production and survival (Tohyama *et al,* 2013). Replacing glucose with lactate markedly increased contracting fields within the 3D gels. I did not test if fibroblasts underwent apoptosis, but by immunofluorescence, the nuclei of non-cardiomyocytes were still present. This indicates that contrary to the results of Tohyama et al, non-cardiomyocytes survived but did not further proliferate within the 3D gels.

2.3.2 Subcellular Localization of MLP

The subcellular localization of MLP has been discussed controversially in the literature (Henderson *et al,* 2003; Geier *et al,* 2008). It has been speculated that the differences in the localization were caused by the use of different antibodies (Gehmlich *et al,* 2008). Fig. 21 illustrates that even commercially available antibodies against MLP are not all specific. $MLP^{-/-}$ cardiomyocytes serve as a very good negative control, as they do not express any MLP. The sequence of CRP1 and CRP2, two other members of the protein family of which MLP is a member, resemble MLP in big parts, making it more complicated to chose an antigen for antibody production.

While the antibody against MLP from GeneTex revealed a Z-disk associated localization of its target in isolated cardiomyocytes of both $MLP^{-/-}$ and $MLP^{+/+}$ strains, none of the other antibodies used in this thesis indicated this highly restricted localization in MLP

expressing mice. The easiest explanation for this finding is that the GeneTex antibody was not detecting MLP but another Z-disk protein. As the company has not disclosed the antigen used for the production of their antibody, I cannot guess what the antibody really is detecting.

Using the home-made 79D2 antibody against MLP or the commercial one from Everest in neonatal cardiomyocytes, endogenous MLP was predominantly distributed diffusely throughout the cytoplasm (fig. 24). Only in tissue slides, MLP displayed an additional weak striated pattern, co-localizing with the Z-disk (fig. 23). But as I never tested for the localization of MLP in neonatal cardiac tissue slices or adult isolated cardiomyocytes, the possibility remains that the striated pattern of MLP is a result of the developmental stage of the cell and present in adult but not neonatal cardiomyocytes. It is possible as well that MLP associated to the Z-disk is not detected in intact cells by immunofluorescence because of cytoplasmic MLP background. If cytoplasmic MLP degrades or is washed out of cut cells from tissue slices prior to fixation, the contrast between cytoplasmic and Z-disk MLP would be accelerated, revealing a striated pattern.

When neonatal cardiomyocytes are stretched, MLP translocates from the cytoplasm to the nucleus (Boateng *et al,* 2007; Boateng *et al,* 2009). I could confirm these findings (fig. 24, fig. 29). However, when I treated 3D cultures of neonatal cardiomyocytes with stretch, I could not detect MLP in the nucleus of the cells (fig. 25). In 2D cultures, a stretch of 10% was a strong enough stimulus to lead to the translocation of MLP. In 3D, stretching of up to 18% did not lead to a change of MLP localization compared to non-stretched controls.
I considered three explanations, why I could not detect MLP in the nucleus of stretched cells in 3D cultures. (1): A mistake in the protocol of immunofluorescence. (2): A misfunction of the machine. The stretch was not applied correctly to the cells within the gel. (3): Stretching the cardiomyocytes does not lead to nuclear relocation of MLP in 3D cultures, only in 2D.
For hypothesis (1), I could show that the problem is not an insufficient permeabilization of the cell membrane or the nuclear membrane. Antibodies against YAP could detect the transcriptional co-activator in the nucleus of cardiomyocytes in 3D with the same protocol for immunofluorescence that did not work for MLP (fig. 26, protocol 2.1.2.9.2 on page 43). Although it is still possible that MLP is washed out of the nucleus until the cells are properly fixed, this is not very likely. Thus, I concluded that the unexpected localization of MLP is not a problem of the staining procedure.
To disprove hypothesis (2) and (3), I wanted to check for markers of cardiomyocte hypertrophy. For example, cardiomyocytes stretched in 2D express ANP and BNP (Knöll *et al,*

2002). If the machine was not working properly and stretch was not properly applied to the 3D cultures, no changes in the expression profile would be expected. However, if the cells were stretched properly and reacted accordingly by expressing a hypertrophic gene program (Frank *et al,* 2008), but MLP did not shuttle into the nucleus, many hypotheses about the function of MLP in the stretch sensing pathway would have been endangered. However, I did not have enough time to establish the protocol for isolation of RNA of 3D cultures, and subsequent qRT PCR for our group, as I was preparing to leave for Paris to work in the cooperation group of Gisèle Bonne as part of my cotutelle contract. Thus we hired a master student to test if stretching the 3D cultures changed the expression pattern of cardiomyocytes (Lange, 2015). However, she could not answer this initial question. Thus unfortunately, neither of the remaining two hypotheses could be proved wrong.

While a misfunction of the stretch machine would simply be annoying, the correct application of the stretch without the shuttling of MLP would be very interesting. However, so far, no report about the behaviour of MLP within cells in 3D cultures has been published. It is known that cells react differently on stimuli, depending on 2D and 3D culture conditions. The differentiation rate of C2C12 cells increased when the cells were plated on harder 2D plates, while it was found to be vice versa in 3D cultures with a higher differentiation rate in softer than harder 3D gels (Boontheekul *et al,* 2007). In the healthy heart, MLP also is not found in the nucleus of the cardiomyocytes, although the cells are constantly and repeatedly stretched (fig. 23, also Ecarnot-Laubriet *et al,* 2000). Thus, more experiments are needed to finally answer the question if MLP shuttles to the nucleus of isolated cardiomyocytes in 3D cell cultures.

3 Nesprin-1 in Mechanotransduction

3.1 Material and Methods

3.1.1 Material

3.1.1.1 Buffer and Solutions

If not further specified, buffers and solutions were prepared as aqueous solutions and stored at room temperature.

Protein extraction buffer	2% SDS, 250 mMol sucrose, 75 mMol urea, 1 mMol DTT, 50 mMol Tris-HCl, pH7,5
1 x TAE	10 x stock, Invitrogen, 15558-026
1 x TBE	10 x stock, Invitrogen, 15581-028
Tris-Glycine-Buffer	Thermo-Fisher, 28363
4% PFA	ChemCruz, sc-281692

3.1.1.2 Cell lines

Name	**Official Name**	**Mutation**	**Description**
LMNA-ΔK32	LMNA-ΔK32 P1 (Bertrand *et al,* 2014)	p.Lys32del	immortalized, CDK4+hTERT, selection neomycin and puromycin, *Gluteus maximus*, 13 years, male
Nesprin1-ΔKASH	Nesprin1, clone 12 (Mamchaoui *et al,* 2011)	p.Glu7854*	immortalized, CDK4+hTERT, selection neomycin and puromycin, paravertebral, 16 years, male
WT	8220, C1, clone 2 (Bertrand *et al,* 2014)	—	immortalized, CDK4+hTERT, selection neomycin and puromycin, paraspinal, 12 years, female

3.1.1.3 Culture media and supplements for *E. coli* and myoblasts

Culture medium	Contents
199 Medium	gibco, 41150-020
Ampicillin	50 mg/mL, sterile filtered
Aprotinin	Sigma-Aldrich, A1153. Stock: 33 mg/mL
C2C12 medium	DMEM, supplemented with 10 % FBS and 1 % Pen/strep
DMEM	gibco, 61965-026
DMSO	Dimethyl Sulphoxide Hybri-Max® (Sigma-Aldrich, D2650)
FBS	fetal bovine serum (gibco, 10270-106, lot 41A0523K)
Fibrinogen	Sigma-Aldrich, F8630. Stock: 200 mg/mL in 0.9% NaCl
Fibronectin	Sigma-Aldrich, F1141
Gentamicine	gibco, 15750
LB agar	32 g/L, autoclave 15 min at 121 °C
Myoblast Complete Medium	DMEM and 199 Medium in a 4:1 ratio, supplemented with 20 % FBS, 5 ng/mL human epithelial growth factor, 0.5 ng/mL bFGF, 0.2 mMol dexamethasone, 50 mg/mL fetuin, 5 mg/mL insulin and 0.25 mg/mL gentamicine
PBS	gibco, 20012-019
Pen/strep	gibco, 15140-122
Thrombin	Sigma-Aldrich, T7513. Stock: 100 U/mL
Trypsin	0.05 % trypsin-EDTA (gibco, 25300-054)

3.1.1.4 Soft Cell Culture Plates

Soft petri dish, 10 cm, 12 kPa	Matrigen, Petrisoft, PS100-EC-12
Soft petri dish, 3.5 cm, 12 kPa, glass bottom	Matrigen, Softview, SV3520-EC-12

3.1.1.5 Kits

Method	**Product, Manufacturer, Reference**
DNA gel extraction	NucleoSpin® Gel and PCR clean-up, Machery-Nagel, 740609
6 x DNA loading buffer	Gel Loading Dye Purple (6X), NEB, B7024S
DNA molecular weight standard	GeneRuler 1 kb Plus DNA Ladder, Fermentas, SM1331
EtBr	Ethidium Bromide Bottle Dropper (0.7 mg/mL, eurobio, GEPBET02
Maxi-Prep DNA	PureLink® HiPure Plasmid Maxiprep Kit, Invitrogen, K210007
Midi-Prep DNA	PureLink® HiPure Plasmid Midiprep Kit, Invitrogen, K210004
Mini-Prep DNA	NucleoSpin® Plasmid, Macherey-Nagel, 740588
Nitrocellulose membrane, 45 µm	Nitrocellulose Pre-Cut Blotting Membranes, Novex, LC2001
PCR cleanup	NucleoSpin® Gel and PCR clean-up, Machery-Nagel, 740609
PCR SuperMix	PCR SuperMix, Invitrogen, 10572-014
Polyacrylamid	40% Acrylamide/Bis Solution (29:1), Biorad, 1610146
Ponceau red staining	ATX Ponceau S red staining solution, Fluka, 09189-1L-F

protein concentration	Pierce BCA Protein Assay Kit, Thermo Scientific, 23227
protein molecular weight standard	PageRuler Prestained Protein Ladder, Thermo Scientific, 26616
siRNA transfection	HiPerFect Transfection Reagent, Quiagen, 301704
SYBR green	LightCycler® 480 SYBR Green I Master, Roche, 04887352001

3.1.1.6 Enzymes

Enzyme	**Manufacturer, Reference**
Antarctic Phosphatase	New England Biolabs, M0289
*Bam*H I	New England Biolabs, R3136
*Bsr*G I	New England Biolabs, R0575
Klenow Fragment	New England Biolabs, M0210
Nae I	New England Biolabs, R0190
Sac I	Promega, R6221
Sca I	New England Biolabs, R3122
T4 DNA ligase	New England Biolabs, M0202
Xba I	Promega, R6181

3.1.1.7 Antibodies & Co

Antigen	**source**	**Dilutions IF/WB**	**Manufacturer, Reference**
Emerin NCL	mouse	1 : 20 / —	Novo Castra, emerin-CE, clone 4G5
Fab fragment	—	1 : 23 / —	Jackson Imm. Res., 015-000-007
FHOD-1	mouse	1 : 100 / 1 : 1000	abcam, ab73443
Flag M2	mouse	1 : 100 / —	Sigma-Aldrich, F1804
GAPDH	rabbit	— / 1 : 1000	Santa Cruz, sc25778, lot I0413
goat, 568	donkey	1 : 500 / —	Life Technologies, A11057
LaminA/C	goat	1 : 100 / —	Santa Cruz, sc6215, lot E0411
mouse, 488	chicken	1 : 250 / —	Life Technologies, A21200
mouse, 488	goat	1 : 250, 1 : 500	Life Technologies, A11001
Nesprin 1, C-term	mouse	1 : 20	Glen Morris, MANNES1-A, 7A12
Nesprin 2	mouse	1 : 100 / —	Glen Morris, MANNES2-G, 4B5
NMMIIA	rabbit	1 : 200 / —	Abcam, ab24762
Phalloidin 568	—	1 : 400 / —	Interchim, FP-AZ0330
rabbit, 488	goat	1 : 500 / —	Life Technologies, A11008
rabbit, 568	goat	1 : 500 / —	Life Technologies, A11011
SUN-1	rabbit	1 : 500 / —	C3286
SUN-2	rabbit	1 : 1000 / —	A9180
Vinculin	mouse	1 : 200 / —	Sigma Aldrich, V9131

3.1.1.8 Oligonucleotides

3.1.1.8.1 Oligonucleotides for Cloning and Sequencing

Name	Sequence
FlagSyne1-part1-fw	5'-ACA AGG ACG ACG ATG ACA AAG ATA TGG CAA CCT CC-3'
FlagSyne1-part2-fw	5'-GAT ATC TAG ACG CCA CCA TGG ACT ACA AGG ACG ACG-3'
FlagSyne1-rev-ScaI	5'-CTT CAG TAC TTT ATC AGA GTG GAG GAG G-3'
GFP-S2	5'-ACC CTG GTG AAC CGC ATC GAG CTG-3'
MiniSyne1-seq-1rev	5'-GGC GAT AGT GAA AGC ATC CTC C-3'
MiniSyne1-seq-2.2	5'-AGT GGG TTC AGT ACA CAG C-3'
MiniSyne1-seq-3.2-rev	5'-GAG CCG ATT TCC AAT AAC ATG G-3'
MiniSyne1-seq-4	5'-GGA ATC CCA ACT CAG AGT AGC C-3'
FlagSyne1-rev-ScaI	5'-CTT CAG TAC TTT ATC AGA GTG GAG GAG G-3'
pRRL-01-fw	5'-GAC AGA TCC ATT CGA TTA GTG AAC G-3'
pRRL-02-fw	5'-AGT ATG GGC AAG CAG GGA GC-3'
pRRL-03-fw	5'-GTT CCA CTG AGC GTC AGA CC-3'
pRRL-04-fw	5'-CAT TCA AAT ATG TAT CCG CTC ATG-3'
pRRL-05-fw	5'-GAA AGC CTG AAC TCA CCG CG-3'
pRRL-Amp-fw	5'-GGA TCA TGT AAC TCG CCT TG-3'
pRRL-ColE1-fw	5'-AAC AGG AGA GCG CAC GAG G-3'
pRRL-Des-fw	5'-ACA TGG CAG GCA GGC TTT GG-3'
pRRL-HIV1-RRE-fw	5'-TTT GCT GAG GGC TAT TGA GG-3'
pRRL-Woodchuck-fw	5'-ACT GTG TTT GCT GAC GCA ACC-3'

3.1.1.8.2 Oligonucleotides for Quantitative Real-Time PCR

Name	Sequence
qRT-β2-microglobulin-fw	5'-AGA TGA GTA TGC CTG CCG TG-3'
qRT-β2-microglobulin-rev	5'-GCG GCA TCT TCA AAC CTC CA-3'
qRT-FHOD1-fw	5'-GCA TTG AGA AGC TAC TGA CC-3'
qRT-FHOD1-rev	5'-CAT TCT GTA CCA GCT GTT CC-3'
qRT-RPLP0-fw	5'-CTC CAA GCA GAT GCA GCA GA-3'
qRT-RPLP0-rev	5'-ATA GCC TTG CGC ATC ATG GT-3'
qRT-SYNE2-fw	5'-TTA CTA AGG GCT TGC TTT GAG G-3'
qRT-SYNE2-rev	5'-GGC AGG TTC ATT TCA AGT TGA G-3'

3.1.1.8.3 Oligonucleotides for Small Interfering RNA

Name	Sequence
si-FHOD1-fw	5'-GCC ACU GUU UGA CCU GAA A-3'
si-FHOD1-rev	5'-UUU CAG GUC AAA CAG UGG C-3'

3.1.2 Methods

3.1.2.1 Nucleic Acids/Cloning

3.1.2.1.1 Polymerase Chain Reaction (PCR)

To multiply specific DNA sequences, PCR SuperMix from Invitrogen was used. For preparative PCR reaction, 45 µL PCR SuperMix was mixed with 10 pmol forward and reverse primer and 15 ng DNA template. A list with the primers used for cloning is given in section 3.1.1.8.1 on page 69. An example for a PCR program is given in table 2 on page 45.
For colony PCR, the tip for picking a bacterial colony (see chapter 3.1.2.1.7) was scratched on the bottom of a PCR tube before its addition to the culture medium. No additional DNA template was added. 9 µL PCR SuperMix and 10 pmol forward and reverse primers were added to the tube. The PCR program was the same as before, but with an elongated initial denaturation of 5 min to 10 min to destroy the bacterial cells and to set free their plasmid DNA.

3.1.2.1.2 Sequencing

For sequencing of double stranded plasmid DNA, 500 ng to 1000 ng plasmid were mixed with 50 pmol primer in a final volume of 15 µL. Sanger sequencing was performed by the Cochin Sequencing core facility from eurofins. A list with the primers used for sequencing is given in section 3.1.1.8.1 on page 69.

3.1.2.1.3 Agarose Gelelectrophoresis

The molecular weight of a DNA fragment was analyzed by agarose gelelectrophoresis. 0,5-2% Agarose were heated in TBE or TAE buffer until melted completely and mixed with EtBr. The samples were mixed with 6 x DNA loading buffer. GeneRuler 1 kb Plus DNA Ladder was prepared according to the manufaturer's specifications and applied to the gel next to the samples as reference for the molecular weight of DNA fragments. The electrophoresis was for 30 min to 180 min at 80 V to 130 V in TBE or TAE buffer, respectively, depending on the molecular weight of the DNA sample. The DNA in the agarose gel was visualized with an UV-transilluminator.

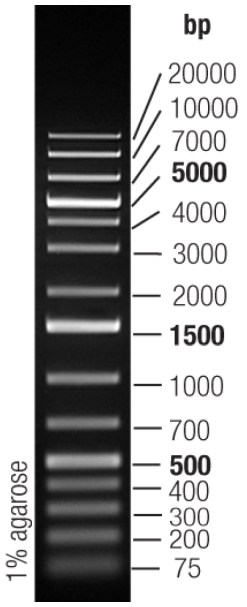

Figure 30: GeneRuler 1 kb Plus DNA Ladder, Fermentas, SM1331.

3.1.2.1.4 Gel Extraction and PCR Cleanup

To extract DNA from an agarose gel or to remove primers, dNTPs, enzyme and salts from a PCR reaction, the NucleoSpin® Gel and PCR cleanup kit from Macherey-Nagel was used according to the manufacturer's instructions.

3.1.2.1.5 Ligation of DNA fragments

Ligation of insert DNA with pGemT-easy: For singularization and further analysis of the products of a PCR reaction (3.1.2.1.1), the cleaned DNA (3.1.2.1.4) was ligated with pGemT-easy vector according to the manufacturer's instructions with a molar ration of vector : insert of 1 : 3.
Ligation of DNA with other vectors: Otherwise, T4 DNA ligase was used according to the manufacturer's instructions with the same molar ration of vector and insert.

3.1.2.1.6 Transformation of *E. coli*

A 20 µL aliquot of XL10-gold was thawed on ice and gently mixed with 5 µL of ligation reaction with pGemT-easy vector or 2 µL ligation reaction with another vector (3.1.2.1.5). After 5 min on ice, the bacteria were exposed to a heat shock of 42 °C for 40 s and again cooled on ice for 5 min. Bacteria containing pGemT-easy were directly plated on agar plates that contained 50 µg/mL ampicillin and that were topped with 100 µL of 0.1 M IPTG and 20 µL of 50 mg/mL X-gal. Bacteria containing other vectors were incubated for 30 min to 90 min at 32 °C in SOC medium prior to plating on agar plates containing 50 µg/mL ampicillin.

3.1.2.1.7 Isolation of Plasmid DNA from Bacteria

Analytical preparation (mini-prep): To isolate plasmid DNA from *E. coli* in an analytical amount, selective LB medium was inoculated with a single colony of a transformation (3.1.2.1.6) and incubated overnight at 32 °C or 37 °C. For isolation of the plasmid DNA, the protocol for high copy plasmids (pGemT-easy) or low copy plasmids (other vectors) was used according to the directions of Macherey-Nagel.
Preparative preparation (midi-prep): For a higher concentration of isolated plasmid DNA, the Midi-Prep Kit from Invitrogen was used according to their specifications for high and low copy number plasmids.
Preparative preparation (maxi-prep): For highest concentration of isolated plasmid DNA, the Maxi-Prep Kit from Invitrogen was used according to their specifications for low copy number plasmids.

3.1.2.1.8 Sequence Specific Restriction Digestion

For sequence specific restriction digestion of DNA, 1 unit restriction endonuclease was used per 1 µg plasmid DNA in an enzyme specific mixture of buffer and BSA in a final volume of 10 µL to 50 µL according to the specifications of the respective manufacturer. If required, the enzyme was inactivated by heating for 20 min at 85 °C. An aliquot of the digestion reaction was used for analysis of the obtained fragments by agarose gel electrophoresis (3.1.2.1.3). For further subcloning, DNA with a specific molecular weight was isolated from the agarose gel by gel extraction (3.1.2.1.4).

3.1.2.1.9 Blunting of Sticky Ends

To fill in 5' overhangs of a restriction digestion, DNA Polymerase I, Large (Klenow) Fragment from NEB was used. After sequence specific restriction digestion (3.1.2.1.8), Klenow fragment and dNTPs were added to the reaction mixture according to the instructions of the manufacturer. After 15 min incubation at 25 °C, the blunted DNA was isolated using the PCR cleanup kit (3.1.2.1.4).

3.1.2.1.10 Dephosphorylation

To prevent re-ligation of a vector that was opened by restriction digestion (3.1.2.1.8), 5' phosphate was removed by antarctic phosphatase from NEB. Antarctic Phosphatase Reaction Buffer and enzyme were added to a heat-inactivated restriction reaction (3.1.2.1.8) and incubated 30 min at 37 °C.

3.1.2.2 Cell Culture

3.1.2.2.1 Primary Human Myoblasts Isolation and Immortalization

In this thesis, I used three different immortalized human myoblast cell lines: WT, Nesprin1-ΔKASH and LMNA-ΔK32 myoblasts (chapter 3.1.1.2 on page 65). Human myoblasts have been isolated and immortalized as described by Mamchaoui *et al,* 2011 and Bertrand *et al,* 2014. Briefly, a muscle biopsy was taken from a patient or control person. The cells from the biopsy were expanded and sorted for myoblasts using anti-CD56 microbeads, which specifically bind myoblasts. For immortalization, cell lines were transduced with retroviral vectors coding for Cdk4 (cyclin-dependent kinase 4) to overcome a premature growth arrest and hTERT (human telomerase reverse transcriptase) for telomere elongation (Zhu *et al,* 2007). Transduced cells were selected by neomycin and puromycin resistancy and single clones were proliferated.

3.1.2.2.2 Culture of Immortalized Myoblasts

Thawing: Frozen cells were shortly warmed between fingers. 1 mL prewarmed culture medium was added to the cells to finally thaw the cells. All cells were transferred to a 10 cm petri dish and kept overnight in the incubator. The next day, the cells were trypsinized, counted and plated as described below.

Culture Conditions: C2C12 cells were cultivated in C2C12 medium and myoblast complete medium was used for human immortalized myoblasts. For 3D cultures, 33 µg/mL aprotinin was added to the myoblast complete medium for preservation of the fibrin matrix. The composition of the media is listed in 3.1.1.3 on page 66. All cells were cultivated at 37 °C and 5 % CO_2. Medium was changed every second day.

Trypsinization: To remove adherent myoblasts from a 10 cm petri dish, cells were washed with PBS and incubated with 3 mL prewarmed trypsin for 3 min to 5 min at 37 °C. The reaction was stopped by adding 7 mL DMEM. A 10 µL-aliquot was used for counting the cells in a Melasses chamber, while the cells were pelleted for 5 min at 400 x g. The cell pellet was resolved in 1 mL culture medium.

Division number: Human immortalized myoblasts divide. To keep track of the age of immortalized human myoblasts, the division number was calculated with the following formula:

$$\text{number of divisions} = \text{previous division number} + \frac{\log(\text{old \# cells}) - \log(\text{new \# cells})}{\log 2}.$$

Plating of myoblasts: For culturing cells in conventional petri dishes, no preparation of the plates was necessary. To cultivate human immortalized myoblasts on glass cover slides for immunofluorescence (see 3.1.2.5.1) or on soft surfaces, coating of the surfaces with 500 µg/mL fibronectin in PBS for at least one hour at 37 °C was mandatory. Before plating the cells, fibronectin was removed and the surface washed once with PBS. For plating C2C12 cells on conventional petri dishes or glass cover slides, no coating was necessary.

Generation of 3D culture gels: 3D cultures with human immortalized myoblasts were generated as described by Hansen *et al,* 2010 and Chiron *et al,* 2012. Briefly, casting molds were prepared with silicone spacers and 1.6 mL 2% agarose/PBS in 24 well plates. After hardening of the agarose, the silicone spacers were replaced by silicone post racks. Myoblasts were trypsinized and counted as described above. Per gel, $0.6 * 10^6$ myoblasts were mixed with 780 ng fibrinogen, 2 DMEM and myoblast complete medium on ice in a final volume of 145.5 µL. This was mixed with 4.5 µL thrombin (0.45 units) to start the polymerization of the fibrin and added to the agarose mold. After 2 h incubation at 37 °C, the gels were transfered to a fresh 24 well plate containing myoblast complete medium with 33 µg/mL aprotinin.

Inhibitors: To test the effect of the inhibition of SRC (SU6656), ROCK kinase (Y27632) and MLC kinase (ML7) on stress fiber formation, the inhibitors were added to the cells during plating in a final concentration of 10 µM (ML7, Y27632) or 25 µM (SU6656). Cells were fixed for immunofluorescence (chapter 3.1.2.5.1) or used for isolation of RNA or protein (chapters 3.1.2.3.1 and 3.1.2.4.1) 16 hours after plating.
siRNA: For knock-down of FHOD1, small interfering RNA (siRNA) was used. Transfection of myoblasts with siRNA was done with HiPerfect kit, according to the instructions of the manufacturer. The effect of the knock-down was analyzed 72 h after transfection.
Freezing and Storage: Myoblasts from one 10 cm petri dish were trypsinized and counted as described above. The cell pellet was resolved in 900 µL sterile filtered FBS and 100 µL DMSO. To assure a slow freezing rate, the tubes with cells were frozen at −80 °C in boites de congelation. After at least one day, the cells were stored in liquid nitrogen.

3.1.2.2.3 Transfection of C2C12 cells

20 000 to 40 000 C2C12 cells were plated in each well of a 6-well-plate with the culture conditions mentioned above. After at least 4 h, the cells were transfected with the Lipofectamine® 2000 kit. Briefly, 2 µg plasmid and 6 µL Lipofectamine® 2000 were each mixed with 100 µL OptiMEM. Both mixtures were combined, vortexed and incubated at room temperature for 10 min. Medium from C2C12 cells was replaced by 3 mL C2C12 medium. Transfection mix was added in drops to the cells. 4 h later at 37 °C, the medium was replaced with 3 mL fresh C2C12 medium. The transfection was analyzed after 48 h.

3.1.2.3 RNA Analysis

3.1.2.3.1 Isolation of mRNA from Immortalized Human Myoblasts

To prepare a culture of myoblasts for mRNA isolation, 600 000 cells were plated per 3 D-gel or 1×10^6 cells per 10 cm petri dish 16 h before RNA isolation.
To isolate mRNA from myoblasts cultured in 3 D-gels, RNeasy fibrous tissue kit was used according to manufacturer's instructions. For isolation of RNA from 2 D cultures, RNeasy kit was used according to manufacturer's instructions. For RNA isolation from transfected cells (chapter 3.1.2.2.3), three wells with the same conditions were merged, as many cells died during the transfection process. To remove the cells from soft surfaces, scratching was not possible, so 1 mL RLT buffer was pipetted over the 10 cm petri dish several times. RNA concentration and quality was measured with a NanoDrop.

3.1.2.3.2 Reverse Transcription

To transcribe isolated mRNA into cDNA, Superscript III was used with 500 ng RNA (from 3.1.2.3.1) and poly(dT)$_{20}$ primers, according to the manufaturer's instructions in a final volume of 21 µL.

3.1.2.3.3 Quantitative Real-Time PCR (qPCR)

For relative quantification of target gene molecules, SYBRgreen was used, that intercalates in double stranded DNA. 4 µL diluted cDNA was mixed with SYBRgreen and 5 pmol forward and reverse primer in a final volume of 10 µL in a LightCycler® 480 from Roche with the software version LCS480 1.5.0.39. Each reaction was performed in triplicates to detect pipetting errors. A list with the primers used for qPCR is given in section 3.1.1.8.2 on page 69.

Table 5: Example for a qPCR program with SYBR green

Initialization	95 °C	10 min	
Denaturation	95 °C	15 sec	40 - 50 cycles
Annealing	60 or 63 °C	30 sec	
Elongation	72 °C	15 sec	
Detection			
Final elongation	72 °C	10 min	

For analysis of the obtained CP values, the ΔΔCP-method was used. The housekeeping genes for *ribosomal protein, large, P0* (*RPLP0*) and β*2 microglobulin* were used as internal controls for normalization.

3.1.2.4 Analysis of Proteins

3.1.2.4.1 Isolation of Proteins from Immortalized Human Myoblasts

To isolate proteins from a common (hard) 10 cm petri dish, the cells were washed once with PBS and the PBS completely removed. The cells were subsequently scratched from the plate with 250 µL cold protein extraction buffer including protease and phosphatase inhibitors.
For protein isolation from soft 10 cm plates, cells were washed once with PBS. The PBS was removed completely. 250 µL cold protein extraction buffer including protease and

phosphatase inhibitors was added to the plate and pipetted over the plate for several times, as scratching was not possible.

3.1.2.4.2 Total Protein Quantification

The total protein content of a sample was measured with the BCA protein assay Kit with 10 µL diluted protein sample (1:10 in water) and 200 µL staining solution. The absorption was measured with an Asys UVM 340 Microplate Reader after either one hour incubation at 37 °C or overnight incubation at room temperature. A standard dilution series with 10 µL of each 2, 1, 0.5, 0.25, 0.125 and 0.0625 ng/µL BSA at the same incubation conditions was used to calculate the protein concentration of the samples. All samples and dilutions were done as triplicates.

3.1.2.4.3 SDS Polyacrylamid Gelelectrophoresis (SDS-PAGE)

20 µg protein was mixed with Laemmli buffer and was separated according to the molecular weight in an SDS polyacrylamid gel in SDS running buffer. As a molecular weight standard, PageRuler prestained protein ladder was used (fig. 31). At first, the proteins were concentrated for 20 min in the stacking gel at the boarder to the running gel at 80 V. The separation of proteins with different molecular weight occured at 130 V to 180 V for 60 min to 90 min in the running gel of 8 % to 10 %.

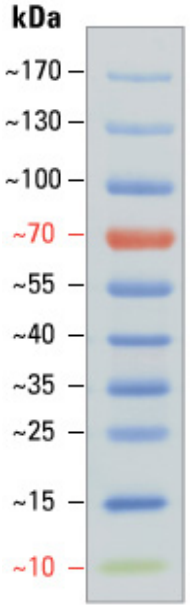

Figure 31: PageRuler Prestained Protein Ladder from Thermo Scientific (26616).

3.1.2.4.4 Western Blot

To transfer the proteins from the SDS-PAGE gel to a nitrocellulose membrane, a tank blot system was used. Precooled transfer buffer, an ice block and the setup in a cold room kept the blot cold during the transfer process. The transfer happened either at 400 mA for 2 h or overnight at 100 mA.
To visualize the success of the transfer, the nitrocellulose membrane was subsequently incubated for 10 min in Ponceau red staining solution. Excessive staining solution was removed with desalted water to reveal the protein bands. A picture was taken with a smartphone camera (Nexus 4). The Ponceau red staining was removed completely with tap water. To saturate free binding sites on the membrane, the membrane was incubated on a rocking shaker with 5 % milk powder/TBST for 1 h at room temperature or overnight at 4 °C. Incubation with the protein specific (primary) or species specific (secondary) antibody happened each for 1 h at room temperature in 1 % milk powder/TBST on a rocking shaker. After each incubation, unbound

antibodies were removed by three washes with TBST. For detection of secondary antibodies indirectly bound to the membrane, the HRP Immobilon Western kit was used in a G-Box from SYNGENE.

3.1.2.5 Microscopic methods

3.1.2.5.1 Immunofluorescence

16 h to 24 h after plating immortalized myoblasts on hard glass cover slides or soft 3.5 cm petri dishes with a glass bottom, cells were rinsed with PBS and fixed for 10 min in 4% PFA. After three washing steps with PBS to remove the PFA, the fixed cells could be stored at 4 °C in PBS.
To proceed the staining procedure, the cells were permeabilized for 5 min with 0.5 % Triton X100/PBS. Subsequent incubation for one hour at room temperature in 5% to 10% BSA/PBS reduced the unspecific background staining. For C2C12 cells, background resulting from mouse-on-mouse staining could further be reduced by incubation with 0.2 mg/mL Fab fragment/PBS for 1 h at room temperature.
Primary antibody incubation was either overnight at 4 °C or for 2 h at room temperature in 1% to 5% BSA/PBS. For double staining, primary antibodies were mixed. For labeling of filamentous actin, phalloidin was added to the primary antibody mixture. Excessive antibodies were removed by three washes with PBS, followed by incubation with secondary antibodies in 1% to 5% BSA/PBS for one hour at room temperature. Again, the cells were washed three times with PBS to remove unbound antibodies. All antibody dilutions are listed in section 3.1.1.7 on page 68.
Samples were mounted with Vectashield® containing DAPI and sealed with nail polish.

3.1.2.5.2 Measuring Cell Orientation

To measure the orientation of cells within 3D culture gels, cells were seeded within fibrin gels as described in chapter 3.1.2.2.2. 24 hours later, the gels were washed once with PBS and fixed for 10 min with 4% PFA. After three more washing steps with PBS, the gel was incubated with Phalloidin-568 in 2% BSA/PBS over night at 4 °C on a rocking shaker to stain for actin fibers. The next day, the gel was washed three times with PBS and mounted with DAPI containing Vectashield. It is important that the gel is oriented along the length of the microscope slide.
With a confocal microscope, pictures of the actin fibers were taken at different parts of the gel. The gel is oriented from left to right in the pictures. The angle θ between the cells towards the lower border of the picture was measured with Fiji and analyzed with Excel (Schindelin *et al,* 2012). The closer $\cos 2\theta$ to 1, the more aligned are the cells from tip to tip of the gel.

3.1.2.5.3 Measuring the Nuclear Size

To compare the size of nuclei from different cell lines, cells were plated on hard glass cover slips, fixed and stained as described for immunofluorescence (section 3.1.2.5.1). Pictures of the DAPI staining of the samples were taken with a Zeiss axiophot fluorescence microscope. The size of the DAPI staining was used as the nuclear size. This was measured with FIJI and analyzed with Excel (Schindelin *et al,* 2012). The nuclei were clustered according to their size. To test if the two datasets were from differed, a two-sided Kolmogorov-Smirnov-test was used.

3.1.2.6 Statistics

Excel 2010 was used to calculate and plot mean values and standard error of the mean. Statistical significance was evaluated with two-sided T-test. Differences between conditions were considered significant at $p < 0.05$.

3.2 Results

3.2.1 Characterization of Nesprin1-ΔKASH Myoblasts

Due to a nonsense mutation, Nesprin1-ΔKASH myoblasts lack the KASH domain of Nesprin-1 (fig. 32 A). The myoblasts were isolated from a patient with congenital muscular dystrophy harboring the mutation c.23560G>T, changing the codon triplet from GAA to TAA. This results in a substitution of the aminoacid E7854 by a stop codon. In this chapter, the immortalized myoblasts are characterized regarding the subcellular localization of Nesprin1-ΔKASH protein and the localization of other proteins of the nuclear envelope. They will be compared with LMNA-ΔK32 myoblasts from another patient with congenital muscular dystrophy with a missing aminoacid in Lamin-A/C.

3.2.1.1 Subcellular Localization of Nesprin1-ΔKASH and LMNA-ΔK32

As the KASH domain integrates Nesprin-1 in the nuclear membrane, I was wondering about the subcellular localization of the mutant protein.
An antibody binding an antigen near the C-term of Nesprin-1 (fig. 32 A) revealed that the WT protein localized to the nucler rim (fig. 32 B, D), but this antibody was not recognizing the mutant protein (fig. 32 C).
7C8, another antibody detecting Nesprin-1, should be able to detect the mutant protein (fig. 32 A). However, the immunofluorescence stainings showed a distribution pattern of Nesprin-1 proteins similar to the MANNES1-A antibody with nuclear rim localization of the WT protein and no detection of Nesprin1-ΔKASH (fig. 32 E-G).
Lamin A/C could be detected at the nuclear rim of all three cell lines (fig. 32 H-J). Additional nucleoplasmic staining of A-type lamins was found in LMNA-ΔK32 myoblasts (fig. 32 J).
Taken together, while Nesprin1-ΔKASH could not be detected, LMNA-ΔK32 showed a nucleoplasmic localization in addition to its normal localization at the nuclear rim.

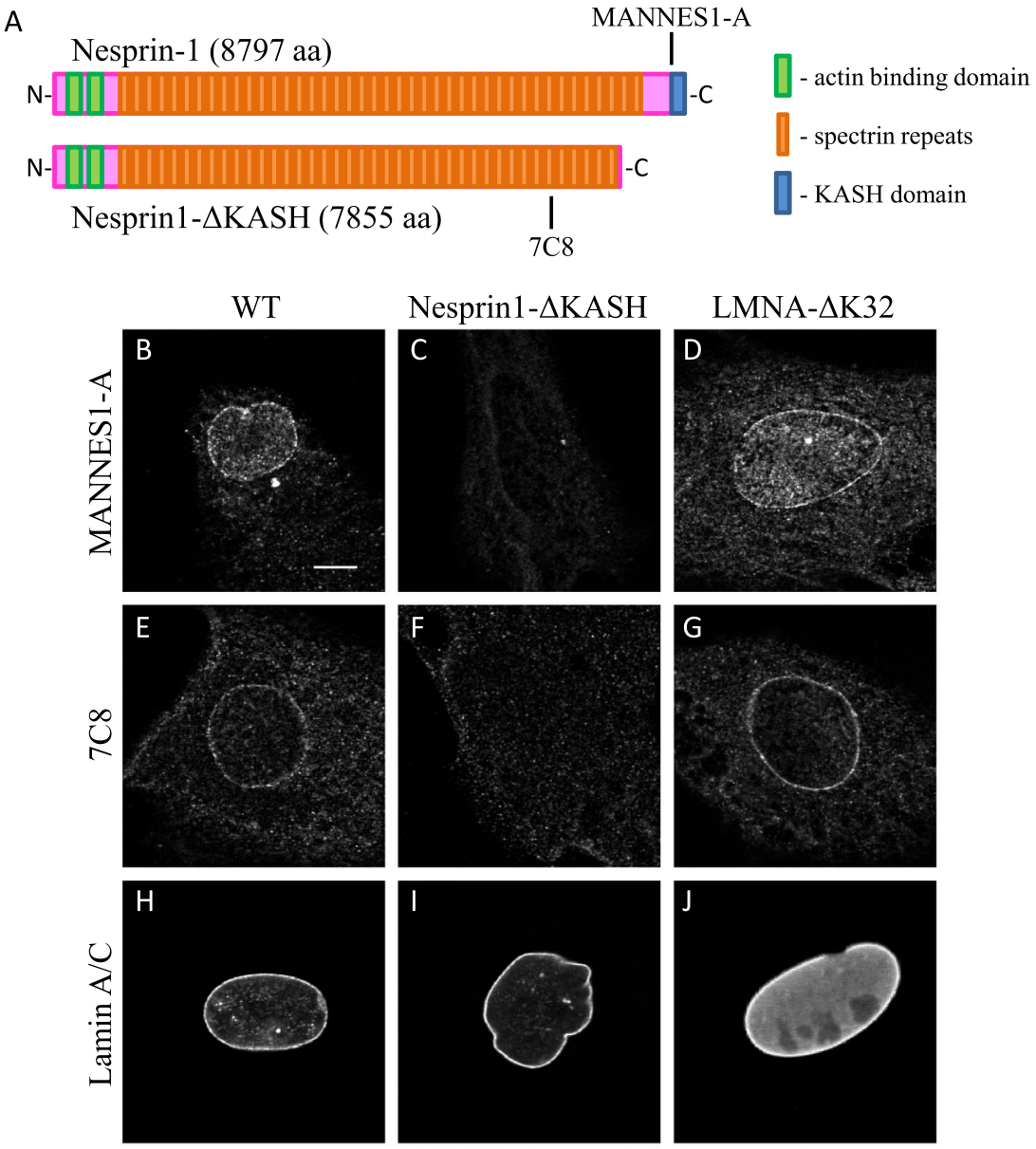

Figure 32: Subcellular Localization of Nesprin-1 and Lamin A/C in WT, Nesprin1-ΔKASH and LMNA-ΔK32 Myoblasts. A: Schematic presentation of the protein domains of Nesprin-1. The mutated protein Nesprin1-ΔKASH misses the C-term of the full-length protein. The binding areas of antibodies against Nesprin-1 are indicated. MANNES1-A, the antibody recognizing the C-terminus of Nesprin-1, indicated a nuclear rim localization in WT and LMNA-ΔK32 myoblasts (B, D), but did not bind to Nesprin1-ΔKASH (C). 7C8, an antibody against Nesprin-1 that binds more N-terminally, showed a similar localization of the WT protein in WT and LMNA-ΔK32 myoblasts (E, G), but did not detect any protein in Nesprin1-ΔKASH cells (F). Lamin A/C localized to the nuclear rim in all three cell lines (H-J), with additional nucleoplasmic localization in LMNA-ΔK32 myoblasts (J). Scale bar: 5 µm.

3.2.1.2 Subcellular Localization of Other Nuclear Envelope Proteins

As Nesprin-1 could not be detected in Nesprin1-ΔKASH myoblasts, I wondered if other proteins from the nuclear envelope were mislocalized. However, the subcellular localization was not different for Emerin, SUN-1 and Nesprin-2 in Nesprin1-ΔKASH and LMNA-ΔK32 myoblasts compared with WT myoblasts (fig 33). SUN-2 showed nucleoplasmic localization in addition to its nuclear rim localization in Nesprin1-ΔKASH myoblasts.

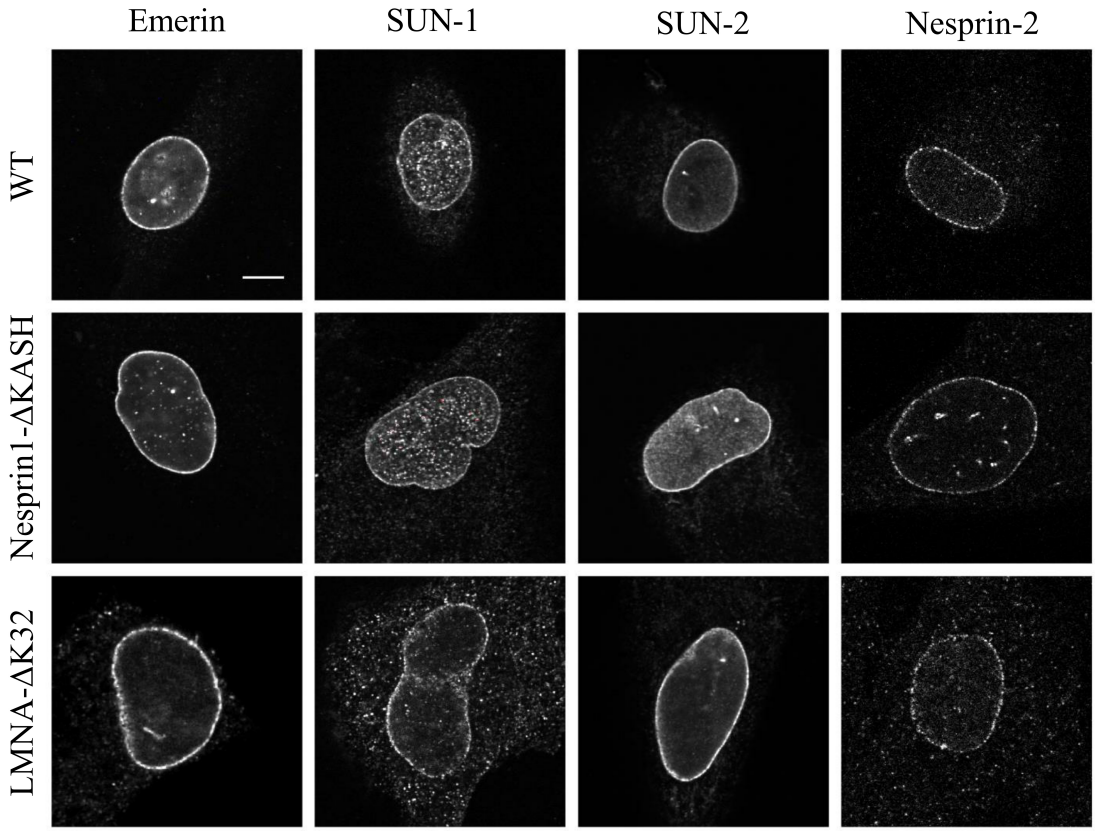

Figure 33: Localization of Emerin, SUN proteins and Nesprin-2 at the Nuclear Envelope. Emerin, SUN-1, SUN-2, and Nesprin-2 that are all localized at the nuclear envelope in WT myoblasts, have a similar localization pattern in Nesprin1-ΔKASH and LMNA-ΔK32 myoblasts. Some nucleoplasmic staining was found for SUN-2 in Nesprin1-ΔKASH myoblasts, but not in WT and LMNA-ΔK32 myoblasts. Note the deformation of the mutant nuclei. Scale bar: 5 µm.

3.2.1.3 A Closer Look at Nesprin-2

As Nesprin-1 and Nesprin-2 share a high homology in their protein structure, I wanted to test if a higher expression of Nesprin-2 compensated for the missing Nesprin-1 KASH domain in Nesprin1-ΔKASH myoblasts. Quantitative realtime PCR analysis showed that *Nesprin-2* was not upregulated on RNA-level in Nesprin1-ΔKASH myoblasts (fig. 34 C).

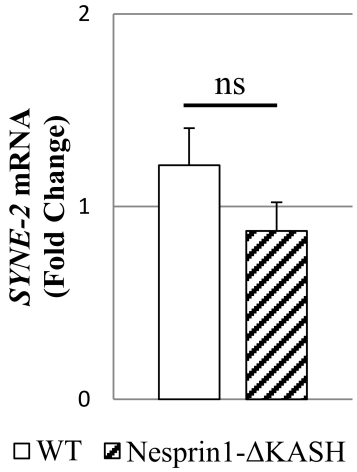

Figure 34: Quantification of Nesprin-2 on RNA Level. Expression of *SYNE-2* mRNA, normalized to *RPLP0* mRNA. n=3 for each cell line. Compared to WT cells, *Nesprin-2* is not upregulated in Nesprin1-ΔKASH myoblasts. ns: no significant difference.

3.2.1.4 Changes in the Nuclear Structure

While looking at the different immunofluorescence stainings, I found that many mutant nuclei differed from WT nuclei in size and form. Nuclear shape abnormalities have been described before for the LMNA-ΔK32 myoblasts (Bertrand *et al,* 2014). Thus I focused on nuclear deformations in Nesprin1-ΔKASH myoblasts.

On average, the Nesprin1-ΔKASH nuclei were 30 µm^2 bigger than WT nuclei (fig. 35 A). The size distribution pattern reveals that many nuclei from WT and Nesprin1-ΔKASH myoblasts had similar sizes, but while many WT nuclei tended to be smaller than 150 µm^2, more mutant nuclei were bigger than 250 µm^2 (fig. 35 B). This distribution pattern validated the observation that nuclei of Nesprin1-ΔKASH myoblasts often were bigger than those of WT cells.
More than 30% of Nesprin1-ΔKASH myoblasts displayed deformed nuclei to various degrees (fig. 35 C). Deformations included nuclear blebbing and invagination, as also seen in fig. 33). Only very few of the WT myoblast displayed similar deformations.

Taken together, the nuclei of Nesprin1-ΔKASH myoblasts were bigger and more often deformed than those of WT myoblasts. This indicates that the KASH domain of nesprin-1 is important to maintain the structure of the nuclear envelope.

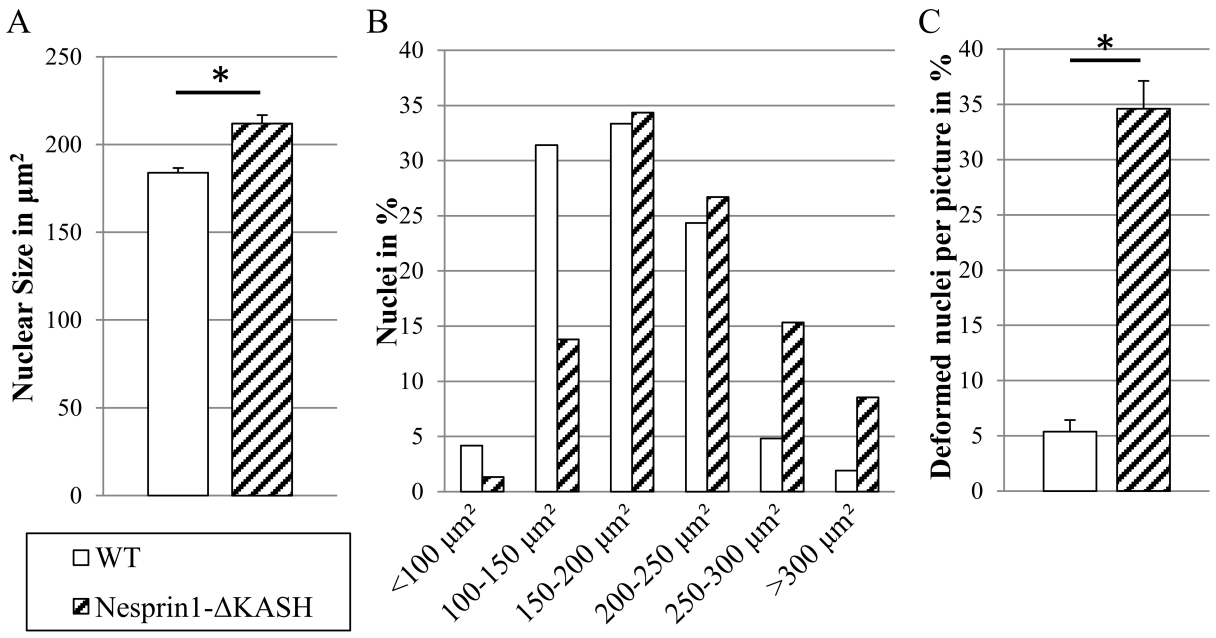

Figure 35: Nuclear Size and Malformation in Nesprin1-ΔKASH and WT myoblasts. A: Mean nuclear size of WT nuclei was smaller than that of Nesprin1-ΔKASH nuclei. *: two-sided T-test with $p<0.001$. B: The size distribution diagram shows that although many nuclei of both cell lines had a similar size, WT nuclei tended to be smaller than nuclei from Nesprin1-ΔKASH myoblasts. Both size distributions were significantly different, according to a two-sided Kolmogorov-Smirnov-test ($p<0.01$). WT n=360, Nesprin1-ΔKASH n=495. C: Nuclear malformations like blebbing and herniations occurred in about one third of the observed Nesprin1-ΔKASH myoblasts, while they were rarely seen in WT cells. WT n=414, Nesprin1-ΔKASH n=561.

3.2.2 Myoblasts in Stiff and Soft Environments

As described in the introduction, the recognition of the stiffness of the environment is important for myoblasts for a proper development (see table 1 on page 11). In this chapter, I will present results which indicate that Nesprin1-ΔKASH myoblasts have a defect in mechanotransduction. I will compare these cells with LMNA-ΔK32 myoblasts. It was shown before that these myoblasts have a defect in mechanotransduction (Bertrand *et al,* 2014).
Afterwards, I will test which pathways are disturbed in Nesprin1-ΔKASH and LMNA-ΔK32 myoblasts to further understand these defects in mechanotransduction.

3.2.2.1 Orientation of Myoblasts in Soft 3D Cultures

In three-dimensional (3D) tissue cultures that are fixed on two posts, internal tensions lead to a longitudinal alignment of myoblasts (Chiron *et al,* 2012). Without this tension, enclosed cells do not align. Our team found that myoblasts with homozygous mutation in the LMNA gene leading to a single missing aminoacid (LMNA-ΔK32) have a defect in mechanotransduction (Bertrand *et al,* 2014). I wanted to know if Nesprin1-ΔKASH

myoblasts displayed a similar phenotype, as Lamin proteins are directly interacting with proteins of the LINC complex.
The orientation of the cells was measured by $\cos 2\theta$ (fig. 36 C). The closer this value equals one, the more aligned the cells are with the gel axis.
Most WT myoblasts oriented themselves from tip to tip of the 3D gel, resulting in a $\cos 2\theta$ close to 1 (fig. 36 A, D). However, Nesprin1-ΔKASH myoblasts did not align properly, as seen in fig. 36 B, resulting in a low $\cos 2\theta$ (fig. 36 D).

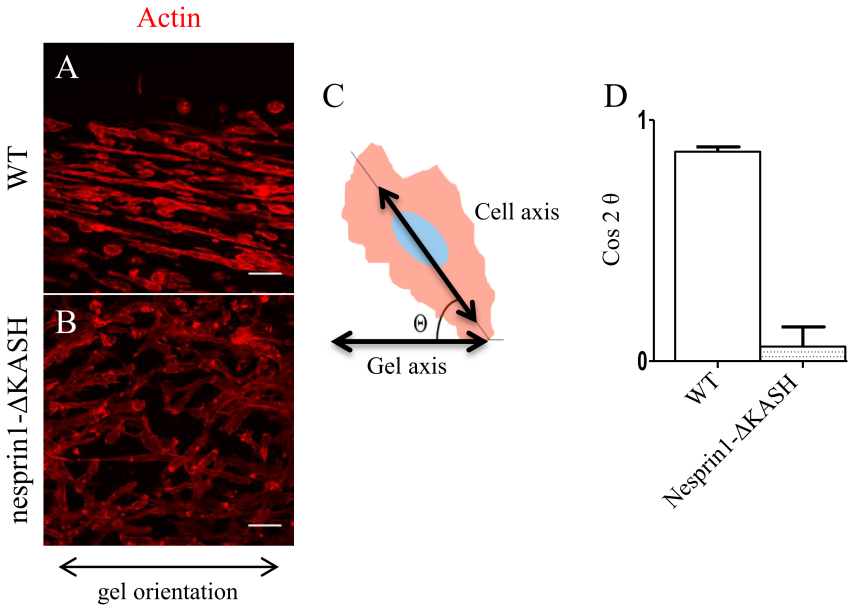

Figure 36: Orientation in 3D cell culture. A, B: In fibrin-based 3D gels, WT myoblasts aligned themselves from tip to tip of the gel along the gel axis. Nesprin1-ΔKASH myoblasts failed to orient themselves in this manner. Cells were stained with Phalloidin. Scale: 50 µm. C: The orientation of the cells was quantified by measuring the angle between the gel axis and the cell axis, θ. D: The closer $\cos 2\theta$ equaled to one, the more the cells aligned along the gel axis.

3.2.2.2 Cell Spreading in Stiff and Soft Environment

While cell spreading of WT myoblasts differs according to their substrate stiffness, LMNA-ΔK32 myoblasts did not adapt their spreading to the surface stiffness (Bertrand *et al,* 2014). I wanted to test to what extent this also is true for Nesprin1-ΔKASH myoblasts.

On glass cover slides, spreading area of WT, Nesprin1-ΔKASH and LMNA-ΔK32 myoblasts did not differ (fig. 37). Conventional cell culture plastic dishes and glass cover slips are quite stiff. This does not resemble the natural environment of myoblasts. To test how WT, Nesprin1-ΔKASH and LMNA-ΔK32 myoblasts react to softer environments, I plated them on soft petri dishes. The stiffness of 12 kPa resembles the stiffness of muscle tissue. With these soft conditions, the spreading area was lower for WT myoblasts, while

both LMNA-ΔK32 and Nesprin1-ΔKASH myoblasts did not reduce their spreading area accordingly but had a spreading area similar to that on stiff glass cover slides.
Together with the data from the 3D-orientation, we can assume that both Nesprin1-ΔKASH and LMNA-ΔK32 myoblasts have a defect in mechanotransduction.

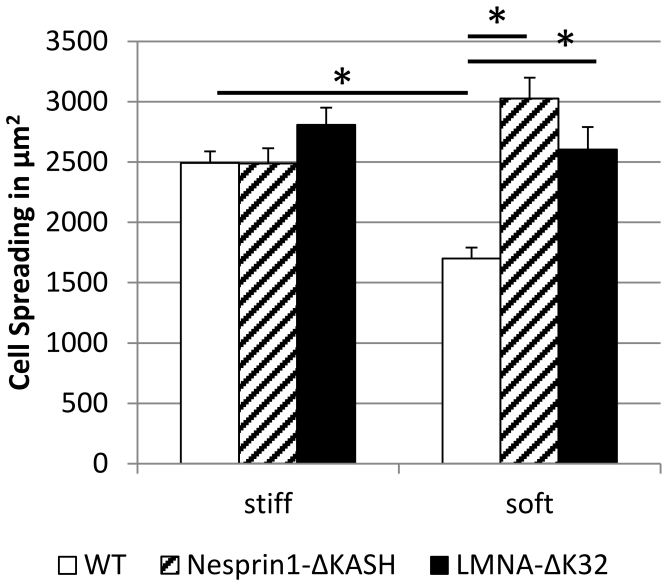

Figure 37: Spreading Area on Stiff and Soft Substrates. On stiff glass cover slides, the spreading area did not differ between the three myoblast cell lines. When cultured on soft tissue culture dishes, spreading area of WT cells was reduced, while Nesprin1-ΔKASH and LMNA-ΔK32 cells spread similar as on stiff surface. *: two-sided T-test with $p<0.001$. Only significant difference is figured. n=50-80 per cell line and culture condition.

3.2.2.3 The Actin Cytoskeleton in Stiff and Soft 2D Culture Conditions

As both Nesprin1-ΔKASH and LMNA-ΔK32 myoblasts were not able to align themselves according to the orientation of the 3D-gel, I was interested if the cells could sense differences regarding the stiffness of their environment.
On conventional stiff glass coverslips, WT, Nesprin1-ΔKASH and LMNA-ΔK32 myoblasts developed strong stress fibers, that were visualized by co-immunofluorescent staining of Actin and NMMIIa (fig. 38 A-C). Stress fibers were present in all parts of the cell, including the area dorsal of the nucleus and at the periphery of the cell (fig. 38 D-E).
When grown on those soft surfaces, differences between the WT and mutant cell lines became more obvious (fig. 39). In WT myoblasts, both actin and NMMIIa stainings were less prominent (fig. 39 A). Although some stress fibers could be found when zooming in (fig. 39 D, D'), they were fewer and thinner than on hard plates. Interestingly, actin fibers along the edges of the cell, that did not co-stain with NMMIIa, were still present (fig. 39 D').
In Nesprin1-ΔKASH and LMNA-ΔK32 mutant myoblasts, stress fibers were prominent also when grown on soft plates (fig. 39 B, C). A closer look at the area dorsal from the nucleus and at the cell periphery shows that stress fibers were strongly developed in both parts of the mutant cells.
Taken together, the differences between WT, Nesprin1-ΔKASH and LMNA-ΔK32 myoblasts were not big as long as the cells were plated on hard plastic dishes or glass. But

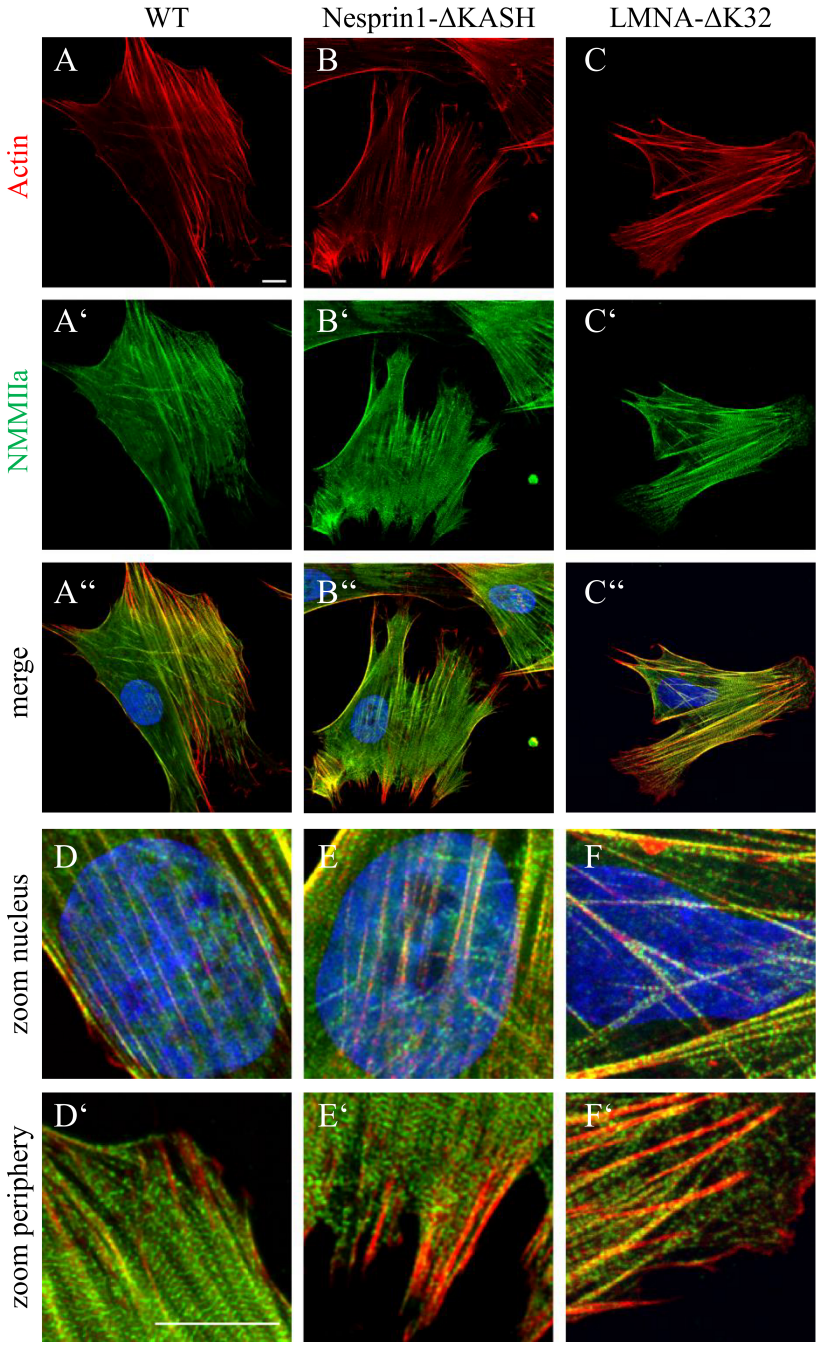

Figure 38: Actin Cytoskeleton on Stiff 2D Substrates. A, B, C: All three cell lines developed a strong actin cytoskeleton when cultured on conventional glass coverslips coated with fibronectin. A', B', C': Presence of NMMIIa at this actin cytoskeleton indicated that those actin fibers were actually contractile stress fibers. A", B", C": merge of actin (red), NMMIIa (green) and DAPI (blue) staining. D, E, F: Zoom to the nuclear area reveals that the stress fibers were also present dorsal of the nucleus. D', E', F': When zooming in at the periphery of the cells, the typical striated pattern of NMMIIa is visible.

when the cells were cultured on softer tissue culture plates that mimic the stiffness of muscle tissue, WT myoblasts reduced their stress fibers, while neither of the mutant cell lines adapted the actin cytoskeleton to the soft surface.

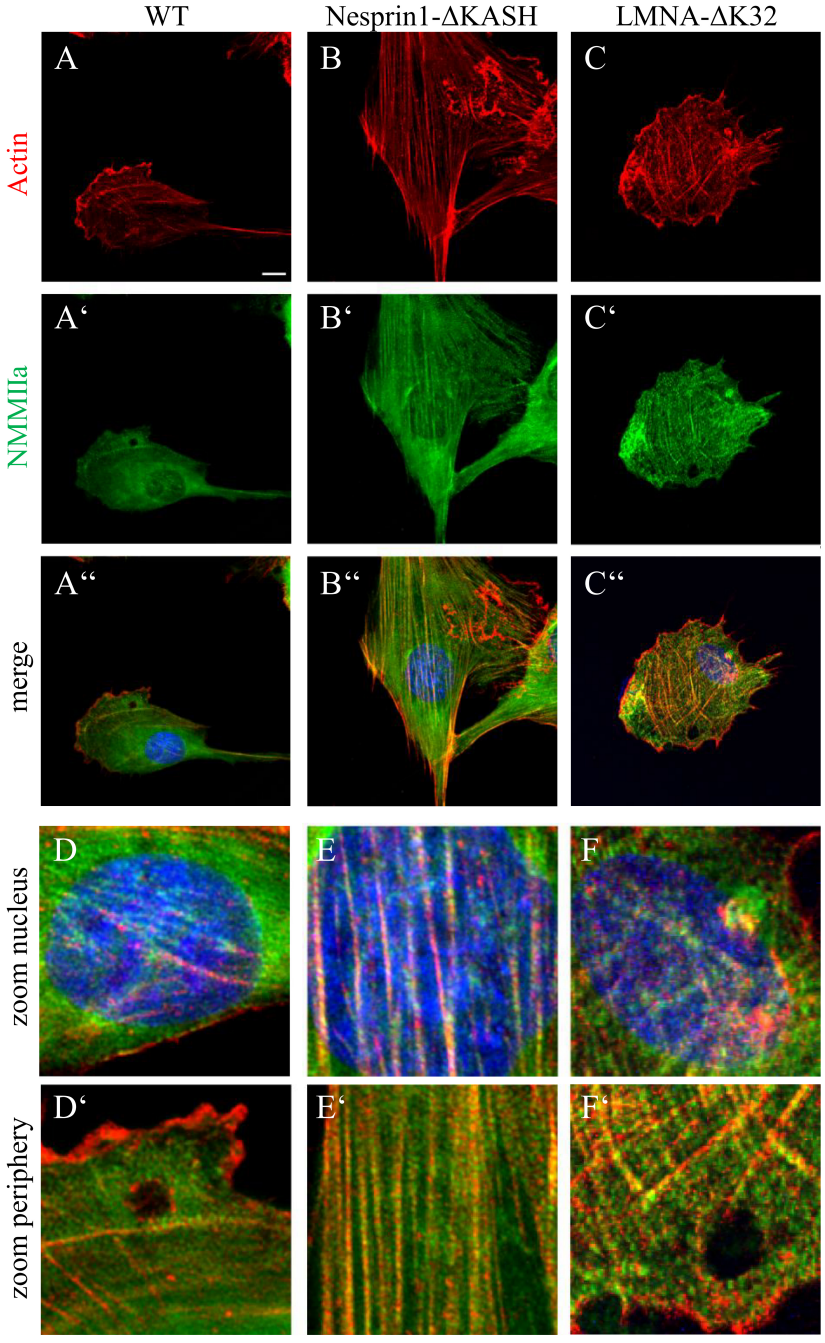

Figure 39: Actin Cytoskeleton on Soft 2D Substrates. A: In WT myoblasts, I found a reduced staining of actin fibers. A': The staining for NMMIIa was less prominent than on hard plates as well. B, C: The actin cytoskeleton of Nesprin1-ΔKASH and LMNA-ΔK32 myoblasts was still strong. B', C': At the same time, the NMMIIa staining was also strong, again indicating the presence of contractile actin stress fibers. A", B", C": Merge of actin (red), NMMIIa (green) and DAPI (blue) staining. D, D': Zooming in, some thin actin stress fibers could be found in WT myoblasts dorsal of the nucleus as well as in the cell periphery. Actin fibers that did not co-stain with NMMIIa were still present at the very edges of the cell membrane. E, E', F, F': Compared to the WT myoblasts, more and thicker stress fibers could be found in Nesprin1-ΔKASH and LMNA-ΔK32 myoblasts both dorsal of the nuclei and at the cell peripheries.

3.2.2.4 Focal Adhesions in Nesprin1-ΔKASH myoblasts

Some types of actin stress fibers are capped with focal adhesions, which connect the stress fibers to the outside of the cell. As I had found prominent stress fibers in Nesprin1-ΔKASH and LMNA-ΔK32 mutant myoblasts on soft surfaces, which were reduced in WT myoblasts, I tested if focal adhesions were more prominent in mutant myoblasts as well (fig. 40). I used vinculin as a marker for focal adhesions.
Focal adhesions were very prominent on stiff glass cover slides in WT, Nesprin1-ΔKASH and LMNA-ΔK32 myoblasts (fig. 40 A, B, C). In WT myoblasts, the vinculin staining was weaker on soft plates, indicating fewer and smaller focal adhesions (fig. 40 D). Compared to WT myoblasts, focal adhesions were more prominent in Nesprin1-ΔKASH and LMNA-ΔK32 myoblasts in soft culture conditions (fig. 40 E, F).
Overall, the mutant myoblasts again failed to adapt to the softer surface.

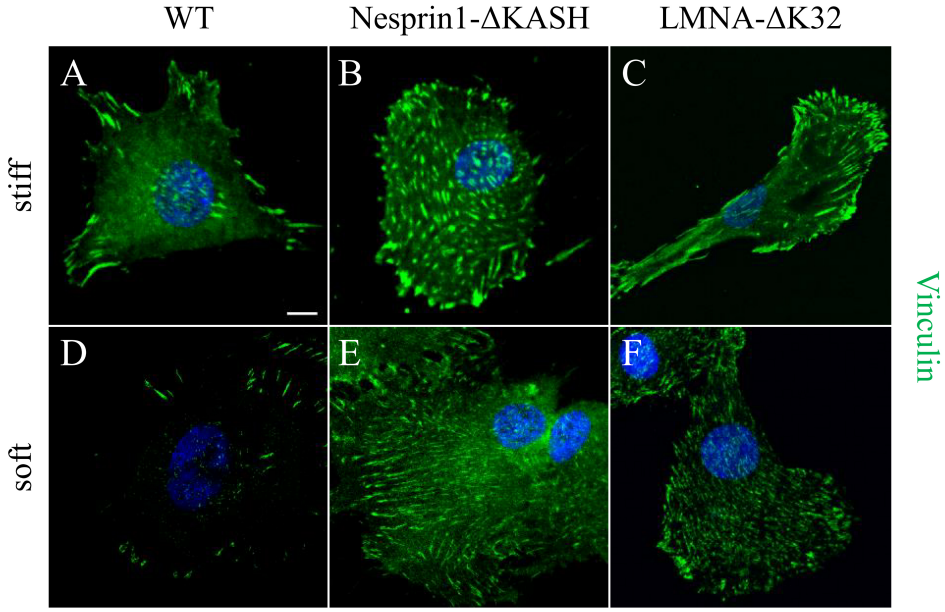

Figure 40: Focal Adhesions in Nesprin1-ΔKASH and LMNA-ΔK32 Myoblasts. A, B, C: When cultivated on stiff glass coverslips, all three cell lines developed many and big focal adhesions. D: When cultivated on softer plates, focal adhesions were reduced in WT myoblasts compared to hard culture conditions. E, F: Compared to stiff culture conditions, focal adhesions were also reduced in Nesprin1-ΔKASH and LMNA-ΔK32 myoblasts on soft surfaces. However, they were still bigger and more prominent than those from WT myoblasts on soft surfaces. Vinculin (green) was used as a marker for focal adhesions. Co-staining with DAPI (blue) for visualization of the nucleus.

3.2.2.5 Which pathway is disturbed in Nesprin1-ΔKASH and LMNA-ΔK32 myoblasts?

As presented in the introduction (chapter 1.2.3.2.3), NMMIIa is important for the generation of stress fibers (Cai *et al,* 2006; Goeckeler *et al,* 2008). NMMIIa can be activated via ROCK and MLC kinase. To figure out which pathway was disturbed in our mutant myoblasts, I treated the cells with different inhibitors targeting proteins upstream of NMMIIa.

3.2.2.5.1 Inhibition of MLC kinase

NMMIIa can be activated by MLC kinase (Katoh *et al,* 2001). This enzyme is inhibited by the compound ML7 (Reig *et al,* 1993). When ML7 was added to the Nesprin1-ΔKASH or LMNA-ΔK32 myoblasts growing on soft tissue culture plates, the cells formed some stress fibers (fig. 41). Stress fibers dorsal from the nucleus were prominent but thinner than without inhibitor (compare to fig. 39).
As ML7 only had a weak effect on Nesprin1-ΔKASH and LMNA-ΔK32 myoblasts on soft surfaces, I concluded that MLC kinase was not involved in the ectopic formation of stress fiber on soft surfaces.

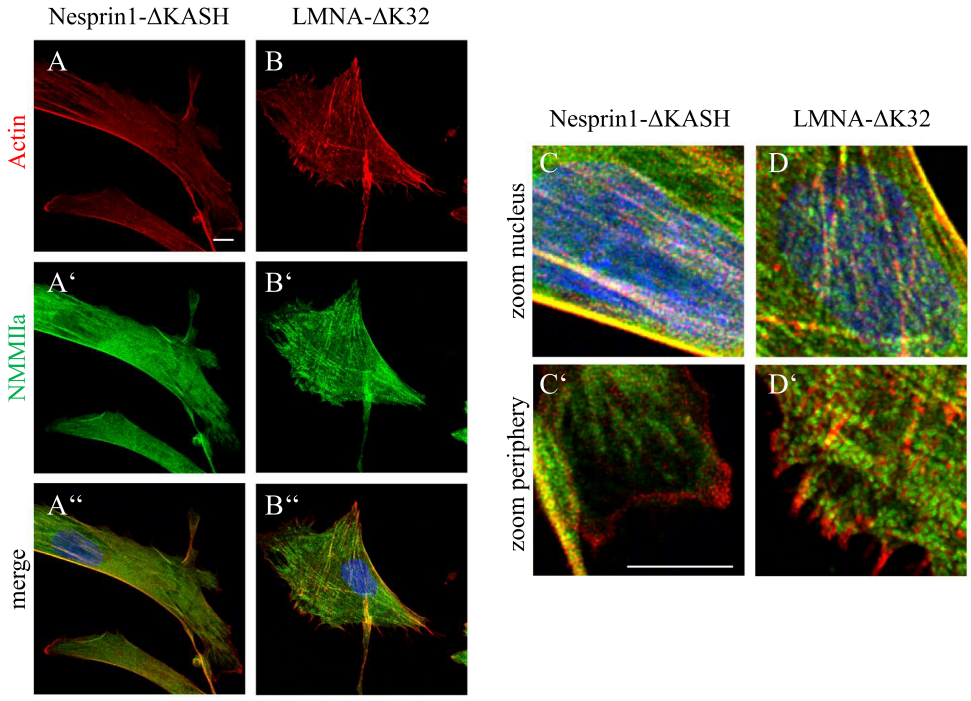

Figure 41: ML7, Inhibitor of MLC Kinase, Reduced Stress Fibers in the Cell Periphery on Soft 2D Substrates. A, B: Some stress fibers were detectable when Nesprin1-ΔKASH or LMNA-ΔK32 myoblasts were treated with the inhibitor of MLC Kinase. C, D: Stress fibers dorsal of the nucleus were more prominent than those at the cellular periphery. Scale bars: 10 µm.

3.2.2.5.2 Inhibition of the SRC-RhoA-ROCK-NMMIIa Pathway

NMMIIa can be activated via phosphorylation by MLC kinase, but also by ROCK proteins (Katoh *et al,* 2001). Y27632 is a specific inhibitor of ROCK (Uehata *et al,* 1997) To test if ROCK proteins are active in Nesprin1-ΔKASH and LMNA-ΔK32 myoblasts on soft substrates, I treated the myoblasts with the compound Y27632 during the plating.

Compared to the amount of actin fibers in myoblasts on soft plates without inhibitor (fig. 39), actin fibers were markedly reduced by the ROCK inhibitor in Nesprin1-ΔKASH and LMNA-ΔK32 myoblasts (fig. 42 A, B, C). Remaining actin fibers were not NMMIIa

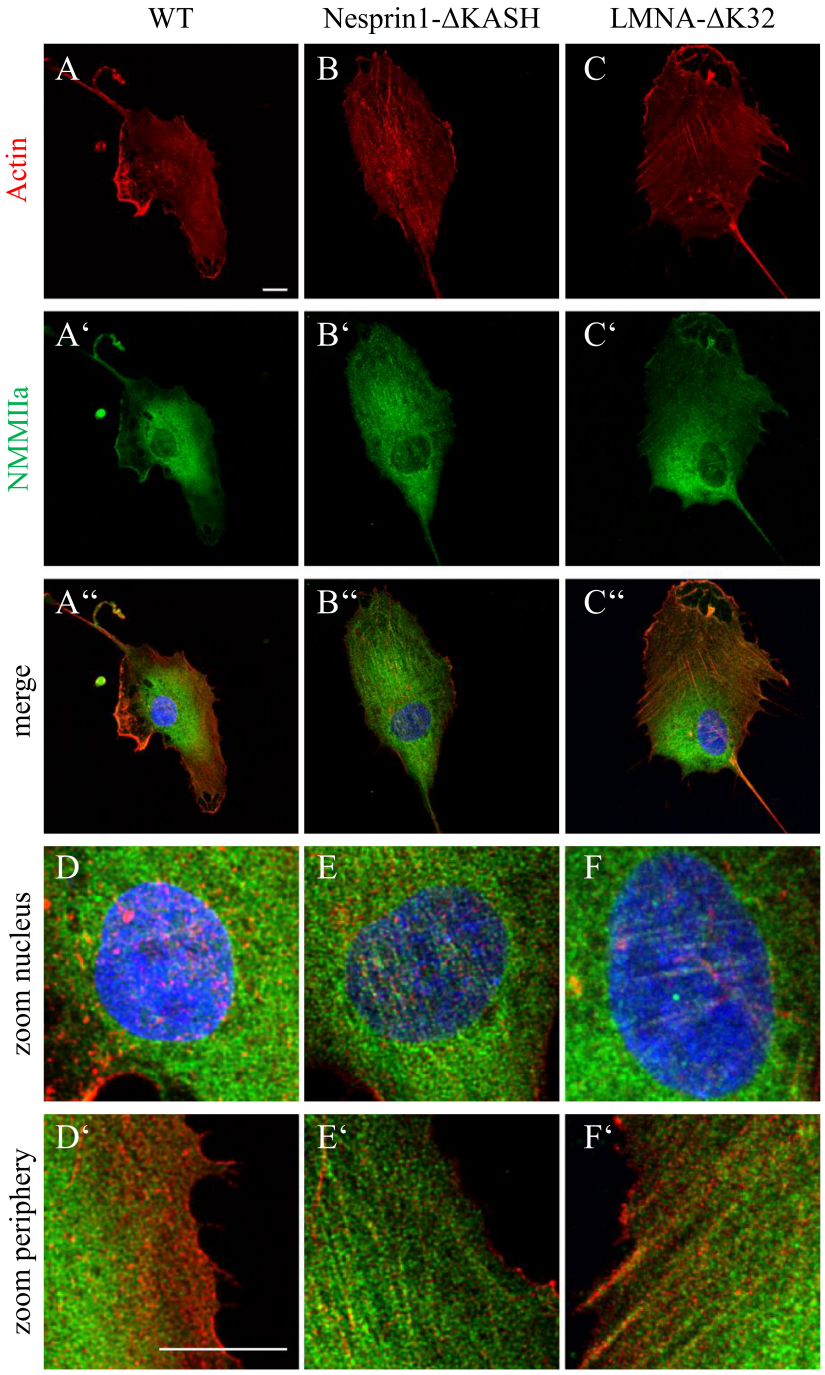

Figure 42: ROCK Inhibitor Y27632 Prevented Stress Fiber Formation on Soft 2D Substrates. A-C: The presence of Y27632 reduced the amount of actin fibers in all three cell lines. A'-C': NMMIIa was no longer organized in fibers. A"-C": merge of actin (red), NMMIIa (green) and DAPI (blue). D-F: No stress fibers were formed dorsal of the nucleus. D'-F': In the peripheral part of the cells, some actin fibers were present, but they did not co-localize with NMMIIa.

positive (fig. 42 A'-C").
Zooming in at the nuclear or peripheral part of the cells, no stress fibers were visible in WT and Nesprin1-ΔKASH myoblasts (fig. 42 D, D', E, E') and only very few and very thin ones in LMNA-ΔK32 myoblasts (fig. 42 F, F').
This indicates that an over-activity of ROCK led to the phenotype of Nesprin1-ΔKASH and LMNA-ΔK32 myoblasts.

Upstream of ROCK proteins, SRC activates RhoA kinase, which in turn activate ROCK. SU6656 is a potent inhibitor of SRC function (Blake *et al,* 2000). When SRC activity is blocked by the inhibitor, Nesprin1-ΔKASH and LMNA-ΔK32 myoblasts fail to develop stress fibers when plated on soft surfaces, neither dorsal of the nucleus nor in more peripheral parts of the cell (fig. 43).

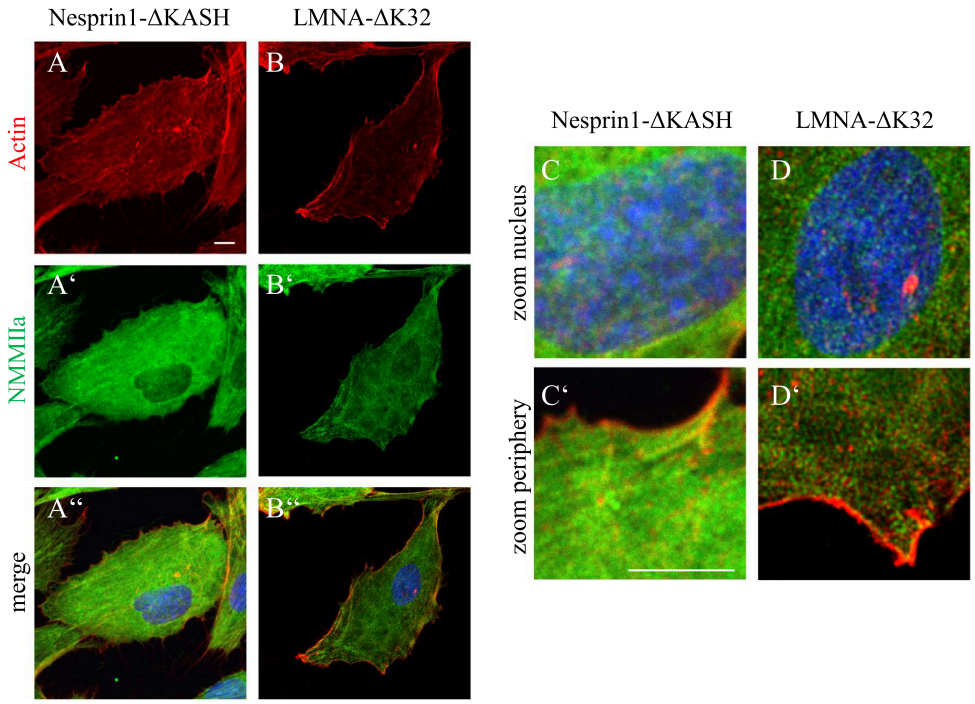

Figure 43: SU6656, Inhibitor of SRC, Prevented Stress Fiber Formation on Soft 2D Substrates. A, B: No stress fibers were visible when Nesprin1-ΔKASH or LMNA-ΔK32 myoblasts were treated with the inhibitor of SRC. C, D: No stress fibers could be found dorsal of the nucleus as well as in the periphery. The actin fibers that did not co-stain with NMMIIa were still present in both cell lines. Scale bars: 10 µm.

These results indicate that indeed the SRC-RhoA-ROCK pathway is active in Nesprin1-ΔKASH and LMNA-ΔK32 myoblasts and that an incorrect activation of this pathway caused the strong development of stress fibers in the mutant myoblasts.

3.2.2.5.3 FHOD1 in Soft Environment

Besides NMMIIa, the formin protein FHOD1 gets activated by ROCK, which leads to actin stress fiber formation (Hannemann *et al,* 2008; Takeya *et al,* 2008). As data from the previous chapter suggested that ROCK is more active in mutant than WT myoblasts on soft surfaces, I wanted to test if FHOD1 also is affected.

In immunofluorescence, there did not seem to be a big difference between WT, Nesprin1-ΔKASH and LMNA-ΔK32 myoblasts regarding FHOD1 on soft surfaces (fig. 44). The protein was found in a perinuclear localization as well as diffusely distributed in the cytoplasm in all three cell lines (fig. 44 A', B', C'). As before, the actin cytoskeleton was very prominent in Nesprin1-ΔKASH and LMNA-ΔK32 myoblasts (fig. 44 B, C), but not in the WT (fig. 44 A).

For quantification, total protein and mRNA were isolated from myoblasts on soft surfaces. On protein level, FHOD1 was upregulated in both mutant cell lines, compared with WT (fig. 45 A). FHOD1 mRNA was upregulated as well in Nesprin1-ΔKASH and LMNA-ΔK32 myoblasts (fig. 45 B).

To further investigate if FHOD1 is involved in the aberrant stress fiber formation in Nesprin1-ΔKASH and LMNA-ΔK32 myoblasts, I knocked-down FHOD1 by small interfering RNA (siRNA) in myoblasts that were cultivated on soft plates (fig. 46). While actin stress fibers were hardly present in WT myoblasts anyway (fig. 46 A and D), stress fibers

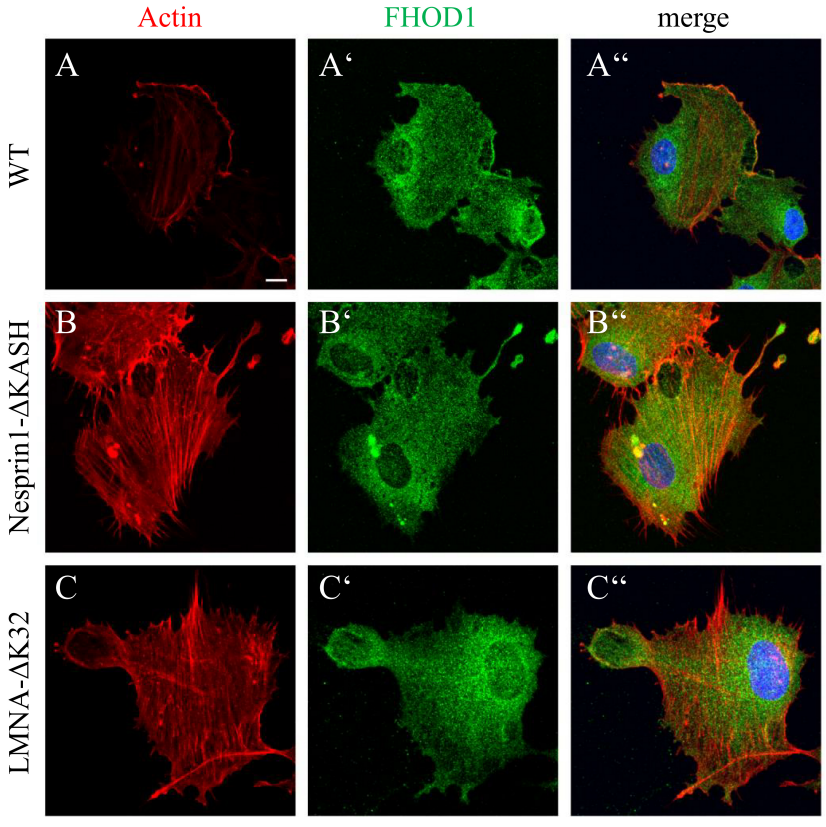

Figure 44: Subcellular Localization of FHOD1 on Soft Surface. A-C: As before, strong actin fibers could be found in mutant, but not in WT myoblasts. A'-C': FHOD1 was found diffusely distributed in the cytoplasm of all three cell lines, as well as concentrated in a perinuclear fashion. A"-C": Merge of Actin (red), FHOD1 (green) and DAPI (blue). Scale bar: 10 µm.

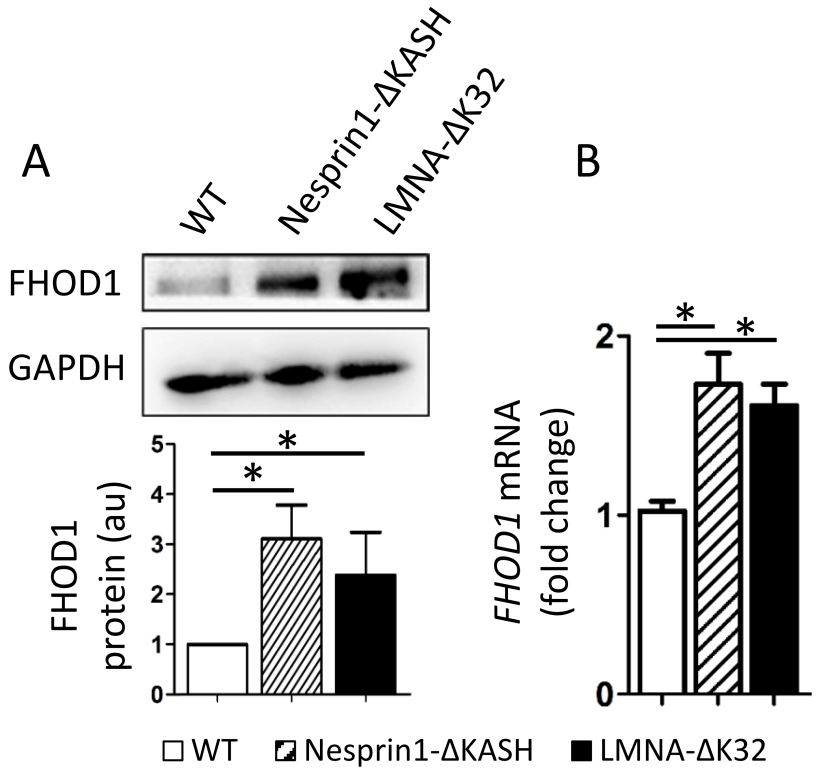

Figure 45: Quantification of FHOD1 on RNA and Protein Level. A: Representative western blot pictures of FHOD1 and loading control GAPDH. Below: quantification of FHOD1 protein over GAPDH, compared to WT. au: arbitrary units. n=3 for each cell line. B: Expression of *FHOD1* mRNA, normalized to β*2 microglobulin* mRNA. n=6 for each cell line. *: $p<0.05$ compared to WT.

were markedly reduced, although not abolished, in Nesprin1-ΔKASH and LMNA-ΔK32 myoblasts (fig. 46 B and E, C and F) compared to untreated mutant myoblasts (fig. 39). Taken together, FHOD1 is overexpressed in Nesprin1-ΔKASH and LMNA-ΔK32 myoblasts on soft surfaces. Knock-down of FHOD1 rescued the phenotype of the mutant myoblasts on soft surfaces by reducing the amount of actin stress fibers. This indicates that FHOD1 is involved in ectopic stress fiber formation in Nesprin1-ΔKASH and LMNA-ΔK32 myoblasts on soft surfaces.

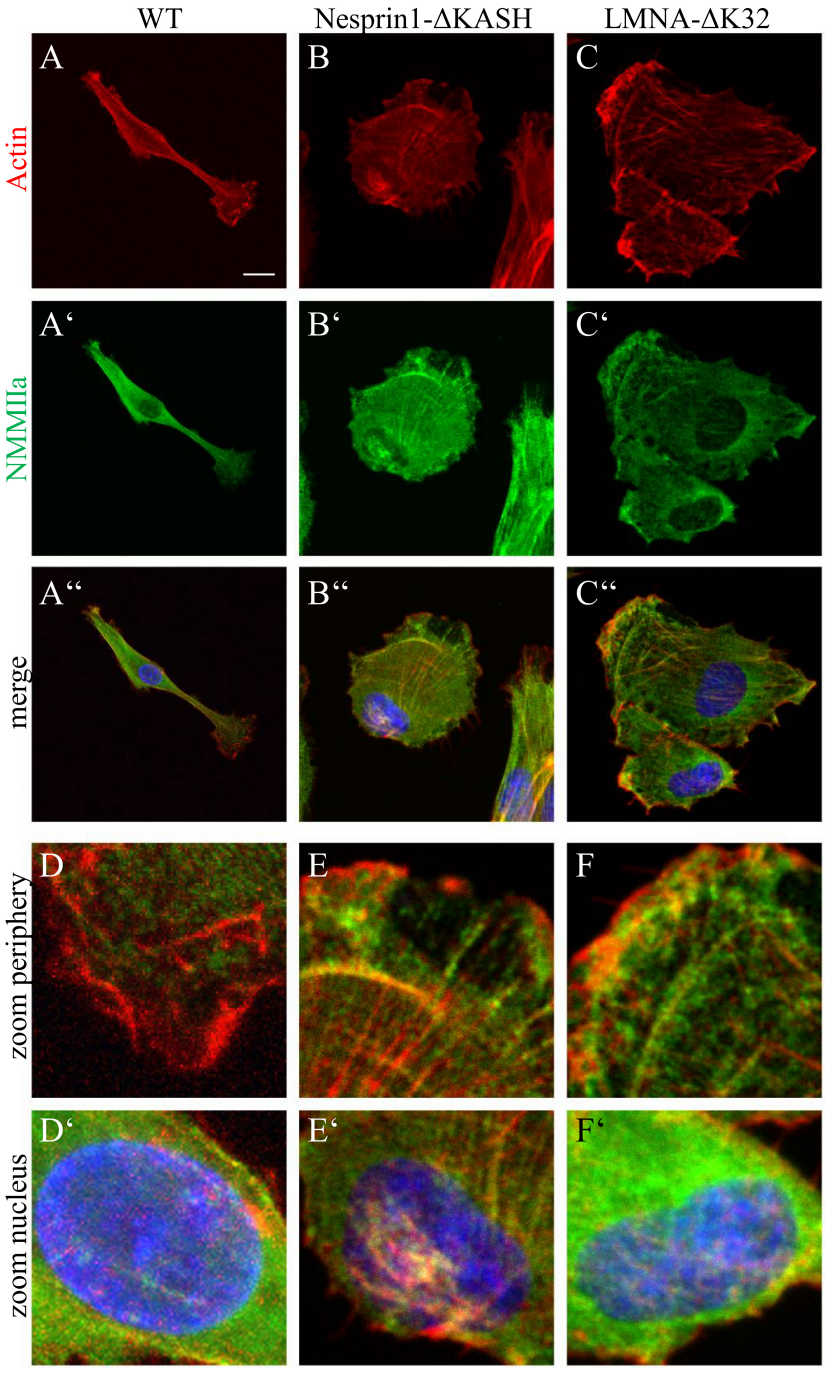

Figure 46: Reduction of Stress Fibers by siRNA Against FHOD1 on Soft Surface. A-C: After knock-down of FHOD1, actin bundles were markedly reduced in Nesprin1-ΔKASH and LMNA-ΔK32 myoblasts. A'-C': Consistantly, NMMIIa was no longer organized in a fibrous structure in all three cell lines. A"-C": Merge of Actin (red), NMMIIa (green) and DAPI (blue). D-F: Despite the general reduction of actin bundles, some stress fibers were still present in the cell periphery. D'-F': No stress fibers were found dorsal of the nucleus. Scale bars: 10 µm.

3.2.3 Cloning for Mini-Nesprin-1

To rescue the phenotype of Nesprin1-ΔKASH myoblasts, I wanted to stably express a mini-Nesprin-1 construct, comparably as described by Lu *et al,* 2012 for Nesprin-2. Mini-Nesprin-1 contains the n-terminal actin binding domains and the c-terminal KASH domain from Nesprin-1, but the long rod of spectrin repeats is missing (fig. 47A).

Starting point for the cloning was an expression vector coding for mini-Nesprin-1 coupled to GFP (Frédéric Aurade and Sestina Falcone) (fig. 47 B). To include the mini-Nesprin-1 sequence in pRRL, a flag and kozak sequence as well as restrictions sites were added by PCR. The GFP from the destination vector pRRL (fig. 47 C) was removed with restriction sites and replaced by mini-Nesprin-1 sequence linked to flag (fig. 47 D). With this construct, flag-mini-Nesprin-1 and a hygromycin resistance will be expressed in a bicistronic way under the regulation of a desmin promotor.

To test the construct, C2C12 cells were transfected with the final vector pRRL-MiniSYNE1 and stained for the flag sequence. However, none of the cells were positive for flag, while transfection with another pRRL vector (Flag-preLaminA, CMV promotor) was successfull (data not shown). To test if the cells were expressing any of the construct, RNA was isolated from the transfected cells 48 hours after transfection, transcribed to cDNA and used as a template for PCR with primers binding to the N- and C-term of the mini-Nesprin-1 construct. As an internal control, a PCR with primers targeting RPLP0 was performed with the same conditions as the qPCR (fig. 48). Controls were non-transfected cells (expected: mini-Nesprin-1 negative, RPLP0 positive) and reverse transcription without transcriptase (expected: both PCR negative). The mini-Nesprin-1 PCR was indeed negative for non-transfected cells, indicating that the PCR was specific. A strong signal was found for mini-Nesprin-1 in the transfected cell sample. However, a weak signal was found for the mini-Nesprin-1 PCR in the transcriptase negative control, indicating that a not all of the plasmid was digested during the RNA isolation procedure.

I concluded that although the plasmid had not been completely digested during the isolation of RNA, mini-Nesprin-1 was transcribed in the transfected myoblasts. Thus, the vector construct was ready for production of lentivirus.

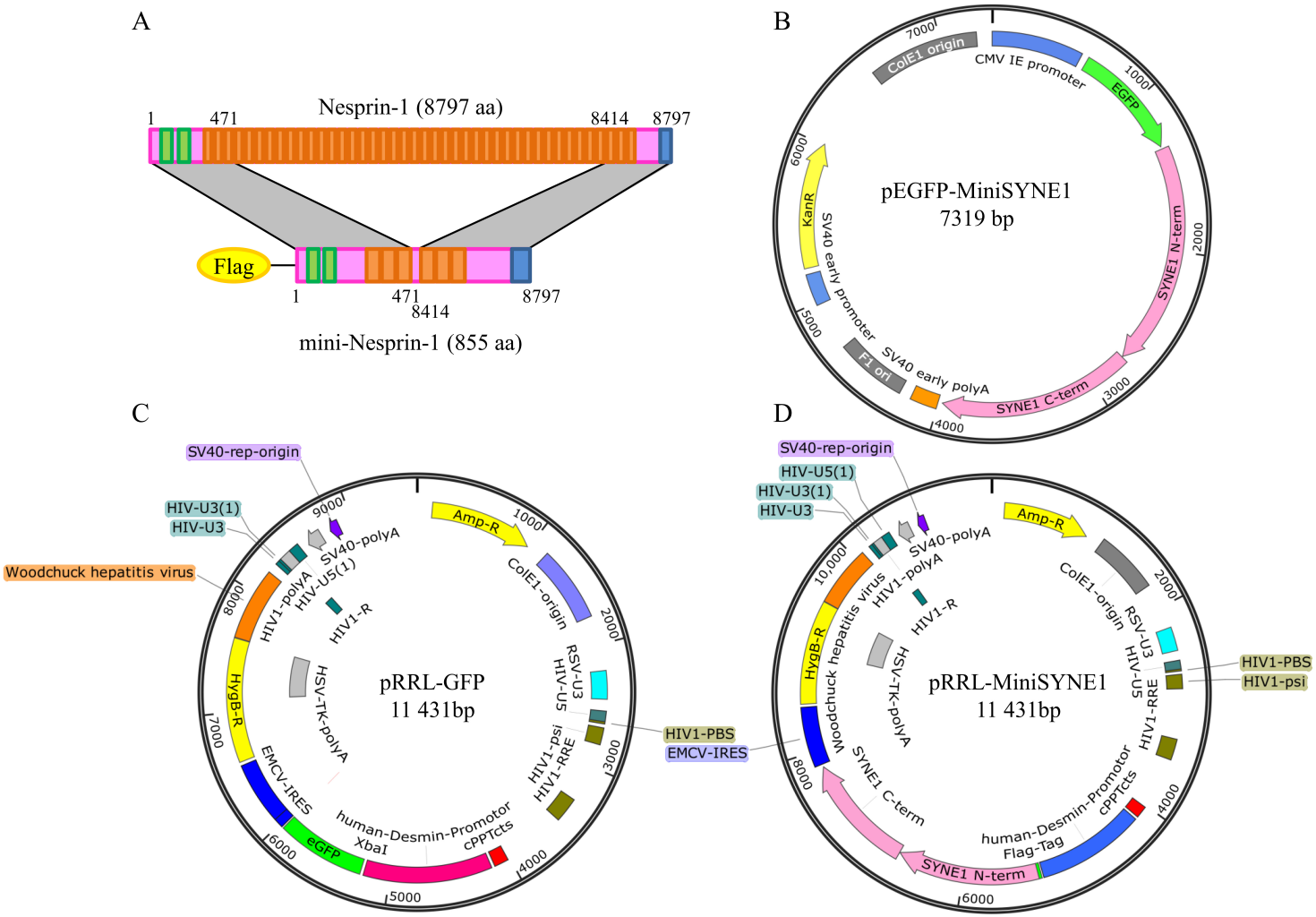

Figure 47: Cloning Strategy for Mini-Nesprin-1. A: Nesprin-1 giant contains a N-terminal actin binding domain (green), a long rod of spectrin repeats (orange) and a C-terminal KASH domain (blue). Mini-Nesprin-1 misses a big part of the rod, but contains the actin binding domain as well as the KASH domain and an additional flag tag (yellow). B: In the starting vector for cloning, the N- and C-termini from Nesprin-1 were already fused (pink), and linked to GFP (green). Additionally, you find a polyA tail (orange), origins of replication (grey), promotor (blue) and a kanamycin resistance (yellow). C: The destination vector contains a construct for bicistronic expression of GFP (green) and a hygromycin resistance (yellow), connected via an IRES sequence (dark blue), that are under the control of a desmin promotor (dark pink). A gene for resistance against ampicillin (yellow) and an origin of replication (blue) were important for amplification of the vector in *E. coli*. Some regions necessary for lentivirus production are indicated. D: To replace GFP with mini-Nesprin-1 and to add the flag tag, it was amplified by PCR and subcloned in pGemT-easy (not shown). For the replacement, restriction enzymes were used and the open destination vector was fused with the flag-mini-Nesprin-1 construct.

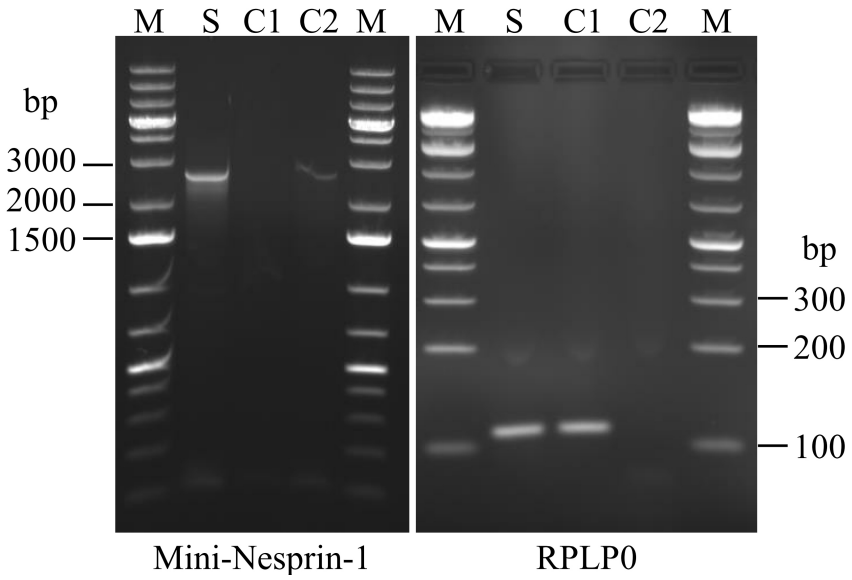

Figure 48: Control of Mini-Nesprin-1 expression by RT-PCR. To test if the mini-Nesprin-1 construct is expressed in C2C12 cells, RNA was isolated from transfected cells, transcribed into cDNA and used as a template for PCR detecting either mini-Nesprin-1 or endogenous RPLP0. S: cDNA from transfected cells. C1: cDNA from non-transfected cells. C2: mRNA from transfected cells, negative control from reverse transcription.

3.3 Discussion

3.3.1 Characterization of Nesprin1-ΔKASH Myoblasts

The LINC complex connects proteins within the nucleus with the different parts of the cytoskeleton. Nesprin proteins interact within the perinuclear space with SUN proteins that span the inner nuclear envelope to interact with nuclear proteins like lamins or emerin.
The patient harbouring a nonsense mutation in *SYNE-1*, the gene coding for Nesprin-1, expresses a truncated Nesprin-1 that lacks the C-terminal KASH domain. All KASH domain containing isoforms of Nesprin-1 should be affected (Rajgor *et al,* 2012). As this domain is important for the interaction of Nesprin-1 with SUN proteins, I was wondering if Nesprin1-ΔKASH still localized to the nuclear envelope.

The antibodies MANNES1-A and 7C8 found WT Nesprin-1 forming a ring around the nucleus (fig. 32). However, Nesprin1-ΔKASH could not be detected in the mutant myoblasts. In addition, 7C8, that according to its antigen should be able to detect the truncated protein, also failed to recognize Nesprin1-ΔKASH in western blot of Nesprin1-ΔKASH myoblasts proteins (Ian Hold, personal communication). This shows that Nesprin1-ΔKASH protein was not present in the mutant myoblasts.
This finding resembles the third mouse line generated to remove the KASH domain from Nesprin-1 (Zhang *et al,* 2010). There, too, a premature stop codon lead to Nesprin-1 knock-out mice. If Nesprin1-ΔKASH in the patient's cells was not properly transcribed or if the protein was translated but highly unstable cannot be answered at the moment. For this, RNA analysis (qRT PCR) would be necessary.
In patients with Emery-Dreifuss muscular dystrophy harboring point mutations in *SYNE-1*, a mislocalization of SUN-2 and Emerin has been found (Zhang *et al,* 2007a). In Nesprin1-ΔKASH myoblasts, only the latter localized only to the nuclear rim, while SUN-2 additionally was found in the nucleoplasm (fig. 33). This mislocalization of SUN-2 probably is a secondary effect not directly caused by a lack of Nesprin-1 at the nuclear rim, as the interaction with SUN proteins has been reported necessary for nuclear rim localization of Nesprin proteins, not vice versa (Crisp *et al,* 2006; Lei *et al,* 2009). The difference in localization of Emerin in cells with point mutations and our truncation of Nesprin-1 can be explained by the difference of the respective mutation. For SUN-1, A-type lamins and Nesprin-2, no difference in the subcellular localization between WT and Nesprin1-ΔKASH myoblasts could be detected.
As Nesprin1-ΔKASH was not present in the mutant myoblasts, I wondered if Nesprin-2 compensated for the missing Nesprin-1. Both proteins share a high homology. However, neither immunofluorescence nor qRT-PCR gave an indication that Nesprin-2 was over-

expressed in Nesprin1-ΔKASH myoblasts (fig. 34). The same was observed previously after knock-down of Nesprin-1 in endothelial cells (Chancellor *et al,* 2010). If the loss of Nesprin-1 at the nuclear envelope is compensated for prevention of a disturbance of the LINC complex, it is not done by Nesprin-2.

In contrast to the truncated Nesprin-1, LMNA-ΔK32 localized to the nuclear rim (fig. 32). However, the mutant Lamin proteins additionally were found in the nucleoplasm of LMNA-ΔK32 myoblasts, indicating some mislocalization. Common theories not only attribute lamin proteins with a stabilizing function of the nucleus, but also a gene regulatory function by its direct interaction with chromatin (Azibani *et al,* 2014). Thus, mislocalized A-type lamins might change the gene expression pattern in LMNA-ΔK32 myoblasts. Subcellular localization of Emerin, SUN-1, SUN-2, Nesprin-1 and Nesprin-2 was not affected by the nucleoplasmic localization of LMNA-ΔK32 protein.
On the other hand, the similarity between the phenotypes of Nesprin1-ΔKASH and LMNA-ΔK32 mutant myoblasts indicate that a change in the interaction between LMNA-ΔK32 and the chromatin is not the main cause of the phenotype. Although an interaction between Nesprin-2 and chromatin has been reported (Rashmi *et al,* 2012), such an interaction is not known from Nesprin-1. Thus rather than directly influencing gene expression, it is more likely that a disturbance in the signal transfer either from the LINC complex into the nucleus or in the other direction from the nucleus to the cytoskeleton through missing Nesprin-1 or mutated A-type lamins is the main cause for the observed defects in mechanotransduction in Nesprin1-ΔKASH and LMNA-ΔK32 myoblasts.

During immunofluorescence, nuclear deformations like blebbing and invaginations in Nesprin1-ΔKASH myoblasts were quite striking (fig. 32, fig. 33, fig. 35). Nuclear deformations are often found in patients harbouring mutations in proteins of the LINC complex, in the LMNA gene or in Emerin (Capell and Collins, 2006; Zhang *et al,* 2007a; Azibani *et al,* 2014; Bertrand *et al,* 2014). This shows that this multiprotein complex is important for maintaining the structure of the nucleus. But how?

It was shown that the small Nesprin-3 interacts with the actin binding domains of Nesprin-1 and Nesprin-2. Thus, both giant Nesprin proteins, anchored in the nuclear envelope by their KASH domains, bend down to interact with Nesprin-3 that is similarly anchored in the nuclear envelope (Lu *et al,* 2012; Taranum *et al,* 2012). That way, while the nuclear lamina stabilizes the nucleus from the inside, Nesprin proteins form a cage around the nucleus, further stabilizing its structure (fig. 49, Dahl *et al,* 2004; Lu *et al,* 2012). If Nesprin1-ΔKASH is no longer located at the nuclear envelope and Nesprin-2 is not compensating for the loss of Nesprin-1, gaps might occur in this cage that allow the nucleus to partially deform. In accordance with this model, if a mini-Nesprin-2 construct is expressed that lacks the long rod domain, the nuclei are significantly smaller (Lu *et al,* 2012). It is easy to imagine that a relaxation of this network leads not only to deformed but also to bigger nuclei.

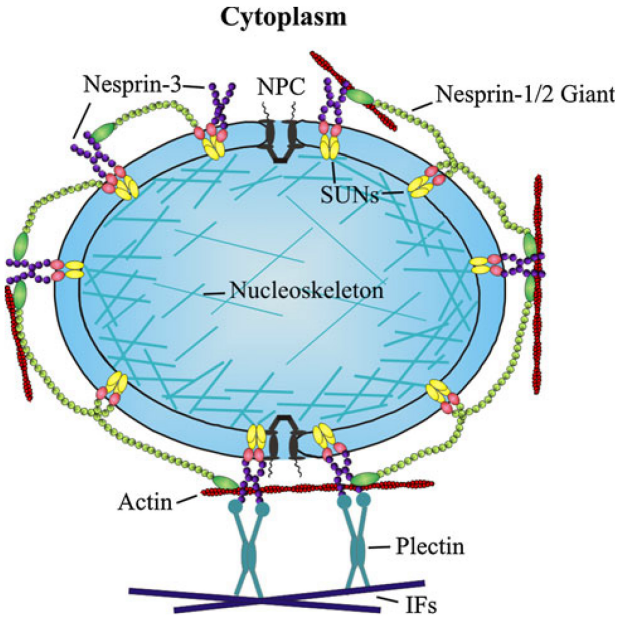

Figure 49: Nesprin Protein Cage Model. In this model, the interaction of nesprin-1, -2 and -3 are depicted around the nucleus together with their connection to actin and IFs. With the actin binding domain at the N-terminus, nesprin-1 and nesprin-2 not only interact with actin but also bind the smaller nesprin-3. That way, the nesprin proteins form a cage around the nucleus. From Lu *et al,* 2012.

Nuclear blebbing is a feature of nuclear envelopathies, that involve mutations in the genes coding for A-type lamins and Emerin (Capell and Collins, 2006). Nuclear deformations that I found in Nesprin1-ΔKASH myoblasts incdicate that mutations in A-type lamins, Emerin and Nesprin proteins disturb a common pathway or protein complex necessary to maintain the nuclear structure.

Taken together, the characterization of Nesprin1-ΔKASH myoblasts revealed that the truncated Nesprin1-ΔKASH is not present. All of the other tested proteins that localize to the nuclear rim in WT myoblasts were found at the nuclear rim both in Nesprin1-ΔKASH and LMNA-ΔK32 myoblasts. Despite this normal localization, deformations of the nuclear structure were present in both mutant cell lines, similar to phenotypes found in other nuclear envelopathies. This shows that both mutations have a severe effect of the integrity of the connection between the cytoplasm and the nucleus.

3.3.2 Myoblasts in Stiff and Soft Environments

I could show that neither Nesprin1-ΔKASH nor LMNA-ΔK32 myoblasts correctly interpreted the physical signals of their environment. They did not properly align in 3D culture gels (fig. 36 and Bertrand *et al,* 2014). Furthermore, stress fibers, (fig. 39), focal adhesions (fig. 40) and spreading area (fig. 37) were not downregulated on soft surfaces, as the WT myoblasts did. This means that both Nesprin1-ΔKASH and LMNA-ΔK32 myoblasts behaved as if they were plated on hard surfaces, even when their surrounding actually was soft.

Two hypotheses are discussed, how mutations in the LMNA gene lead to the phenotypes observed in human patients, mouse models and cell culture dishes: the "structural hypothesis" proposing that a destabilization of the nuclear envelope leaves the nucleus more sensitive towards physical stretch and the "gene regulation hypothesis" that suggests that mutations in the LMNA gene lead to a change in interaction of the protein with the chromatin. It is not easy to disprove one hypothesis or the other, as A-type lamins interact with many different proteins (Worman and Bonne, 2007).

Nesprin proteins stabilize the nucleus from the outside, similar to the lamina that stabilizes the nucleus from the inside (fig. 49). This, together with the fact that a knock-down of Nesprin-1 due to Nesprin1-ΔKASH leads to a similar phenotype as the LMNA-ΔK32 mutation, favors the structural hypothesis.

However, although the structural hypothesis might explain the deformed nuclei, it does not explain why Nesprin1-ΔKASH and LMNA-ΔK32 myoblasts do not recognize soft surfaces. If information about the physical environment are transferred from the cytoskeleton via LINC complex and Lamin proteins into the nucleus (as shown by Guilluy *et al,* 2014), or if information for a feedback-loop for adaptation of the cell to changes in the environment are transferred in the other direction by the same proteins, distubances of the LINC complex as well as mutations in Lamin A/C might block the flow of information, leaving the cell ignorant of its surroundings.

Taken together, LMNA-ΔK32 and Nesprin1-ΔKASH myoblasts were not able to recognize and adapt to the tension within the 3D gel nor to the stiffness of their surrounding in 2D. However, the question still remains which pathways of mechanotransduction are misfunctioning in these cells.

As ectopic stress fibers were present in Nesprin1-ΔKASH and LMNA-ΔK32 myoblasts when plated on a soft surface, I decided to identify the pathway(s) that were active on soft surfaces to generate these pronounced stress fibers. NMMIIa, which is part of stress fibers, also is necessary for stress fiber formation (Goeckeler *et al,* 2008). It can be activated via phosphorylation by two different kinases: MLC kinase and ROCK kinase (Katoh *et*

al, 2001). I could show that inhibition of ROCK or SRC kinase reduced stress fibers in Nesprin1-ΔKASH and LMNA-ΔK32 myoblasts on soft surfaces (fig. 42, fig. 43), while inhibition of MLC kinase did not have this effect (fig. 41).

Not only NMMIIa, but also formin proteins are important for stress fiber formation. The formin FHOD1 gets activated by ROCK in an SRC-dependant manner (Hannemann *et al,* 2008). Furthermore, FHOD1 interacts with Nesprin-2, thus it is present at the nuclear envelope (Kutscheidt *et al,* 2014).
FHOD1 was upregulated on protein level in Nesprin1-ΔKASH and LMNA-ΔK32 myoblasts on soft surfaces (fig. 45), while its subcellular localization was similar in all three cell lines. The upregulation does not prove a higher activity of FHOD1. To test for this, an antibody specific for phosphorylated FHOD1 would have been necessary. This will be future work. However, siRNA-mediated knock-down of FHOD1 largely rescued the actin stress fiber phenotype of Nesprin1-ΔKASH and LMNA-ΔK32 on soft surfaces (fig. 46). This is another indication that this formin protein is involved in the mis-interpretation of Nesprin1-ΔKASH and LMNA-ΔK32 myoblasts of the physical properties in their environment.
Taken together, ROCK and SRC but not MLC kinase were active in the formation of stress fibers in Nesprin1-ΔKASH and LMNA-ΔK32 myoblasts on soft surfaces. ROCK and SRC influence NMMIIa and the formin FHOD1, which are both important for the formation of actin stress fibers. Future work will connect these pathways with mutations in the LINC complex and proteins associated to this protein complex.

4 Bibliography

Akin, O and Mullins, RD (2008). Capping protein increases the rate of actin-based motility by promoting filament nucleation by the Arp2/3 complex. *Cell* 133, 841–851.

Amann, KJ and Pollard, TD (2001). Direct real-time observation of actin filament branching mediated by Arp2/3 complex using total internal reflection fluorescence microscopy. *Proceedings of the National Academy of Sciences* 98, 15009–15013.

Amano, M, Ito, M, Kimura, K, Fukata, Y, Chihara, K, Nakano, T, Matsuura, Y, and Kaibuchi, K (1996). Phosphorylation and activation of myosin by Rho-associated kinase (Rho-kinase). *Journal of Biological Chemistry* 271, 20246–20249.

Arber, S, Halder, G, and Caroni, P (1994). Muscle LIM protein, a novel essential regulator of myogenesis, promotes myogenic differentiation. *Cell* 79, 221–231.

Arber, S, Hunter, JR, Hongo, M, Sansig, G, Borg, J, Perriard, J-C, Chien, KR, and Caroni, P (1997). MLP-Deficient Mice Exhibit a Disruption of Cardiac Cytoarchitetural Organization, Dilated Cardiomyopathy, *Cell* 88, 393–403.

Arthur, WT, Petch, LA, and Burridge, K (2000). Integrin engagement suppresses RhoA activity via a c-Src-dependent mechanism. *Current Biology* 10, 719–722.

Azibani, F, Muchir, A, Vignier, N, Bonne, G, and Bertrand, AT (2014). Striated muscle laminopathies. *Seminars in Cell & Developmental Biology* 29, 107–115.

Bach, I (2000). The LIM domain: regulation by association. *Mechanisms of Development* 91, 5–17.

Banerjee, I, Fuseler, JW, Price, RL, Borg, TK, and Baudino, TA (2007). Determination of cell types and numbers during cardiac development in the neonatal and adult rat and mouse. *American Journal of Physiology - Heart and Circulatory Physiology* 293, 1883–1891.

Bang, M-L, Centner, T, Fornoff, F, Geach, AJ, Gotthardt, M, McNabb, M, Witt, CC, Labeit, D, Gregorio, CC, Granzier, H, and Labeit, S (2001). The complete gene sequence of titin, expression of an unusual 700-kDa titin isoform, and its interaction with obscurin identify a novel Z-line to I-band linking system. *Circulation Research* 89, 1065–1072.

Barash, IA, Mathew, L, Lahey, M, Greaser, ML, and Lieber, RL (2005). Muscle LIM protein plays both structural and functional roles in skeletal muscle. *American Journal of Physiology - Cell Physiology* 289, C1312–C1320.

Barletta, MR di, Ricci, E, Galluzzi, G, Tonali, P, Mora, M, Morandi, L, Romorini, A, Voit, T, Orstavik, KH, Merlini, L, Trevisan, C, Biancalana, V, Housmanowa-Petrusewicz, I, Bione, S, Ricotti, R, Schwartz, K, Bonne, G, and Toniolo, D (2000). Different mutations in the LMNA gene cause autosomal dominant and autosomal recessive Emery-Dreifuss muscular dystrophy. *The American Journal of Human Genetics* 66, 1407–1412.

Barry, JM and Maron, MS (2013). Hypertrophic cardiomyopathy. *The Lancet* 381, 242–255.

Basso, C, Thiene, G, Corrado, D, Buja, G, Melacini, P, and Nava, A (2000). Hypertrophic cardiomyopathy and sudden death in the young: pathologic evidence of myocardial ischemia. *Human Pathology* 31, 988–998.

Ben Yaou, RB, Toutain, A, Arimura, T, Demay, L, Massart, C, Peccate, C, Muchir, A, Llense, S, Deburgrave, N, Leturcq, F, Litim, KE, Rahmoun-Chiali, N, Richard, P, Babuty, D, Récan-Budiartha, D, and Bonne, G (2007). Multitissular involvement in a family with LMNA and EMD mutations: Role of digenic mechanism? *Neurology* 68, 1883–1894.

Bertrand, AT, Chikhaoui, K, Yaou, RB, and Bonne, G (2011). Clinical and genetic heterogeneity in laminopathies. *Biochemical Society Transactions* 39, 1687–1692.

Bertrand, AT, Ziaei, S, Ehret, C, Duchemin, H, Mamchaoui, K, Bigot, A, Mayer, M, Quijano-Roy, S, Desguerre, I, Lainé, J, Ben Yaou, R, Bonne, G, and Coirault, C (2014). Cellular microenvironments reveal defective mechanosensing responses and elevated YAP signaling in LMNA-mutated muscle precursors. *Journal of Cell Science* 127, 2873–2884.

Bertz, M, Wilmanns, M, and Rief, M (2009). The titin-telethonin complex is a directed, superstable molecular bond in the muscle Z-disk. *Proceedings of the National Academy of Sciences* 106, 13307–13310.

Biagini, E, Coccolo, F, Ferlito, M, Perugini, E, Rocchi, G, Bacchi-Reggiani, L, Lofiego, C, Boriani, G, Prandstraller, D, Picchio, FM, Branzi, A, and Rapezzi, C (2005). Dilated-hypokinetic evolution of hypertrophic cardiomyopathy: prevalence, incidence, risk factors, and prognostic implications in pediatric and adult patients. *Journal of the American College of Cardiology* 46, 1543–1550.

Bione, S, Maestrini, E, Rivella, S, Mancini, M, Regis, S, Romeo, G, and Toniolo, D (1994). Identification of a novel X-linked gene responsible for Emery-Dreifuss muscular dystrophy. *Nature Genetics* 8, 323–327.

Blake, RA, Broome, MA, Liu, X, Wu, J, Gishizky, M, Sun, L, and Courtneidge, SA (2000). SU6656, a selective src family kinase inhibitor, used to probe growth factor signaling. *Molecular and Cellular Biology* 20, 9018–9027.

Blanchard, A, Ohanian, V, and Critchley, D (1989). The structure and function of α-actinin. *Journal of Muscle Research and Cell Motility* 10, 280–289.

Blondel, B, Roijen, I, and Cheneval, JP (1971). Heart Cells in Culture: A Simple Method for Increasing the Proportion of Myoblasts. *Specialia* 27, 356–358.

Boateng, SY, Belin, RJ, Geenen, DL, Margulies, KB, Martin, JL, Hoshijima, M, Tombe, PP de, and Russell, B (2007). Cardiac dysfunction and heart failure are associated with abnormalities in the subcellular distribution and amounts of oligomeric muscle LIM protein. *American Journal of Physiology - Heart and Circulatory Physiology* 61, H259–H269.

Boateng, SY, Senyo, SE, Qi, L, Goldspink, PH, and Russell, B (2009). Myocyte remodeling in response to hypertrophic stimuli requires nucleocytoplasmic shuttling of muscle LIM protein. *Journal of Molecular and Cellular Cardiology* 47, 426–435.

Bombardier, JP, Eskin, JA, Jaiswal, R, Corrêa Jr, IR, Xu, M-Q, Goode, BL, and Gelles, J (2015). Single-molecule visualization of a formin-capping protein 'decision complex' at the actin filament barbed end. *Nature Communications* 6.

Bonne, G, Di Barletta, MR, Varnous, S, Bécane, H-M, Hammouda, E-H, Merlini, L, Muntoni, F, Greenberg, CR, Gary, F, Urtizberea, J-A, Duboc, D, Fardeau, M, Toniolo, D, and Schwartz, K (1999). Mutations in the gene encoding lamin A/C cause autosomal dominant Emery-Dreifuss muscular dystrophy. *Nature Genetics* 21, 285–288.

Boontheekul, T, Hill, EE, Kong, H-J, and Mooney, DJ (2007). Regulating myoblast phenotype through controlled gel stiffness and degradation. *Tissue Engineering* 13, 1431–1442.

Bos, JM, Poley, RN, Ny, M, Tester, DJ, Xu, X, Vatta, M, Towbin, JA, Gersh, BJ, Ommen, SR, and Ackerman, MJ (2006). Genotype–phenotype relationships involving hypertrophic cardiomyopathy-associated mutations in titin, muscle LIM protein, and telethonin. *Molecular Genetics and Metabolism* 88, 78–85.

Bouaouina, M, Jani, K, Long, JY, Czerniecki, S, Morse, EM, Ellis, SJ, Tanentzapf, G, Schöck, F, and Calderwood, DA (2012). Zasp regulates integrin activation. *Journal of Cell Science* 125, 5647–5657.

Brack, AS, Conboy, IM, Conboy, MJ, Shen, J, and Rando, TA (2008). A temporal switch from notch to Wnt signaling in muscle stem cells is necessary for normal adult myogenesis. *Cell Stem Cell* 2, 50–59.

Brakebusch, C and Fässler, R (2003). The integrin–actin connection, an eternal love affair. *The EMBO Journal* 22, 2324–2333.

Brodsky, GL, Muntoni, F, Miocic, S, Sinagra, G, Sewry, C, and Mestroni, L (2000). Lamin A/C gene mutation associated with dilated cardiomyopathy with variable skeletal muscle involvement. *Circulation* 101, 473–476.

Brosig, M, Ferralli, J, Gelman, L, Chiquet, M, and Chiquet-Ehrismann, R (2010). Interfering with the connection between the nucleus and the cytoskeleton affects nuclear rotation, mechanotransduction and myogenesis. *The International Journal of Biochemistry & Cell Biology* 42, 1717–1728.

Burgoyne, T, Morris, EP, and Luther, PK (2015). Three-Dimensional Structure of Vertebrate Muscle Z-Band: The Small-Square Lattice Z-Band in Rat Cardiac Muscle. *Journal of Molecular Biology* 427, 3527–3537.

Burke, B and Stewart, CL (2002). Life at the edge: the nuclear envelope and human disease. *Nature Reviews Molecular Cell Biology* 3, 575–585.

Burridge, K (1986). Substrate adhesions in normal and transformed fibroblasts: organization and regulation of cytoskeletal, membrane and extracellular matrix components at focal contacts. *Cancer Rev* 4, 18–78.

Burridge, K and Wittchen, ES (2013). The tension mounts: stress fibers as force-generating mechanotransducers. *The Journal of Cell Biology* 200, 9–19.

Cai, Y, Biais, N, Giannone, G, Tanase, M, Jiang, G, Hofman, JM, Wiggins, CH, Silberzan, P, Buguin, A, Ladoux, B, and Sheetz, MP (2006). Nonmuscle myosin IIA-dependent force inhibits cell spreading and drives F-actin flow. *Biophysical Journal* 91, 3907–3920.

Capell, BC and Collins, FS (2006). Human laminopathies: nuclei gone genetically awry. *Nature Reviews Genetics* 7, 940–952.

Carlsson, L, Nyström, L-E, Sundkvist, Il, Markey, F, and Lindberg, Uj (1977). Actin polymerizability is influenced by profilin, a low molecular weight protein in non-muscle cells. *Journal of Molecular Biology* 115, 465–483.

Chancellor, TJ, Lee, J, Thodeti, CK, and Lele, T (2010). Actomyosin tension exerted on the nucleus through nesprin-1 connections influences endothelial cell adhesion, migration, and cyclic strain-induced reorientation. *Biophysical Journal* 99, 115–123.

Cheng, W, Li, B, Kajstura, J, Li, P, Wolin, MS, Sonnenblick, EH, Hintze, TH, Olivetti, G, and Anversa, P (1995). Stretch-induced programmed myocyte cell death. *Journal of Clinical Investigation* 96, 2247–2259.

Chhabra, ES and Higgs, HN (2006). INF2 Is a WASP homology 2 motif-containing formin that severs actin filaments and accelerates both polymerization and depolymerization. *Journal of Biological Chemistry* 281, 26754–26767.

Chien, KR, Knowlton, KU, Zhu, H, and Chien, S (1991). Regulation of cardiac gene expression during myocardial growth and hypertrophy: molecular studies of an adaptive physiologic response. *The FASEB Journal* 5, 3037–3046.

Chiron, S, Tomczak, C, Duperray, A, Lainé, J, Bonne, G, Eder, A, Hansen, A, Eschenhagen, T, Verdier, C, and Coirault, C (2012). Complex interactions between human myoblasts and the surrounding 3D fibrin-based matrix. *PloS one* 7, e36173.

Cicha, I, Zitzmann, R, and Goppelt-Struebe, M (2014). Dual inhibition of Src family kinases and Aurora kinases by SU6656 modulates CTGF (connective tissue growth factor) expression in an ERK-dependent manner. *The International Journal of Biochemistry & Cell Biology* 46, 39–48.

Conte, G and Gioja, L (1836). Scrofola del sistema muscolare. *Annali Clinici dell'Ospedale degli Incurabili* 2, 66–79.

Cook, JR, Carta, L, Bénard, L, Chemaly, ER, Chiu, E, Rao, SK, Hampton, TG, Yurchenco, P, Costa, KD, Hajjar, RJ, and Ramirez, F (2014). Abnormal muscle mechanosignaling triggers cardiomyopathy in mice with Marfan syndrome. *The Journal of Clinical Investigation* 124, 1329–1339.

Costa, N da, Edgar, J, Ooi, P-T, Su, Y, Meissner, JD, and Chang, K-C (2007). Calcineurin differentially regulates fast myosin heavy chain genes in oxidative muscle fibre type conversion. *Cell and Tissue Research* 329, 515–527.

Cozzarelli, NR (1977). The mechanism of action of inhibitors of DNA synthesis. *Annual Review of Biochemistry* 46, 641–668.

Cramer, LP, Siebert, M, and Mitchison, TJ (1997). Identification of novel graded polarity actin filament bundles in locomoting heart fibroblasts: implications for the generation of motile force. *The Journal of Cell Biology* 136, 1287–1305.

Crisp, M, Liu, Q, Roux, K, Rattner, JB, Shanahan, C, Burke, B, Stahl, PD, and Hodzic, D (2006). Coupling of the nucleus and cytoplasm role of the LINC complex. *The Journal of Cell Biology* 172, 41–53.

Dahl, KN, Kahn, SM, Wilson, KL, and Discher, DE (2004). The nuclear envelope lamina network has elasticity and a compressibility limit suggestive of a molecular shock absorber. *Journal of Cell Science* 117, 4779–4786.

Dawe, HR, Adams, M, Wheway, G, Szymanska, K, Logan, CV, Noegel, AA, Gull, K, and Johnson, CA (2009). Nesprin-2 interacts with meckelin and mediates ciliogenesis via remodelling of the actin cytoskeleton. *Journal of Cell Science* 122, 2716–2726.

DeMali, KA, Barlow, CA, and Burridge, K (2002). Recruitment of the Arp2/3 complex to vinculin coupling membrane protrusion to matrix adhesion. *The Journal of Cell Biology* 159, 881–891.

Dhein, S, Schreiber, A, Steinbach, S, Apel, D, Salameh, A, Schlegel, F, Kostelka, M, Dohmen, PM, and Mohr, FW (2014). Mechanical control of cell biology. Effects of cyclic mechanical stretch on cardiomyocyte cellular organization. *Progress in Biophysics and Molecular Biology* 115, 93–102.

Ding, X, Xu, R, Yu, J, Xu, T, Zhuang, Y, and Han, M (2007). SUN1 is required for telomere attachment to nuclear envelope and gametogenesis in mice. *Developmental Cell* 12, 863–872.

Dittmer, TA and Misteli, T (2011). The lamin protein family. *Genome Biology* 12, 222.

Dorn, GW, Robbins, J, and Sugden, PH (2003). Phenotyping Hypertrophy: Eschew Obfuscation. *Circulation Research* 92, 1171–1175.

Duong, NG, MorrisMorris GE, LT, Zhang, Q, Sewry, CA, Shanahan, CM, and Holt, I (2014). Nesprins: Tissue-Specific Expression of Epsilon and Other Short Isoforms. *PlosOne* 9.

Dupré, N, Gros-Louis, F, Chrestian, N, Verreault, S, Brunet, D, Verteuil, D de, Brais, B, Bouchard, J-P, and Rouleau, GA (2007). Clinical and genetic study of autosomal recessive cerebellar ataxia type 1. *Annals of Neurology* 62, 93–98.

Ecarnot-Laubriet, A, De Luca, K, Vandroux, D, Moisant, M, Bernard, C, Assem, M, Rochette, L, and Teyssier, J-R (2000). Downregulation and nuclear relocation of MLP during the progression of right ventricular hypertrophy induced by chronic pressure overload. *Journal of Molecular and Cellular Cardiology* 32, 2385–2395.

Edwards, M, Zwolak, A, Schafer, DA, Sept, D, Dominguez, R, and Cooper, JA (2014). Capping protein regulators fine-tune actin assembly dynamics. *Nature Reviews Molecular Cell Biology* 15, 677–689.

Eghbali, M, Czaja, MJ, Zeydel, M, Weiner, FR, Zern, MA, Seifter, S, and Blumenfeld, OO (1988). Collagen chain mRNAs in isolated heart cells from young and adult rats. *Journal of Molecular and Cellular Cardiology* 20, 267–276.

Elliott, P, Andersson, B, Arbustini, E, Bilinska, Z, Cecchi, F, Charron, P, Dubourg, O, Kühl, U, Maisch, B, McKenna, WJ, Monserrat, L, Pankuzeit, S, Rapezzi, C, Seferovic,

P, Tavazzi, L, and Keren, A (2007). Classification of the cardiomyopathies: a position statement from the European Society Of Cardiology Working Group on Myocardial and Pericardial Diseases. *European Heart Journal*.

Engler, AJ, Griffin, MA, Sen, S, Bönnemann, CG, Sweeney, HL, and Discher, DE (2004). Myotubes differentiate optimally on substrates with tissue-like stiffness: pathological implications for soft or stiff microenvironments. *The Journal of Cell Biology* 166, 877–887.

Engler, AJ, Sen, S, Sweeney, HL, and Discher, DE (2006). Matrix elasticity directs stem cell lineage specification. *Cell* 126, 677–689.

Engler, AJ, Carag-Krieger, C, Johnson, CP, Raab, M, Tang, H-Y, Speicher, DW, Sanger, JW, Sanger, JM, and Discher, DE (2008). Embryonic cardiomyocytes beat best on a matrix with heart-like elasticity: scar-like rigidity inhibits beating. *Journal of Cell Science* 121, 3794–3802.

Enriquez, AD and Goldman, ME (2014). Management of hypertrophic cardiomyopathy. *Annals of Global Health* 80, 35–45.

Fan, D, Takawale, A, Lee, J, and Kassiri, Z (2012). Cardiac fibroblasts, fibrosis and extracellular matrix remodeling in heart disease. *Fibrogenesis Tissue Repair* 5, 15–15.

Fedorchak, GR, Kaminski, A, and Lammerding, J (2014). Cellular mechanosensing: getting to the nucleus of it all. *Progress in Biophysics and Molecular Biology* 115, 76–92.

Finsen, AV, Lunde, IG, Sjaastad, I, Østli, EK, Lyngra, M, Jarstadmarken, HO, Hasic, A, Nygård, S, Wilcox-Adelman, SA, Goetinck, PF, Lyberg, T, Skrbic, B, Florholmen, G, Tønnessen, T, Louch, WE, Djurovic, S, Carlson, CR, and Christensen, G (2011). Syndecan-4 is essential for development of concentric myocardial hypertrophy via stretch-induced activation of the calcineurin-NFAT pathway. *PloS One* 6, e28302.

Flick, MJ and Konieczny, SF (2000). The muscle regulatory and structural protein MLP is a cytoskeletal binding partner of βI-spectrin. *Journal of Cell Science* 113, 1553–1564.

Flier, A van der and Sonnenberg, A (2001). Function and interactions of integrins. *Cell and Tissue Research* 305, 285–298.

Frank, D, Kuhn, C, Brors, B, Hanselmann, C, Lüdde, M, Katus, HA, and Frey, N (2008). Gene expression pattern in biomechanically stretched cardiomyocytes: evidence for a stretch-specific gene program. *Hypertension* 51, 309–318.

Freyd, G, Kim, SK, and Horvitz, HR (1990). Novel cysteine-rich motif and homeodomain in the product of the *Caenorhabditis elegans* cell lineage gene lin-II. *Nature* 344, 876–879.

Fusco, S, Panzetta, V, Embrione, V, and Netti, PA (2015). Crosstalk between focal adhesions and material mechanical properties governs cell mechanics and functions. *Acta Biomaterialia* 23, 63–71.

Gasteier, JE, Madrid, R, Krautkrämer, E, Schröder, S, Muranyi, W, Benichou, S, and Fackler, OT (2003). Activation of the Rac-binding partner FHOD1 induces actin stress fibers via a ROCK-dependent mechanism. *Journal of Biological Chemistry* 278, 38902–38912.

Gehmlich, K, Geier, C, Osterziel, KJ, Ven, PFM Van der, and Fürst, DO (2004). Decreased interactions of mutant muscle LIM protein (MLP) with N-RAP and α-actinin and their implication for hypertrophic cardiomyopathy. *Cell and Tissue Research* 317, 129–136.

Gehmlich, K, Geier, C, Milting, H, Fürst, DO, and Ehler, E (2008). Back to square one: what do we know about the functions of muscle LIM protein in the heart? *Journal of Muscle Research and Cell Motility* 29, 155–158.

Gehmlich, K, Ehler, E, Perrot, A, Fürst, DO, and Geier, C (2010). Letter to the Editor regarding "MLP: A Stress Sensor Goes Nuclear" By Sylvia Gunkel, Jörg Heineke, Denise Hilfiker-Kleiner, Ralph Knöll, J Mol Cell Cardiol. 2009; 47 (4): 423–425. *Journal of Molecular and Cellular Cardiology* 48, 424–425.

Geier, C, Perrot, A, Özcelik, C, Binner, P, Counsell, D, Hoffmann, K, Pilz, B, Martiniak, Y, Gehmlich, K, Ven, PF van der, Fürst, DO, Vornwald, A, Hodenberg, E von, Nürnberg, P, Scheffold, T, Dietz, R, and Osterziel, KJ (2003). Mutations in the human muscle LIM protein gene in families with hypertrophic cardiomyopathy. *Circulation* 107, 1390–1395.

Geier, C, Gehmlich, K, Ehler, E, Hassfeld, S, Perrot, A, Hayess, K, Cardim, N, Wenzel, K, Erdmann, B, Krackhardt, F, Posch, M, Osterziel, Bublak, A, Nägele, H, Scheffold, T, Dietz, R, Chien, K, Spuler, S, Fürst, D, Nürnberg, P, and Özcelik, C (2008). Beyond the sarcomere: CSRP3 mutations cause hypertrophic cardiomyopathy. *Human Molecular Genetics* 17, 2753–2765.

Geiger, B, Bershadsky, A, Pankov, R, and Yamada, KM (2001). Transmembrane crosstalk between the extracellular matrix and the cytoskeleton. *Nature Reviews Molecular Cell Biology* 2, 793–805.

Geurts, AM, Cost, GJ, Freyvert, Y, Zeitler, B, Miller, JC, Choi, VM, Jenkins, SS, Wood, A, Cui, X, Meng, X, Vincent, A, Lam, S, Michalkiewicz, M, Schilling, R, Foeckler, J, Kalloway, S, Weiler, H, Ménoret, S, Anegon, I, Davis, GD, Zhang, L, Rebar, EJ, Gregory, PD, Urnov, FD, Jacob, HJ, and Buelow, R (2009). Knockout rats via embryo microinjection of zinc-finger nucleases. *Science* 325, 433–433.

Goeckeler, ZM, Bridgman, PC, and Wysolmerski, RB (2008). Nonmuscle myosin II is responsible for maintaining endothelial cell basal tone and stress fiber integrity. *American Journal of Physiology - Cell Physiology* 295, C994–C1006.

Goldyn, AM, Rioja, BA, Spatz, JP, Ballestrem, C, and Kemkemer, R (2009). Force-induced cell polarisation is linked to RhoA-driven microtubule-independent focal-adhesion sliding. *Journal of Cell Science* 122, 3644–3651.

Goley, ED and Welch, MD (2006). The ARP2/3 complex: an actin nucleator comes of age. *Nature Reviews Molecular Cell Biology* 7, 713–726.

Goode, BL and Eck, MJ (2007). Mechanism and function of formins in the control of actin assembly. *Annual Review of Biochemistry* 76, 593–627.

Grady, RM, Starr, DA, Ackerman, GL, Sanes, JR, and Han, M (2005). Syne proteins anchor muscle nuclei at the neuromuscular junction. *Proceedings of the National Academy of Sciences of the United States of America* 102, 4359–4364.

Granzier, HL and Irving, TC (1995). Passive tension in cardiac muscle: contribution of collagen, titin, microtubules, and intermediate filaments. *Biophysical Journal* 68, 1027–1044.

Gros-Louis, F, Dupré, N, Dion, P, Fox, MA, Laurent, S, Verreault, S, Sanes, JR, Bouchard, J-P, and Rouleau, GA (2007). Mutations in SYNE1 lead to a newly discovered form of autosomal recessive cerebellar ataxia. *Nature Genetics* 39, 80–85.

Guelen, L, Pagie, L, Brasset, E, Meuleman, W, Faza, MB, Talhout, W, Eussen, BH, Klein, A de, Wessels, L, Laat, W de, and Steensel, B van (2008). Domain organization of human chromosomes revealed by mapping of nuclear lamina interactions. *Nature* 453, 948–951.

Guilluy, C, Swaminathan, V, Garcia-Mata, R, O'Brien, ET, Superfine, R, and Burridge, K (2011). The Rho GEFs LARG and GEF-H1 regulate the mechanical response to force on integrins. *Nature Cell Biology* 13, 722–727.

Guilluy, C, Osborne, LD, Van Landeghem, L, Sharek, L, Superfine, R, Garcia-Mata, R, and Burridge, K (2014). Isolated nuclei adapt to force and reveal a mechanotransduction pathway in the nucleus. *Nature Cell Biology* 16, 376–381.

Gupta, MP, Samant, SA, Smith, SH, and Shroff, SG (2008). HDAC4 and PCAF bind to cardiac sarcomeres and play a role in regulating myofilament contractile activity. *Journal of Biological Chemistry* 283, 10135–10146.

Hannemann, S, Madrid, R, Stastna, J, Kitzing, T, Gasteier, J, Schönichen, A, Bouchet, J, Jimenez, A, Geyer, M, Grosse, R, Benichou, S, and Fackler, OT (2008). The Diaphanous-related Formin FHOD1 associates with ROCK1 and promotes Src-dependent plasma membrane blebbing. *Journal of Biological Chemistry* 283, 27891–27903.

Hansen, A, Eder, A, Bönstrup, M, Flato, M, Mewe, M, Schaaf, S, Aksehirlioglu, B, Schwörer, A, Uebeler, J, and Eschenhagen, T (2010). Development of a drug screening platform based on engineered heart tissue. *Circulation Research* 107, 35–44.

Haque, F, Mazzeo, D, Patel, JT, Smallwood, DT, Ellis, JA, Shanahan, CM, and Shackleton, S (2010). Mammalian SUN protein interaction networks at the inner nuclear membrane and their role in laminopathy disease processes. *Journal of Biological Chemistry* 285, 3487–3498.

Haque, Farhana, Lloyd, David J, Smallwood, Dawn T, Dent, Carolyn L, Shanahan, Catherine M, Fry, Andrew M, Trembath, Richard C, and Shackleton, Sue (2006). SUN1 interacts with nuclear lamin A and cytoplasmic nesprins to provide a physical connection between the nuclear lamina and the cytoskeleton. *Molecular and Cellular Biology* 26, 3738–3751.

Harris, AK, Stopak, D, and Wild, P (1981). Fibroblast traction as a mechanism for collagen morphogenesis. *Nature* 290, 249–251.

Harris, ES, Li, F, and Higgs, HN (2004). The mouse formin, FRLα, slows actin filament barbed end elongation, competes with capping protein, accelerates polymerization from monomers, and severs filaments. *Journal of Biological Chemistry* 279, 20076–20087.

Harris, ES, Rouiller, I, Hanein, D, and Higgs, HN (2006). Mechanistic differences in actin bundling activity of two mammalian formins, FRL1 and mDia2. *Journal of Biological Chemistry* 281, 14383–14392.

Hasan, S, Güttinger, S, Mühlhäusser, P, Anderegg, F, Bürgler, S, and Kutay, U (2006). Nuclear envelope localization of human UNC84A does not require nuclear lamins. *FEBS Letters* 580, 1263–1268.

Heath, JP (1983). Behaviour and structure of the leading lamella in moving fibroblasts. I. Occurrence and centripetal movement of arc-shaped microfilament bundles beneath the dorsal cell surface. *Journal of Cell Science* 60, 331–354.

Heath, JP and Dunn, GA (1978). Cell to substratum contacts of chick fibroblasts and their relation to the microfilament system. A correlated interference-reflexion and high-voltage electron-microscope study. *Journal of Cell Science* 29, 197–212.

Heidenhain, M (1899). Über die Struktur der Darmepithelzellen. *Archiv für Mikroskopische Anatomie* 54, 184–224.

Heineke, J, Ruetten, H, Willenbockel, C, Gross, SC, Naguib, M, Schaefer, A, Kempf, T, Hilfiker-Kleiner, D, Caroni, P, Kraft, T, Kaiser, RA, Molkentin, JD, Drexler, H, and Wollert, KC (2005). Attenuation of cardiac remodeling after myocardial infarction by muscle LIM protein-calcineurin signaling at the sarcomeric Z-disc. *Proceedings of the National Academy of Sciences of the United States of America* 102, 1655–1660.

Heineke, J, Wollert, KC, Osinska, H, Sargent, MA, York, J, Robbins, J, and Molkentin, JD (2010). Calcineurin protects the heart in a murine model of dilated cardiomyopathy. *Journal of Molecular and Cellular Cardiology* 48, 1080–1087.

Henderson, JR, Pomies, P, Auffray, C, and Beckerle, MC (2003). ALP and MLP distribution during myofibrillogenesis in cultured cardiomyocytes. *Cell Motility and the Cytoskeleton* 54, 254–265.

Herman, DS, Lam, L, Taylor, MRG, Wang, L, Teekakirikul, P, Christodoulou, D, Conner, L, DePalma, SR, McDonough, B, Sparks, E, Teodorescu, DL, Cirino, AL, Banner, NR, Pennell, DJ, Graw, S, Merlo, M, DiLenarda, A, Sinagra, G, Bos, JM, Ackerman, MJ, Mitchell, RN, Murry, CE, Lakdawala, NK, Ho, CY, Barton, PJR, Cook, SA, Mestroni, L, Seidman, JG, and Seidman, CE (2012). Truncations of titin causing dilated cardiomyopathy. *New England Journal of Medicine* 366, 619–628.

Herrmann, H and Aebi, U (2004). Intermediate filaments: molecular structure, assembly mechanism, and integration into functionally distinct intracellular scaffolds. *Annual Review of Biochemistry* 73, 749–789.

Hershberger, RE, Parks, SB, Kushner, JD, Li, D, Ludwigsen, S, Jakobs, P, Nauman, D, Burgess, D, Partain, J, and Litt, M (2008). Coding sequence mutations identified in MYH7, TNNT2, SCN5A, CSRP3, LBD3, and TCAP from 313 patients with familial or idiopathic dilated cardiomyopathy. *Clinical and Translational Science* 1, 21–26.

Higgs, HN and Peterson, KJ (2005). Phylogenetic analysis of the formin homology 2 domain. *Molecular Biology of the Cell* 16, 1–13.

Hoffmann, C, Moreau, F, Moes, M, Luthold, C, Dieterle, M, Goretti, E, Neumann, K, Steinmetz, A, and Thomas, C (2014). Human Muscle LIM Protein Dimerizes along the Actin Cytoskeleton and Cross-Links Actin Filaments. *Molecular and Cellular Biology* 34, 3053–3065.

Højlund, K, Bowen, BP, Hwang, H, Flynn, CR, Madireddy, L, Geetha, T, Langlais, P, Meyer, C, Mandarino, LJ, and Yi, Z (2009). *In vivo* phosphoproteome of human skeletal muscle revealed by phosphopeptide enrichment and HPLC- ESI- MS/MS. *Journal of Proteome Research* 8, 4954–4965.

Holdsworth, DA, Cox, AT, Boos, C, Hardman, R, and Sharma, S (2015). Cardiomyopathies and the Armed Forces. *Journal of the Royal Army Medical Corps* 161, 259–267.

Horn, HF, Kim, DI, Wright, GD, Wong, ESM, Stewart, CL, Burke, B, and Roux, KJ (2013). A mammalian KASH domain protein coupling meiotic chromosomes to the cytoskeleton. *The Journal of Cell Biology* 202, 1023–1039.

Hotulainen, P and Lappalainen, P (2006). Stress fibers are generated by two distinct actin assembly mechanisms in motile cells. *The Journal of Cell Biology* 173, 383–394.

Hu, P and Luo, B-H (2013). Integrin bi-directional signaling across the plasma membrane. *Journal of Cellular Physiology* 228, 306–312.

Humphries, JD, Byron, A, and Humphries, MJ (2006). Integrin ligands at a glance. *Journal of Cell Science* 119, 3901–3903.

Humphries, JD, Wang, P, Streuli, C, Geiger, B, Humphries, MJ, and Ballestrem, C (2007). Vinculin controls focal adhesion formation by direct interactions with talin and actin. *The Journal of Cell Biology* 179, 1043–1057.

Huxley, AF and Niedergerke, R (1954). Structural changes in muscle during contraction. *Nature* 173, 971–973.

Huxley, H and Hanson, J (1954). Changes in the cross-striations of muscle during contraction and stretch and their structural interpretation. *Nature* 173, 973–976.

Hynes, RO (2002). Integrins: bidirectional, allosteric signaling machines. *Cell* 110, 673–687.

Ieda, M, Tsuchihashi, T, Ivey, KN, Ross, RS, Hong, T-T, Shaw, RM, and Srivastava, D (2009). Cardiac fibroblasts regulate myocardial proliferation through β1 integrin signaling. *Developmental Cell* 16, 233–244.

Imamura, H, Tanaka, K, Hihara, T, Umikawa, M, Kamei, T, Takahashi, K, Sasaki, T, and Takai, Y (1997). Bni1p and Bnr1p: downstream targets of the Rho family small G-proteins which interact with profilin and regulate actin cytoskeleton in *Saccharomyces cerevisiae*. *The EMBO journal* 16, 2745–2755.

Isenberg, G, Rathke, PC, Hülsmann, N, Franke, WW, and Wohlfarth-Bottermann, KE (1976). Cytoplasmic actomyosin fibrils in tissue culture cells. *Cell and Tissue Research* 166, 427–443.

Isenberg, G, Aebi, U, and Pollard, TD (1980). An actin-binding protein from Acanthamoeba regulates actin filament polymerization and interactions. *Nature* 288, 455–459.

Isermann, P and Lammerding, J (2013). Nuclear mechanics and mechanotransduction in health and disease. *Current Biology* 23, R1113–R1121.

Ishizaki, T, Uehata, M, Tamechika, I, Keel, J, Nonomura, K, Maekawa, M, and Narumiya, S (2000). Pharmacological properties of Y-27632, a specific inhibitor of rho-associated kinases. *Molecular Pharmacology* 57, 976–983.

Iwamoto, DV and Calderwood, DA (2015). Regulation of integrin-mediated adhesions. *Current Opinion in Cell Biology* 36, 41–47.

Iwanaga, Y, Nishi, I, Furuichi, S, Noguchi, T, Sase, K, Kihara, Y, Goto, Y, and Nonogi, H (2006). B-Type Natriuretic Peptide Strongly Reflects Diastolic Wall Stress in Patients With Chronic Heart Failure. *Journal of the American College of Cardiology* 47, 742–748.

Jacobs, M, Hayakawa, K, Swenson, L, Bellon, S, Fleming, M, Taslimi, P, and Doran, J (2006). The structure of dimeric ROCK I reveals the mechanism for ligand selectivity. *Journal of Biological Chemistry* 281, 260–268.

Jacot, JG, McCulloch, AD, and Omens, JH (2008). Substrate stiffness affects the functional maturation of neonatal rat ventricular myocytes. *Biophysical Journal* 95, 3479–3487.

Jugdutt, BI (2003). Ventricular remodeling after infarction and the extracellular collagen matrix when is enough enough? *Circulation* 108, 1395–1403.

Kandert, S, Lüke, Y, Kleinhenz, T, Neumann, S, Lu, W, Jaeger, VM, Munck, M, Wehnert, M, Müller, CR, Zhou, Z, Noegel, AA, Dabauvalle, M-C, and Karakesisoglou, I (2007). Nesprin-2 giant safeguards nuclear envelope architecture in LMNA S143F progeria cells. *Human Molecular Genetics* 16, 2944–2959.

Karlsson, O, Thor, S, Norberg, T, Ohlsson, H, and Edlund, T (1990). Insulin gene enhancer binding protein Isl-1 is a member of a novel class of proteins containing both a homeo-and a Cys His domain. *Nature* 344, 879–882.

Katoh, K, Kano, Y, Masuda, M, Onishi, H, and Fujiwara, K (1998). Isolation and contraction of the stress fiber. *Molecular Biology of the Cell* 9, 1919–1938.

Katoh, K, Kano, Y, Amano, M, Kaibuchi, K, and Fujiwara, K (2001). Stress fiber organization regulated by MLCK and Rho-kinase in cultured human fibroblasts. *American Journal of Physiology-Cell Physiology* 280, C1669–C1679.

Kawaharada, K, Kawamata, M, and Ochiya, T (2015). Rat embryonic stem cells create new era in development of genetically manipulated rat models. *World Journal of Stem Cells* 7, 1054–1063.

Khatau, SB, Hale, CM, Stewart-Hutchinson, PJ, Patel, MS, Stewart, CL, Searson, PC, Hodzic, D, and Wirtz, D (2009). A perinuclear actin cap regulates nuclear shape. *Proceedings of the National Academy of Sciences* 106, 19017–19022.

Kim, D-H, Khatau, SB, Feng, Y, Walcott, S, Sun, SX, Longmore, G D, and Wirtz, D (2012). Actin cap associated focal adhesions and their distinct role in cellular mechanosensing. *Scientific Reports* 2, 1–13.

Kim, D-H, Cho, S, and Wirtz, D (2014). Tight coupling between nucleus and cell migration through the perinuclear actin cap. *Journal of Cell Science* 127, 2528–2541.

Kim, DI, KC, B, and Roux, KJ (2015). Making the LINC: SUN and KASH protein interactions. *Biological Chemistry* 396, 295–310.

Kimura, K, Ito, M, Amano, M, Chihara, K, Fukata, Y, Nakafuku, M, Yamamori, B, Feng, J, Nakano, T, Okawa, K, Iwamatsu, A, and Kaibuchi, K (1996). Regulation of myosin phosphatase by Rho and Rho-associated kinase (Rho-kinase). *Science* 273, 245–248.

Klede, S (2011). "Untersuchung von Z-Scheiben Proteinen in quergestreiften Muskeln mittels 2-D Elektrophorese". PhD thesis. Westfälische Wilhelms-Universität Münster.

Knock, GA, Shaifta, Y, Snetkov, VA, Vowles, B, Drndarski, S, Ward, JPT, and Aaronson, PI (2008). Interaction between src family kinases and rho-kinase in agonist-induced Ca2+-sensitization of rat pulmonary artery. *Cardiovascular Research* 77, 570–579.

Knöll, R, Hoshijima, M, Hoffman, HM, Person, V, Lorenzen-Schmidt, I, Bang, M, Hayashi, T, Shiga, N, Yasukawa, H, Schaper, W, McKenna, W, Yokoyama, M, Schork, NJ, Omens, JH, McCulloch, AD, Kimura, A, Gregorio, CC, Poller, W, Schaper, J, Schultheiss, HP, and Chien, KR (2002). The cardiac mechanical stretch sensor machinery involves a Z disc complex that is defective in a subset of human dilated cardiomyopathy. *Cell* 111, 943–955.

Knöll, R, Kostin, S, Klede, S, Savvatis, K, Klinge, L, Stehle, I, Gunkel, S, Kötter, S, Babicz, K, Sohns, M, Miocic, S, Didié, M, Knöll, G, Zimmermann, W, Thelen, P, Bickeböller, H, Maier, L, Schaper, W, Schaper, J, Kraft, T, Tschöpe, C, Linke, W, and Chien, K (2010). A common MLP (muscle LIM protein) variant is associated with cardiomyopathy. *Circulation Research* 106, 695–704.

Knöll, R, Linke, WA, Zou, P, Miočić, S, Kostin, S, Buyandelger, B, Ku, C-H, Neef, S, Bug, M, Schäfer, K, Knöll, G, Felkin, LE, Wessels, J, Toischer, K, Hagn, F, Kessler, H, Didié, M, Quentin, T, Maier, LS, Teucher, N, Unsöld, B, Schmidt, A, Birks, EJ, Gunkel, S, Lang, P, Granzier, H, Zimmermann, WH, Field, LJ, Faulkner, G, Doppelstein, M, Barton, PJ, Sattler, M, Wilmanns, M, and Chien, KR (2011). Telethonin deficiency is associated with maladaptation to biomechanical stress in the mammalian heart. *Circulation Research* 109, 758–769.

Kobayashi, Y, Katanosaka, Y, Iwata, Y, Matsuoka, M, Shigekawa, M, and Wakabayashi, S (2006). Identification and characterization of GSRP-56, a novel Golgi-localized spectrin repeat-containing protein. *Experimental Cell Research* 312, 3152–3164.

Koch, AJ and Holaska, JM (2012). Loss of emerin alters myogenic signaling and miRNA expression in mouse myogenic progenitors. *PloS One* 7, e37262.

Koch, AJ and Holaska, JM (2014). Emerin in health and disease. *Seminars in Cell & Developmental Biology* 29, 95–106.

Koivisto, E, Acosta, AJ, Moilanen, A-M, Tokola, H, Aro, J, Pennanen, H, Säkkinen, H, Kaikkonen, L, Ruskoaho, H, and Rysä, J (2014). Characterization of the Regulatory Mechanisms of Activating Transcription Factor 3 by Hypertrophic Stimuli in Rat Cardiomyocytes. *PLoS ONE* 9, e105168.

Koka, S, Neudauer, CL, Li, X, Lewis, RE, McCarthy, JB, and Westendorf, JJ (2003). The formin-homology-domain-containing protein FHOD1 enhances cell migration. *Journal of Cell Science* 116, 1745–1755.

Kong, Y, Flick, MJ, Kudla, AJ, and Konieczny, SF (1997). Muscle LIM protein promotes myogenesis by enhancing the activity of MyoD. *Molecular and Cellular Biology* 17, 4750–4760.

Kook, S-H, Lee, H-J, Chung, W-T, Hwang, I-H, Lee, S-A, Kim, B-S, and Lee, J-C (2008). Cyclic mechanical stretch stimulates the proliferation of C2C12 myoblasts and inhibits their differentiation via prolonged activation of p38 MAPK. *Molecules and Cells* 25, 479–486.

Kovar, DR and Pollard, TD (2004). Insertional assembly of actin filament barbed ends in association with formins produces piconewton forces. *Proceedings of the National Academy of Sciences of the United States of America* 101, 14725–14730.

Kovar, DR, Kuhn, JR, Tichy, AL, and Pollard, TD (2003). The fission yeast cytokinesis formin Cdc12p is a barbed end actin filament capping protein gated by profilin. *The Journal of Cell Biology* 161, 875–887.

Kreis, TE and Birchmeier, W (1980). Stress fiber sarcomeres of fibroblasts are contractile. *Cell* 22, 555–561.

Krimm, I, Östlund, C, Gilquin, B, Couprie, J, Hossenlopp, P, Mornon, J-P, Bonne, G, Courvalin, J-C, Worman, HJ, and Zinn-Justin, S (2002). The Ig-like structure of the C-terminal domain of lamin A/C, mutated in muscular dystrophies, cardiomyopathy, and partial lipodystrophy. *Structure* 10, 811–823.

Kuhn, C, Frank, D, Dierck, F, Oehl, U, Krebs, J, Will, R, Lehmann, LH, Backs, J, Katus, HA, and Frey, N (2012). Cardiac remodeling is not modulated by overexpression of muscle LIM protein (MLP). *Basic Research in Cardiology* 107, 1–14.

Kuo, J-C (2014). Focal adhesions function as a mechanosensor. *Progress in Molecular Biology and Translational Science* 126, 55–73.

Kutscheidt, S, Zhu, R, Antoku, S, Luxton, GW, Stagljar, I, Fackler, OT, and Gundersen, GG (2014). FHOD1 interaction with nesprin-2G mediates TAN line formation and nuclear movement. *Nature Cell Biology* 16, 708–715.

Lammerding, J, Schulze, PC, Takahashi, T, Kozlov, S, Sullivan, T, Kamm, RD, Stewart, CL, and Lee, RT (2004). Lamin A/C deficiency causes defective nuclear mechanics and mechanotransduction. *Journal of Clinical Investigation* 113, 370.

Lammerding, J, Hsiao, J, Schulze, PC, Kozlov, S, Stewart, CL, and Lee, RT (2005). Abnormal nuclear shape and impaired mechanotransduction in emerin-deficient cells. *The Journal of Cell Biology* 170, 781–791.

Lange, A (2015). "Expression von Hypertrophiemarkern bei isolierten neonatalen Mauskardiomyozyten". MA thesis. Technische Universität Berlin.

Lange, S, Xiang, F, Yakovenko, A, Vihola, A, Hackman, P, Rostkova, E, Kristensen, J, Brandmeier, B, Franzen, G, Hedberg, B, Gunnarsson, LG, Hughes, SM, Marchand, S,

Sejersen, T, Richard, I, Edström, L, Ehler, E, Udd, B, and Gautel, M (2005). The kinase domain of titin controls muscle gene expression and protein turnover. *Science* 308, 1599–1603.

Lazarides, E and Burridge, K (1975). α-Actinin: immunofluorescent localization of a muscle structural protein in nonmuscle cells. *Cell* 6, 289–298.

Lee, JSH, Hale, CM, Panorchan, P, Khatau, SB, George, JP, Tseng, Y, Stewart, CL, Hodzic, D, and Wirtz, D (2007). Nuclear lamin A/C deficiency induces defects in cell mechanics, polarization, and migration. *Biophysical Journal* 93, 2542–2552.

Lee, KK, Starr, D, Cohen, M, Liu, J, Han, M, Wilson, KL, and Gruenbaum, Y (2002). Lamin-dependent localization of UNC-84, a protein required for nuclear migration in Caenorhabditis elegans. *Molecular Biology of the Cell* 13, 892–901.

Lei, K, Zhang, X, Ding, X, Guo, X, Chen, M, Zhu, B, Xu, T, Zhuang, Y, Xu, R, and Han, M (2009). SUN1 and SUN2 play critical but partially redundant roles in anchoring nuclei in skeletal muscle cells in mice. *Proceedings of the National Academy of Sciences* 106, 10207–10212.

Leung, T, Manser, E, Tan, L, and Lim, L (1995). A novel serine/threonine kinase binding the Ras-related RhoA GTPase which translocates the kinase to peripheral membranes. *Journal of Biological Chemistry* 270, 29051–29054.

Leung, T, Chen, X-Q, Manser, E, and Lim, L (1996). The p160 RhoA-binding kinase ROK alpha is a member of a kinase family and is involved in the reorganization of the cytoskeleton. *Molecular and Cellular Biology* 16, 5313–5327.

Levin, E, Leibinger, M, Andreadaki, A, and Fischer, D (2014). Neuronal Expression of Muscle LIM Protein in Postnatal Retinae of Rodents. *PloS One* 9, e100756.

Lewis, WH and Lewis, MR (1924). Behavior of cells in tissue cultures. *General Cytology*. Ed. by EV Cowdry. The University of Chicago Press. Chicago, Illinois, 385–447.

Li, F and Higgs, HN (2003). The mouse Formin mDia1 is a potent actin nucleation factor regulated by autoinhibition. *Current Biology* 13, 1335–1340.

Li, F, Wang, X, Capasso, JM, and Gerdes, AM (1996). Rapid transition of cardiac myocytes from hyperplasia to hypertrophy during postnatal development. *Journal of Molecular and Cellular Cardiology* 28, 1737–1746.

Li, M, Zhang, M, Huang, L, Zhou, J, Zhuang, H, Taylor, JT, Keyser, BM, and Whitehurst, RM (2005). T-Type Ca2+ Channels Are Involved in High Glucose–Induced Rat Neonatal Cardiomyocyte Proliferation. *Pediatric research* 57, 550–556.

Li, P, Meinke, P, Huong, LTT, Wehnert, M, and Noegel, AA (2014). Contribution of SUN1 mutations to the pathomechanism in muscular dystrophies. *Human Mutation* 35, 452–461.

Limouze, J, Straight, AF, Mitchison, T, and Sellers, JR (2004). Specificity of blebbistatin, an inhibitor of myosin II. *Journal of Muscle Research & Cell Motility* 25, 337–341.

Lloyd, DJ, Trembath, RC, and Shackleton, S (2002). A novel interaction between lamin A and SREBP1: implications for partial lipodystrophy and other laminopathies. *Human Molecular Genetics* 11, 769–777.

Lo, C-M, Wang, H-B, Dembo, M, and Wang, Y-l (2000). Cell movement is guided by the rigidity of the substrate. *Biophysical Journal* 79, 144–152.

Louis, HA, Pino, JD, Schmeichel, KL, Pomiès, P, and Beckerle, MC (1997). Comparison of three members of the cysteine-rich protein family reveals functional conservation and divergent patterns of gene expression. *Journal of Biological Chemistry* 272, 27484–27491.

Lu, W, Schneider, M, Neumann, S, Jaeger, V-M, Taranum, S, Munck, M, Cartwright, S, Richardson, C, Carthew, J, Noh, K, Goldberg, M, Noegel, AA, and I, Karakesisoglou (2012). Nesprin interchain associations control nuclear size. *Cellular and Molecular Life Sciences* 69, 3493–3509.

Luo, T, Mohan, K, Iglesias, PA, and Robinson, DN (2013). Molecular mechanisms of cellular mechanosensing. *Nature Materials* 12, 1064–1071.

Luxton, GWG, Gomes, ER, Folker, ES, Worman, H, and Gundersen, GG (2011). TAN lines: A novel nuclear envelope structure involved in nuclear positioning. *Nucleus* 2, 173–181.

Lyon, RC, Zanella, F, Omens, JH, and Sheikh, F (2015). Mechanotransduction in Cardiac Hypertrophy and Failure. *Circulation Research* 116, 1462–1476.

Majkut, S, Idema, T, Swift, J, Krieger, C, Liu, A, and Discher, DE (2013). Heart-specific stiffening in early embryos parallels matrix and myosin expression to optimize beating. *Current Biology* 23, 2434–2439.

Mamchaoui, K, Trollet, C, Bigot, A, Negroni, E, Chaouch, S, Wolff, A, Kandalla, PK, Marie, S, Di Santo, J, St Guily, JL, Muntoni, F, Kim, J, Philippi, S, Spuler, S, Levy, N, Blumen, SC, Voit, T, Wright, WE, Aamiri, A, Butler-Browne, G, and Mouly, V (2011). Immortalized pathological human myoblasts: towards a universal tool for the study of neuromuscular disorders. *Skeletal Muscle* 1, 1–11.

Manilal, S, Nguyen, TM, Sewry, CA, and Morris, GE (1996). The Emery-Dreifuss muscular dystrophy protein, emerin, is a nuclear membrane protein. *Human Molecular Genetics* 5, 801–808.

Maron, BJ, Julius, M, Flack, JM, Gidding, SS, Kurosaki, TT, and Bild, DE (1995). Prevalence of hypertrophic cardiomyopathy in a general population of young adults. Echocardiographic analysis of 4111 subjects in the CARDIA Study. *Circulation* 92, 785–789.

Maron, BJ, Maron, MS, and Semsarian, C (2012). Genetics of hypertrophic cardiomyopathy after 20 years: clinical perspectives. *Journal of the American College of Cardiology* 60, 705–715.

Martinac, B (2014). The ion channels to cytoskeleton connection as potential mechanism of mechanosensitivity. *Biochimica et Biophysica Acta - Biomembranes* 1838, 682–691.

Maruyama, K, Natori, R, and Nonomura, Y (1976). New elastic protein from muscle. *Nature* 262, 58–60.

Maruyama, K, Kimura, S, Ishi, T, Kuroda, M, and Ohashi, K (1977). Beta-actinin, a regulatory protein of muscle. Purification, characterization and function. *Journal of Biochemistry* 81, 215–232.

McNally, EM, Golbus, JR, and Puckelwartz, MJ (2013). Genetic mutations and mechanisms in dilated cardiomyopathy. *The Journal of Clinical Investigation* 123, 19–26.

Meier, J, Campbell, KH, Ford, CC, Stick, R, and Hutchison, CJ (1991). The role of lamin LIII in nuclear assembly and DNA replication, in cell-free extracts of Xenopus eggs. *Journal of Cell Science* 98, 271–279.

Meinke, P and Schirmer, EC (2015). LINC'ing form and function at the nuclear envelope. *FEBS letters*.

Méjat, A (2010). LINC complexes in health and disease. *Nucleus* 1, 40–52.

Melcon, G, Kozlov, S, Cutler, DA, Sullivan, T, Hernandez, L, Zhao, P, Mitchell, S, Nader, G, Bakay, M, Rottman, JN, Hoffman, EP, and Stewart, CL (2006). Loss of emerin at the nuclear envelope disrupts the Rb1/E2F and MyoD pathways during muscle regeneration. *Human Molecular Genetics* 15, 637–651.

Mercuri, E and Muntoni, F (2013). Muscular dystrophies. *The Lancet* 381, 845–860.

Michelsen, JW, Schmeichel, KL, Beckerle, MC, and Winge, DR (1993). The LIM motif defines a specific zinc-binding protein domain. *Proceedings of the National Academy of Sciences* 90, 4404–4408.

Minajeva, A, Kulke, M, Fernandez, JM, and Linke, WA (2001). Unfolding of titin domains explains the viscoelastic behavior of skeletal myofibrils. *Biophysical Journal* 80, 1442–1451.

Miner, JH, Miller, JB, and Wold, BJ (1992). Skeletal muscle phenotypes initiated by ectopic MyoD in transgenic mouse heart. *Development* 114, 853–860.

Mislow, JMK, Holaska, JM, Kim, MS, Lee, KK, Segura-Totten, M, Wilson, KL, and McNally, EM (2002). Nesprin-1α self-associates and binds directly to emerin and lamin A in vitro. *FEBS Letters* 525, 135–140.

Miyoshi, T, Tsuji, T, Higashida, C, Hertzog, M, Fujita, A, Narumiya, S, Scita, G, and Watanabe, N (2006). Actin turnover–dependent fast dissociation of capping protein in the dendritic nucleation actin network: evidence of frequent filament severing. *The Journal of cell biology* 175, 947–955.

Moese, S, Selbach, M, Brinkmann, V, Karlas, A, Haimovich, B, Backert, S, and Meyer, TF (2007). The *Helicobacter pylori* CagA protein disrupts matrix adhesion of gastric epithelial cells by dephosphorylation of vinculin. *Cellular Microbiology* 9, 1148–1161.

Mohapatra, B, Jiminez, S, Lin, JH, Bowles, KR, Coveler, KJ, Marx, JG, Chrisco, MA, Murphy, RT, Lurie, PR, Schwartz, RJ, Elliott, PM, Vatta, M, McKenna, W, Towbin, JA, and Bowles, NE (2003). Mutations in the muscle LIM protein and alpha-actinin-2 genes in dilated cardiomyopathy and endocardiac fibroelastosis. *Molecular Genetics and Metabolism* 1, 207–215.

Molkentin, JD, Lu, J-R, Antos, CL, Markham, B, Richardson, J, Robbins, J, Grant, SR, and Olson, EN (1998). A calcineurin-dependent transcriptional pathway for cardiac hypertrophy. *Cell* 93, 215–228.

Morawietz, H, Ma, Y-H, Vives, F, Wilson, E, Sukhatme, VP, Holtz, J, and Ives, HE (1999). Rapid induction and translocation of Egr-1 in response to mechanical strain in vascular smooth muscle cells. *Circulation Research* 84, 678–687.

Morimoto, A, Shibuya, H, Zhu, X, Kim, J, Ishiguro, K, Han, M, and Watanabe, Y (2012). A conserved KASH domain protein associates with telomeres, SUN1, and dynactin during mammalian meiosis. *The Journal of Cell Biology* 198, 165–172.

Moseley, JB and Goode, BL (2005). Differential activities and regulation of Saccharomyces cerevisiae formin proteins Bni1 and Bnr1 by Bud6. *Journal of Biological Chemistry* 280, 28023–28033.

Muchir, A, Bonne, G, Kooi, AJ van der, Meegen, M van, Baas, F, Bolhuis, PA, Visser, M de, and Schwartz, K (2000). Identification of mutations in the gene encoding lamins A/C in autosomal dominant limb girdle muscular dystrophy with atrioventricular conduction disturbances (LGMD1B). *Human Molecular Genetics* 9, 1453–1459.

Mullins, RD, Heuser, JA, and Pollard, TD (1998). The interaction of Arp2/3 complex with actin: nucleation, high affinity pointed end capping, and formation of branching networks of filaments. *Proceedings of the National Academy of Sciences* 95, 6181–6186.

Nag, AC (1979). Study of non-muscle cells of the adult mammalian heart: a fine structural analysis and distribution. *Cytobios* 28, 41–61.

Narumiya, S, Tanji, M, and Ishizaki, T (2009). Rho signaling, ROCK and mDia1, in transformation, metastasis and invasion. *Cancer and Metastasis Reviews* 28, 65–76.

Newman, B, Cescon, D, Woo, A, Rakowski, H, Erikkson, MJ, Sole, M, Wigle, ED, and Siminovitch, KA (2005). W4R variant in CSRP3 encoding muscle LIM protein in a patient with hypertrophic cardiomyopathy. *Molecular Genetics and Metabolism* 84, 374–375.

Niu, A, Wang, B, and Li, Y-P (2015). TNFα Shedding in Mechanically Stressed Cardiomyocytes is Mediated by Src Activation of TACE. *Journal of Cellular Biochemistry* 116, 559–565.

Nolen, BJ, Littlefield, RS, and Pollard, TD (2004). Crystal structures of actin-related protein 2/3 complex with bound ATP or ADP. *Proceedings of the National Academy of Sciences of the United States of America* 101, 15627–15632.

Omary, MB, Ku, NO, Tao, GZ, Toivola, DM, and Liao, J (2006). "Heads and tails" of intermediate filament phosphorylation: multiple sites and functional insights. *Trends in Biochemical Sciences* 31, 383–394.

Östlund, C, Sullivan, T, Stewart, CL, and Worman, HJ (2006). Dependence of diffusional mobility of integral inner nuclear membrane proteins on A-type lamins. *Biochemistry* 45, 1374–1382.

Ottenheijm, CA, Heunks, LM, and Dekhuijzen, RP (2008). Diaphragm adaptations in patients with COPD. *Respiratory Research* 9.

Ozawa, R, Hayashi, YK, Ogawa, M, Kurokawa, R, Matsumoto, H, Noguchi, S, Nonaka, I, and Nishino, I (2006). Emerin-lacking mice show minimal motor and cardiac dysfunctions with nuclear-associated vacuoles. *The American Journal of Pathology* 168, 907–917.

Pansters, NAM, Velden, JLJ van der, Kelders, MCJM, Laeremans, H, Schols, AMWJ, and Langen, RCJ (2011). Segregation of myoblast fusion and musce-specific gene expression by distinct ligand-dependent inaltivation of GSK-3β. *Cellular and Molecular Life Sciences: CMLS* 68, 523–535.

Paradis, AN, Gay, MS, Wilson, CG, and Zhang, L (2015). Newborn hypoxia/anoxia inhibits cardiomyocyte proliferation and decreases cardiomyocyte endowment in the developing heart: role of endothelin-1. *PloS One* 10.

Paterson, HF, Self, AJ, Garrett, MD, Just, I, Aktories, K, and Hall, A (1990). Microinjection of recombinant p21rho induces rapid changes in cell morphology. *The Journal of Cell Biology* 111, 1001–1007.

Pellegrin, S and Mellor, H (2007). Actin stress fibres. *Journal of Cell Science* 120, 3491–3499.

Perdue, JF (1973). The distribution, ultrastructure, and chemistry of microfilaments in cultured chick embryo fibroblasts. *The Journal of Cell Biology* 58, 265–283.

Petretta, M, Pirozzi, F, Sasso, L, Paglia, A, and Bonaduce, D (2011). Review and meta-analysis of the frequency of familial dilated cardiomyopathy. *The American Journal of Cardiology* 108, 1171–1176.

Pollard, TD and Cooper, JA (1984). Quantitative analysis of the effect of Acanthamoeba profilin on actin filament nucleation and elongation. *Biochemistry* 23, 6631–6641.

Pollard, TD, Blanchoin, L, and Mullins, RD (2000). Molecular mechanisms controlling actin filament dynamics in nonmuscle cells. *Annual Review of Biophysics and Biomolecular Structure* 29, 545–576.

Pring, M, Weber, A, and Bubb, MR (1992). Profilin-actin complexes directly elongate actin filaments at the barbed end. *Biochemistry* 31, 1827–1836.

Pring, M, Evangelista, M, Boone, C, Yang, C, and Zigmond, SH (2003). Mechanism of formin-induced nucleation of actin filaments. *Biochemistry* 42, 486–496.

Pruyne, D, Evangelista, M, Yang, C, Bi, E, Zigmond, S, Bretscher, A, and Boone, C (2002). Role of formins in actin assembly: nucleation and barbed-end association. *Science* 297, 612–615.

Puchner, EM, Alexandrovich, A, Kho, AL, Hensen, U, Schäfer, LV, Brandmeier, B, Gräter, F, Grubmüller, H, Gaub, HE, and Gautel, M (2008). Mechanoenzymatics of titin kinase. *Proceedings of the National Academy of Sciences* 105, 13 385–13 390.

Puckelwartz, MJ, Kessler, E, Zhang, Y, Hodzic, D, Randles, KN, Morris, G, Earley, JU, Hadhazy, M, Holaska, JM, Mewborn, SK, Pytel, P, and McNally, EM (2009). Disruption of nesprin-1 produces an Emery Dreifuss muscular dystrophy-like phenotype in mice. *Human Molecular Genetics* 18, 607–620.

Quijano-Roy, S, Mbieleu, B, Bönnemann, CG, Jeannet, P-Y, Colomer, J, Clarke, NF, Cuisset, J-M, Roper, H, De Meirleir, L, D'Amico, A, Ben Yaou, R, Nascimento, A, Barois, A, Demay, L, Bertini, E, Ferreiro, A, Sewry, CA, Romero, NB, Ryan, M, Muntoni, F, Guacheney, P, Richard, P, Bonne, G, and Estournet, B (2008). De novo LMNA mutations cause a new form of congenital muscular dystrophy. *Annals of Neurology* 64, 177–186.

Rajgor, D, Mellad, JA, Autore, F, Zhang, Q, and Shanahan, CM (2012). Multiple novel nesprin-1 and nesprin-2 variants act as versatile tissue-specific intracellular scaffolds. *PLoS ONE* 7.

Randles, KN, Lam, LT, Sewry, CA, Puckelwartz, M, Furling, D, Wehnert, M, McNally, EM, and Morris, GE (2010). Nesprins, but not sun proteins, switch isoforms at the nuclear envelope during muscle development. *Developmental Dynamics* 239, 998–1009.

Rashmi, RN, Eckes, B, Glöckner, G, Groth, M, Neumann, S, Gloy, J, Sellin, L, Walz, G, Schneider, M, Karakesisoglou, I, Eichinger, L, and Noegel, AN (2012). The nuclear envelope protein Nesprin-2 has roles in cell proliferation and differentiation during wound healing. *Nucleus* 3, 172–186.

Reig, JA, Viniegra, S, Ballesta, JJ, Palmero, M, and Gutierrez, LM (1993). Naphthalenesulfonamide derivatives ML9 and W7 inhibit catecholamine secretion in intact and permeabilized chromaffin cells. *Neurochemical Research* 18, 317–323.

Robinson, RC, Turbedsky, K, Kaiser, DA, Marchand, J-B, Higgs, HN, Choe, S, and Pollard, TD (2001). Crystal structure of Arp2/3 complex. *Science* 294, 1679–1684.

Roma-Rodrigues, C and Fernandes, AR (2014). Genetics of hypertrophic cardiomyopathy: advances and pitfalls in molecular diagnosis and therapy. *The Application of Clinical Genetics* 7, 195.

Roux, KJ, Crisp, ML, Liu, Q, Kim, D, Kozlov, S, Stewart, CL, and Burke, B (2009). Nesprin 4 is an outer nuclear membrane protein that can induce kinesin-mediated cell polarization. *Proceedings of the National Academy of Sciences* 106, 2194–2199.

Ruwhof, C, Van Wamel, JET, Noordzij, LAW, Aydin, S, Harper, JCR, and Van Der Laarse, A (2001). Mechanical stress stimulates phospholipase C activity and intracellular calcium ion levels in neonatal rat cardiomyocytes. *Cell Calcium* 29, 73–83.

Sadler, Ingrid, Crawford, Aaron W, Michelsen, James W, and Beckerle, Mary C (1992). Zyxin and cCRP: two interactive LIM domain proteins associated with the cytoskeleton. *The Journal of cell biology* 119, 1573–1587.

Safer, D, Elzinga, M, and Nachmias, VT (1991). Thymosin-β4 and F_x, an actin-sequestering peptide, are indistinguishable. *Journal of Biological Chemistry* 266, 4029–4032.

Safer, D, Sosnick, TR, and Elzinga, M (1997). Thymosin β4 binds actin in an extended conformation and contacts both the barbed and pointed ends. *Biochemistry* 36, 5806–5816.

Sagot, I, Rodal, AA, Moseley, J, Goode, BL, and Pellman, D (2002). An actin nucleation mechanism mediated by Bni1 and profilin. *Nature Cell Biology* 4, 626–631.

Sakaki, M, Koike, H, Takahashi, N, Sasagawa, N, Tomioka, S, Arahata, K, and Ishiura, S (2001). Interaction between emerin and nuclear lamins. *Journal of Biochemistry* 129, 321–327.

Salameh, A, Wustmann, A, Karl, S, Blanke, K, Apel, D, Rojas-Gomez, D, Franke, H, Mohr, FW, Janousek, J, and Dhein, S (2010). Cyclic mechanical stretch induces cardiomyocyte orientation and polarization of the gap junction protein connexin43. *Circulation Research* 106, 1592–1602.

Sánchez-García, I and Rabbits, TH (1994). The LIM domain: a new structural motif found in zinc-finger-like proteins. *Trends in Genetics* 10, 315–320.

Schallus, T, Fehér, K, Ulrich, AS, Stier, G, and Muhle-Goll, C (2009). Structure and dynamics of the human muscle LIM protein. *FEBS Letters* 583, 1017–1022.

Scharner, J, Gnocchi, VF, Ellis, JA, and Zammit, PS (2010). Genotype-phenotype correlations in laminopathies: how does fate translate? *Biochemical Society Transactions* 38, 257.

Scharner, J, Lu, H-C, Fraternali, F, Ellis, JA, and Zammit, PS (2014). Mapping disease-related missense mutations in the immunoglobulin-like fold domain of lamin A/C reveals novel genotype–phenotype associations for laminopathies. *Proteins: Structure, Function, and Bioinformatics* 82, 904–915.

Schindelin, J, Arganda-Carreras, I, Frise, E, Kaynig, V, Longair, M, Pietzsch, T, Preibisch, S, Rueden, C, Saalfeld, S, Schmid, B, Tinevez, J-Y, White, DJ, Hartenstein, V, Eliceiri, K, Tomancak, P, and Cardona, A (2012). Fiji: an open-source platform for biological-image analysis. *Nature Methods* 9, 676–682.

Schmeichel, KL and Beckerle, MC (1994). The LIM domain is a modular protein-binding interface. *Cell* 79, 211–219.

Schneider, AG, Sultan, KR, and Pette, D (1999). Muscle LIM protein: expressed in slow muscle and induced in fast muscle by enhanced contractile activity. *American Journal of Physiology-Cell Physiology* 276, 900–906.

Schönichen, A, Mannherz, HG, Behrmann, E, Mazur, AJ, Kühn, S, Silván, U, Schoenenberger, C-A, Fackler, OT, Raunser, S, Dehmelt, L, and Geyer, M (2013). FHOD1 is a combined actin filament capping and bundling factor that selectively associates with actin arcs and stress fibers. *Journal of Cell Science* 126, 1891–1901.

Schramp, M, Ying, O, Kim, TY, and Martin, GS (2008). ERK5 promotes Src-induced podosome formation by limiting Rho activation. *The Journal of Cell Biology* 181, 1195–1210.

Schutt, CE, Myslik, JC, Rozycki, MD, Goonesekere, NC, and Lindberg, U (1993). The structure of crystalline profilin-β-actin. *Nature* 365, 810–816.

Schweizer, PA, Schröter, J, Greiner, S, Haas, J, Yampolsky, P, Mereles, D, Buss, SJ, Seyler, C, Bruehl, C, Draguhn, A, Koenen, M, Meder, B, Katus, HA, and Thomas, D (2014). The symptom complex of familial sinus node dysfunction and myocardial noncompaction is associated with mutations in the HCN4 channel. *Journal of the American College of Cardiology* 64, 757–767.

Seidman, JG and Seidman, C (2001). The genetic basis for cardiomyopathy: from mutation identification to mechanistic paradigms. *Cell* 104, 557–567.

Selden, LA, Kinosian, HJ, Estes, JE, and Gershman, LC (1999). Impact of profilin on actin-bound nucleotide exchange and actin polymerization dynamics. *Biochemistry* 38, 2769–2778.

Sharili, AS and Connelly, JT (2014). Nucleocytoplasmic shuttling: a common theme in mechanotransduction. *Biochemical Society Transactions* 42, 645–649.

Sharma, S, Merghani, A, and Gati, S (2015a). Cardiac screening of young athletes prior to participation in sports: difficulties in detecting the fatally flawed among the fabulously fit. *JAMA Internal Medicine* 175, 125–127.

Sharma, S, Merghani, A, and Mont, L (2015b). Exercise and the heart: the good, the bad, and the ugly. *European Heart Journal* 36, 1445–1453.

Shekhar, S, Kerleau, M, Kühn, S, Pernier, J, Romet-Lemonne, G, Jégou, A, and Carlier, M-F (2015). Formin and capping protein together embrace the actin filament in a ménage à trois. *Nature Communications* 6.

Shen, B, Delaney, MK, and Du, X (2012). Inside-out, outside-in, and inside–outside-in: G protein signaling in integrin-mediated cell adhesion, spreading, and retraction. *Current Opinion in Cell Biology* 24, 600–606.

Small, JV, Rottner, K, Kaverina, I, and Anderson, KI (1998). Assembling an actin cytoskeleton for cell attachment and movement. *Biochimica et Biophysica Acta - Molecular Cell Research* 1404, 271–281.

Snider, P, Standley, KN, Wang, J, Azhar, M, Doetschman, T, and Conway, SJ (2009). Origin of cardiac fibroblasts and the role of periostin. *Circulation Research* 105, 934–947.

Soonpaa, MH, Kim, KK, Pajak, L, Franklin, M, and Field, LJ (1996). Cardiomyocyte DNA synthesis and binucleation during murine development. *American Journal of Physiology - Heart and Circulatory Physiology* 271, 2183–2189.

Soranno, T and Bell, E (1982). Cytostructural dynamics of spreading and translocating cells. *The Journal of Cell Biology* 95, 127–136.

Sosa, BA, Rothballer, A, Kutay, U, and Schwartz, TU (2012). LINC complexes form by binding of three KASH peptides to domain interfaces of trimeric SUN proteins. *Cell* 149, 1035–1047.

Souders, CA, Bowers, SLK, and Baudino, TA (2009). Cardiac fibroblast the renaissance cell. *Circulation Research* 105, 1164–1176.

Spaendonck-Zwarts, KY van, Rijsingen, IAW van, Berg, MP van den, Deprez, RHL, Post, JG, Mil, AM van, Asselbergs, FW, Christiaans, I, Langen, IM van, Wilde, AAM, Boer, RA de, Jongbloed, JDH, Pinto, YM, and Tintelen, JP van (2013). Genetic analysis in 418 index patients with idiopathic dilated cardiomyopathy: overview of 10 years' experience. *European Journal of Heart Failure* 15, 628–636.

Starling, EH (1918). The Linacre lecture on the law of the heart. Given at Cambridge, 1915. Longmans, Green, & Company.

Stewart-Hutchinson, PJ, Hale, CM, Wirtz, D, and Hodzic, D (2008). Structural requirements for the assembly of LINC complexes and their function in cellular mechanical stiffness. *Experimental Cell Research* 314, 1892–1905.

Straight, AF, Cheung, A, Limouze, J, Chen, I, Westwood, NJ, Sellers, JR, and Mitchison, TJ (2003). Dissecting temporal and spatial control of cytokinesis with a myosin II Inhibitor. *Science* 299, 1743–1747.

Straub, FB and Feuer, G (1950). Adenosinetriphosphate the functional group of actin. *Biochimica et Biophysica Acta* 4, 455–470.

Swift, J and Discher, DE (2014). The nuclear lamina is mechano-responsive to ECM elasticity in mature tissue. *Journal of Cell Science* 127, 3005–3015.

Swift, J, Ivanovska, IL, Buxboim, A, Harada, T, Dingal, PCDP, Pinter, J, Pajerowski, JD, Spinler, KR, Shin, J-W, Tewari, M, Rehfeldt, F, Speicher, DW, and Discher, DE (2013). Nuclear lamin-A scales with tissue stiffness and enhances matrix-directed differentiation. *Science* 341, 1240104.

Tadokoro, Se, Shattil, SJ, Eto, K, Tai, V, Liddington, RC, Pereda, JM de, Ginsberg, MH, and Calderwood, DA (2003). Talin binding to integrin ß tails: a final common step in integrin activation. *Science* 302, 103–106.

Takeya, R, Taniguchi, K, Narumiya, S, and Sumimoto, H (2008). The mammalian formin FHOD1 is activated through phosphorylation by ROCK and mediates thrombin-induced stress fibre formation in endothelial cells. *The EMBO Journal* 27, 618–628.

Takito, J, Otsuka, H, Yanagisawa, Ni, Arai, H, Shiga, M, Inoue, M, Nonaka, N, and Nakamura, M (2015). Regulation of osteoclast multinucleation by the actin cytoskeleton signaling network. *Journal of Cellular Physiology* 230, 395–405.

Tamiello, C, Bouten, CVC, and Baaijens, FPT (2015). Competition between cap and basal actin fiber orientation in cells subjected to contact guidance and cyclic strain. *Scientific Reports* 5.

Tamkun, JW, DeSimone, DW, Fonda, D, Patel, RS, Buck, C, Horwitz, AF, and Hynes, RO (1986). Structure of integrin, a glycoprotein involved in the transmembrane linkage between fibronectin and actin. *Cell* 46, 271–282.

Taranum, S, Sur, I, Müller, R, Lu, W, Rashmi, RN, Munck, M, Neumann, S, Karakesisoglou, I, and Noegel, AA (2012). Cytoskeletal interactions at the nuclear envelope mediated by nesprins. *International Journal of Cell Biology* 2012.

Tesson, F, Saj, M, Uvaize, MM, Nicolas, H, Płoski, R, and Bilińska, Z (2013). Lamin A/C mutations in dilated cardiomyopathy. *Cardiology Journal* 21, 331–342.

Thierfelder, L, Watkins, H, MacRae, C, Lamas, R, McKenna, W, Vosberg, H-P, Seldman, JG, and Seidman, CE (1994). α-Tropomyosin and cardiac troponin T mutations cause familial hypertrophic cardiomyopathy: a disease of the sarcomere. *Cell* 77, 701–712.

Tibazarwa, K, Sliwa, K, Wonkam, A, and Mayosi, BM (2013). Peripartum cardiomyopathy and familial dilated cardiomyopathy: a tale of two cases: online article-case report. *Cardiovascular Journal of Africa* 24, e4–e7.

Tilney, LG, Bonder, EM, Coluccio, LM, and Mooseker, MS (1983). Actin from Thyone sperm assembles on only one end of an actin filament: a behavior regulated by profilin. *The Journal of Cell Biology* 97, 112–124.

Tohyama, S, Hattori, F, Sano, M, Hishiki, T, Nagahata, Y, Matsuura, T, Hashimoto, H, Suzuki, T, Yamashita, H, Satoh, Y, Egashira, T, Seki, T, Muraoka, N, Yamakawa, H, Ohgino, Y, Tanaka, T, Yoichi, M, Yuasa, S, Murata, M, Suematsu, M, and Fukada, K (2013). Distinct metabolic flow enables large-scale purification of mouse and human pluripotent stem cell-derived cardiomyocytes. *Cell Stem Cell* 12, 127–137.

Tokola, H, Hautala, N, Marttila, M, Magga, J, Pikkarainen, S, Kerkelä, R, Vuolteenaho, O, and Ruskoaho, H (2001). Mechanical load-induced alterations in B-type natriuretic peptide gene expression. *Canadian Journal of Physiology and Pharmacology* 79, 646–653.

Trombitás, K, Jin, J-P, and Granzier, H (1995). The mechanically active domain of titin in cardiac muscle. *Circulation Research* 77, 856–861.

Tunnah, D, Sewry, CA, Vaux, D, Schirmer, EC, and Morris, GE (2005). The apparent absence of lamin B1 and emerin in many tissue nuclei is due to epitope masking. *Journal of Molecular Histology* 36, 337–344.

Uehata, M, Ishizaki, T, Satoh, H, Ono, T, Kawahara, T, Morishita, T, Tamakawa, H, Yamagami, K, Inui, J, Maekawa, M, and Narumiya, S (1997). Calcium sensitization of smooth muscle mediated by a Rho-associated protein kinase in hypertension. *Nature* 389, 990–994.

Unsöld, B, Schotola, H, Jacobshagen, C, Seidler, T, Sossalla, S, Emons, J, Klede, S, Knöll, R, Guan, K, El-Armouche, A, Linke, W, Kögler, H, and Hasenfuss, G (2012). Age-dependent changes in contractile function and passive elastic properties of myocardium from mice lacking muscle LIM protein (MLP). *European Journal of Heart Failure* 14, 430–437.

Van Rijsingen, IAW, Ast, JF Hermans-van, Arens, YHJM, Schalla, SM, Die-Smulders, CEM de, Wijngaard, A van den, and Pinto, YM (2009). Hypertrophic cardiomyopathy family with double-heterozygous mutations; does disease severity suggest doubleheterozygosity? *Netherlands Heart Journal* 17, 458–463.

Voit, T, Parano, E, Straub, V, Schröder, JM, Schaper, J, Pavone, P, Falsaperla, R, Pavone, L, and Herrmann, R (2002). Congenital muscular dystrophy with adducted thumbs, ptosis, external ophthalmoplegia, mental retardation and cerebellar hypoplasia: a novel form of CMD. *Neuromuscular Disorders* 12, 623–630.

Voit, T, Cirak, S, Abraham, S, Karakesisoglou, I, Parano, E, Pavone, P, Falsaperla, R, Amthor, H, Schroeder, J, Muntoni, F, Guacheney, P, Nurnberg, P, Noegel, A, and Herrmann, R (2007). CO 4 Congenital muscular dystrophy with adducted thumbs, mental retardation, cerebellar hypoplasia and cataracts is caused by mutation of Enaptin (Nesprin-1): The third nuclear envelopathy with muscular dystrophy. *Neuromuscular Disorders* 17, 833–834.

Wang, J-Y, Yu, I-S, Huang, C-C, Chen, C-Y, Wang, W-P, Lin, S-W, Jeang, K-T, and Chi, Y-H (2015). Sun1 deficiency leads to cerebellar ataxia in mice. *Disease Models & Mechanisms* 8, 957–967.

Wang, K, McClure, J, and Tu, A (1979). Titin: major myofibrillar components of striated muscle. *Proceedings of the National Academy of Sciences* 76, 3698–3702.

Wang, N, Tytell, JD, and Ingber, DE (2009). Mechanotransduction at a distance: mechanically coupling the extracellular matrix with the nucleus. *Nature Reviews: Molecular Cell Biology* 10, 75–82.

Warren, DT, Zhang, Q, Weissberg, PL, and Shanahan, CM (2005). Nesprins: intracellular scaffolds that maintain cell architecture and coordinate cell function? *Expert Reviews in Molecular Medicine* 7, 1–15.

Way, JC and Chalfie, M (1988). mec-3, a homeobox-containing gene that specifies differentiation of the touch receptor neurons in *C. elegans*. *Cell* 54, 5–16.

Weber, K and Groeschel-Stewart, U (1974). Antibody to myosin: the specific visualization of myosin-containing filaments in nonmuscle cells. *Proceedings of the National Academy of Sciences* 71, 4561–4564.

Weiskirchen, R and Günther, K (2003). The CRP/MLP/TLP family of LIM domain proteins: acting by connecting. *Bioessays* 25, 152–162.

Wen, K-K, Rubenstein, PA, and DeMali, KA (2009). Vinculin nucleates actin polymerization and modifies actin filament structure. *Journal of Biological Chemistry* 284, 30463–30473.

Wheeler, MA, Davies, JD, Zhang, Q, Emerson, LJ, Hunt, J, Shanahan, CM, and Ellis, JA (2007). Distinct functional domains in nesprin-1α and nesprin-2β bind directly to emerin and both interactions are disrupted in X-linked Emery–Dreifuss muscular dystrophy. *Experimental Cell Research* 313, 2845–2857.

Wilding, JR, Lygate, CA, Davies, KE, Neubauer, S, and Clarke, K (2006). MLP accumulation and remodelling in the infarcted rat heart. *European Journal of Heart Failure* 8, 343–346.

Wilhelmsen, K, Litjens, SHM, Kuikman, I, Tshimbalanga, N, Janssen, H, Bout, I van den, Raymond, K, and Sonnenberg, A (2005). Nesprin-3, a novel outer nuclear membrane protein, associates with the cytoskeletal linker protein plectin. *The Journal of Cell Biology* 171, 799–810.

Willmann, R, Kusch, J, Sultan, KR, Schneider, AG, and Pette, D (2001). Muscle LIM protein is upregulated in fast skeletal muscle during transition toward slower phenotypes. *American Journal of Physiology - Cell Physiology* 280, C273–C279.

Wong, S, Guo, W-H, and Wang, Y-L (2014). Fibroblasts probe substrate rigidity with filopodia extensions before occupying an area. *Proceedings of the National Academy of Sciences* 111, 17176–17181.

Worman, HJ and Bonne, G (2007). "Laminopathies": a wide spectrum of human diseases. *Experimental Cell Research* 313, 2121–2133.

Xue, B and Robinson, RC (2013). Guardians of the actin monomer. *European Journal of Cell Biology* 92, 316–332.

Xue, B, Leyrat, C, Grimes, JM, and Robinson, RC (2014). Structural basis of thymosin-β4/profilin exchange leading to actin filament polymerization. *Proceedings of the National Academy of Sciences* 111, E4596–E4605.

Yarmola, EG, Parikh, S, and Bubb, MR (2001). Formation and implications of a ternary complex of profilin, thymosin β4, and actin. *Journal of Biological Chemistry* 276, 45555–45563.

Young, JL, Kretchmer, K, Ondeck, MG, Zambon, AC, and Engler, AJ (2014). Mechanosensitive kinases regulate stiffness-induced cardiomyocyte maturation. *Scientific Reports* 4.

Yu, F-X, Lin, SC, Morrison-Bogorad, M, Atkinson, MA, and Yin, HL (1993). Thymosin beta 10 and thymosin beta 4 are both actin monomer sequestering proteins. *Journal of Biological Chemistry* 268, 502–509.

Yu, J, Lei, K, Zhou, M, Craft, CM, Xu, G, Xu, T, Zhuang, Y, Xu, R, and Han, M (2011). KASH protein Syne-2/Nesprin-2 and SUN proteins SUN1/2 mediate nuclear migration during mammalian retinal development. *Human Molecular Genetics* 20, 1061–1073.

Yu, OM and Brown, JH (2015). G Protein–Coupled Receptor and RhoA-Stimulated Transcriptional Responses: Links to Inflammation, Differentiation, and Cell Proliferation. *Molecular Pharmacology* 88, 171–180.

Zhang, J, Felder, A, Liu, Y, Guo, LT, Lange, S, Dalton, ND, Gu, Y, Peterson, KL, Mizisin, AP, Shelton, GD, Lieber, RL, and Chen, J (2010). Nesprin 1 is critical for nuclear positioning and anchorage. *Human Molecular Genetics* 19, 329–341.

Zhang, Q, Skepper, JN, Yang, F, Davies, JD, Hegyi, L, Roberts, RG, Weissberg, PL, Ellis, JA, and Shanahan, CM (2001). Nesprins: a novel family of spectrin-repeat-containing proteins that localize to the nuclear membrane in multiple tissues. *Journal of Cell Science* 114, 4485–4498.

Zhang, Q, Ragnauth, C, Greener, MJ, Shanahan, CM, and Roberts, RG (2002). The nesprins are giant actin-binding proteins, orthologous to Drosophila melanogaster muscle protein MSP-300. *Genomics* 80, 473–481.

Zhang, Q, Bethmann, C, Worth, NF, Davies, JD, Wasner, C, Feuer, A, Ragnauth, CD, Yi, Q, Mellad, JA, Warren, DT, Wheeler, MA, Ellis, JA, Skepper, JN, Vorgerd, M, Schlotter-Weigel, B, Weissberg, PL, Roberts, RG, Wehnert, M, and Shanahan, C (2007a). Nesprin-1 and-2 are involved in the pathogenesis of Emery–Dreifuss muscular dystrophy and are critical for nuclear envelope integrity. *Human Molecular Genetics* 16, 2816–2833.

Zhang, X, Xu, R, Zhu, B, Yang, X, Ding, X, Duan, S, Xu, T, Zhuang, Y, and Han, M (2007b). Syne-1 and Syne-2 play crucial roles in myonuclear anchorage and motor neuron innervation. *Development* 134, 901–908.

Zhao, X-H, Laschinger, C, Arora, P, Szászi, K, Kapus, A, and McCulloch, CA (2007). Force activates smooth muscle α-actin promoter activity through the Rho signaling pathway. *Journal of Cell Science* 120, 1801–1809.

Zhu, C-H, Mouly, V, Cooper, RN, Mamchaoui, K, Bigot, A, Shay, J W, Di Santo, JP, Butler-Browne, GS, and Wright, WE (2007). Cellular senescence in human myoblasts

is overcome by human telomerase reverse transcriptase and cyclin-dependent kinase 4: consequences in aging muscle and therapeutic strategies for muscular dystrophies. *Aging Cell* 6, 515–523.

Zigmond, SH, Evangelista, M, Boone, C, Yang, C, Dar, AC, Sicheri, F, Forkey, J, and Pring, M (2003). Formin leaky cap allows elongation in the presence of tight capping proteins. *Current Biology* 13, 1820–1823.

Zolk, Oliver, Caroni, Pico, and Böhm, Michael (2000). Decreased expression of the cardiac LIM domain protein MLP in chronic human heart failure. *Circulation* 101, 2674–2677.

Zou, P, Pinotsis, N, Lange, S, Song, YH, Popov, A, Mavridis, I, Mayans, OM, Gautel, M, and Wilmanns, M (2006). Palindromic assembly of the giant muscle protein titin in the sarcomeric Z-disk. *Nature* 439, 229–233.

A Abbreviations

Abbreviation	Full name
ADP	adenosine diphosphate
AraC	cytosine arabinoside
ATP	adenosine triphosphate
DAPI	4', 6-diamidino-2-phenylindole
DNA	deoxyribonucleic acid
dNTP	deoxyribose nucleoside triphosphate
E. coli	*Escherichia coli*
FHOD1	Formin Homology 2 Domain Containing Protein 1
HIV	human immunodeficiency virus
IF	immunofluorescence
IPTG	isopropyl β-D-1-thiogalactopyranoside
KASH	Klarsicht, ANC-1, Syne homology
LINC	Linker of Nucleus and Cytoplasm
MKL1	Megakaryoblastic Leukemia 1
ML7	1-(5-Iodonaphthalene-l-sulfonyl)-lH-hexahydro-l,4 diazepine hydrochlorid
MLC kinase	Myosin Light Chain kinase
MLP	Muscle LIM Protein
MOI	multiplicity of infection
mRNA	messenger ribonucleic acid
NEB	New England Biolabs
NMMIIa	Non-Muscle Myosin IIa
PCR	polymerase chain reaction
qPCR	quanitative real-time poymerase chain reaction
RhoA	Rat Sarcoma Virus (Ras) Homolog Family Member A
RNA	ribonucleic acid
ROCK	Rho-associated Coiled-coil Forming Protein Serine/Threonine Kinase
RPLP0	Ribosomal Protein, Large, P0
siRNA	small interfering RNA
SRC	from the word SaRComa
WB	western blot
WT	wildtype
X-gal	5-bromo-4-chloro-3-indolyl-β-D-galactopyranoside
YAP	Yes-associated Protein

B List of Figures

C List of Tables